COPPER VAPOR GENERATOR

Robert B. Keller, et al

Atlantic Research Corporation

Prepared for:

Advanced Research Projects Agency
Air Force Weapons Laboratory
Polytechnic Institute of New York

September 1974

AFWL-TR-73-223

This final report was prepared by Atlantic Research Corporation, Alexandria, Virginia, and the Polytechnic Institute of Brooklyn, Farmingdale, New York, under Contract F29601-72-C-0080, Job Order 08700301, with the Air Force Weapons Laboratory, Kirtland AFB, NM. Captain G. W. Rhodes (ALD) was the former project officer. Major Robert F. Weber (ALD) was the Laboratory Project Officer-in-Charge.

When US Government drawings, specifications, or other data are used for any purpose other than a defintiely related Government procurement operation, the Government thereby incurs no responsibility nor any obligation whatsoever, and the fact that the Government may have formulated, furnished, or in any way supplied the said drawings, specifications, or other data is not to be regarded by implication or otherwise as in any manner licensing the holder or any other person or corporation or conveying any rights or permission to manufacture, use, or sell any patented invention that may in any way be related thereto.

This technical report has been reviewed and is approved for publication.

ROBERT F. WEBER
Major, USAF
Project Officer

FOR THE COMMANDER

G. DANA BRABSON
Lt Colonel, USAF
Chief, Device Branch

JOHN C. RICH
Lt Colonel, USAF
Chief, Advanced Laser Technology Division

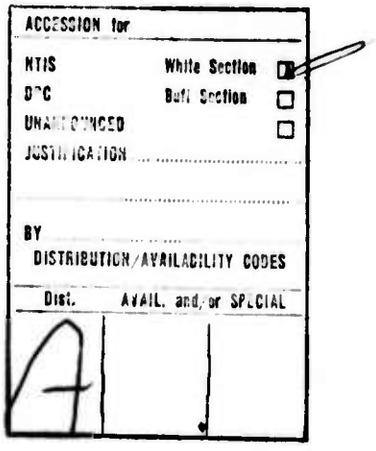

DO NOT RETURN THIS COPY. RETAIN OR DESTROY.

ic

UNCLASSIFIED

SECURITY CLASSIFICATION OF THIS PAGE (When Data Entered)

REPORT DOCUMENTATION PAGE		READ INSTRUCTIONS BEFORE COMPLETING FORM
1. REPORT NUMBER AFWL-TR-73-223	2. GOVT ACCESSION NO.	3. RECIPIENT'S CATALOG NUMBER AD/A-000 555
4. TITLE (and Subtitle) COPPER VAPOR GENERATOR		5. TYPE OF REPORT & PERIOD COVERED Final Report; 31 May 1972-31 May 1973
		6. PERFORMING ORG. REPORT NUMBER
7. AUTHOR(s) Robert B. Keller; Sandor Holly (Atlantic Research Corporation); William T. Walter; Nicholas Solimene; James T. LaTourrette (PIB)		8. CONTRACT OR GRANT NUMBER(s) F29601-72-C-0080; ARPA Order 870, Amdmt 14
9. PERFORMING ORGANIZATION NAME AND ADDRESS Atlantic Research Corporation Alexandria, VA 22314		10. PROGRAM ELEMENT, PROJECT, TASK AREA & WORK UNIT NUMBERS 62301D; 08700301
11. CONTROLLING OFFICE NAME AND ADDRESS Advanced Research Prjoects Agency 1400 Wilson Blvd Arlington, VA 22209		12. REPORT DATE September 1974 13. NUMBER OF PAGES 118
14. MONITORING AGENCY NAME & ADDRESS(if different from Controlling Office) Air Force Weapons Laboratory (ALD) Kirtland AFB, NM 87117		15. SECURITY CLASS. (of this report) UNCLASSIFIED 15a. DECLASSIFICATION/DOWNGRADING SCHEDULE

16. DISTRIBUTION STATEMENT (of this Report)

Approved for public release; distribution unlimited.

17. DISTRIBUTION STATEMENT (of the abstract entered in Block 20, if different from Report)

18. SUPPLEMENTARY NOTES

19. KEY WORDS (Continue on reverse side if necessary and identify by block number)

Copper-vapor laser; Metal-vapor laser; Electronic transitions

20. ABSTRACT (Continue on reverse side if necessary and identify by block number)

Solid fuel propellants seeded with copper powder have been examined as an example of chemical generation of the copper vapor in a copper-vapor laser that has the potential of generating a visible output (510.6 nm) with high efficiency. Chemical generation of the copper vapor is the only approach capable of producing an overall electrical efficiency of 10 percent in a flowing copper-vapor laser. The effect of Ar, N_2, CO_2, CO, H_2, and H_2O as additive gases on the laser's performance has been determined. A simulated propellant-generated

DD FORM 1 JAN 73 1473 EDITION OF 1 NOV 65 IS OBSOLETE

UNCLASSIFIED

SECURITY CLASSIFICATION OF THIS PAGE (When Data Entered)

ABSTRACT (cont'd)

copper-vapor laser was demonstrated by flowing the expected mixture of tank gases over molten copper upstream of the laser cavity. Laser performance was seriously degraded due to the presence of the additive gas mixture. The propellant-generated tests were unsuccessful in part due to insufficient vaporization of the copper seed particles which were distributed in the solid fuel propellant. A heat-pipe copper-vapor laser was also demonstrated.

Block 9 (cont'd)

Polytechnic Institute of Brooklyn
Farmingdale, New York 11735

TABLE OF CONTENTS

LIST OF ILLUSTRATIONS

LIST OF ILLUSTRATIONS (continued)

LIST OF ILLUSTRATIONS (continued)

SECTION I

INTRODUCTION AND SUMMARY

Efficiency and brightness are two of the most important parameters for high-power laser systems. The copper vapor laser (CVL) has already demonstrated a 1 percent efficiency (Refs 1,2), the highest for a visible gas laser, and a peak brightness (Ref 3) of 10^{11} W/cm^2-sr, the highest for a gas laser. In Section II-1 of this report, it is shown that 23 percent represents a practical limiting efficiency for the pulsed CVL and 10 percent is a reasonable goal. Peak brightnesses of 10^{13} W/cm^2-sr appear attainable from present static systems.

Flowing systems have been proposed to allow operation at higher pulse repetition rates and thereby generate higher average powers. The goals set for a flowing system were

a. Generation of 0.25 joule/liter in a single pulse which can be repeated at a 1000 pps rate.

b. An overall electrical efficiency of 10 percent.

In the following discussion "overall electrical efficiency" as a term includes energy expanded to vaporize copper, if electrical energy is used in the process. Reasons for this view are mostly practical; i.e., the power source must be designed to supply the total electrical energy demand of the copper vapor laser system.

In order to meet the above listed goals, an order of magnitude increase is required over what has been achieved in static systems. It is anticipated that a tenfold increase in the copper vapor density over the highest densities achieved so far in static systems, in conjunction with an improved electrical excitation mechanism (fast risetime, quasimonochromatic electron temperatures), makes the first goal achievable. For the second goal, however, fundamental limitations must be considered involving the heat of vaporization of copper to produce the vapor, the fraction of copper atoms which can be utilized due to the large collisional-mixing cross section of the upper and lower laser levels, and efficient transfer of electrical energy into the appropriate population inversions. In Section II-3 it is shown that

a. Approximately 3.86 electron volts (eV) of input energy is required to generate each copper atom in the vapor phase at 1800°K.

b. Not more than one fifth represents the maximum fraction of copper atoms which can be excited to the upper laser level.

c. If electrical energy is used to produce the copper vapor in a flowing system, the overall electrical efficiency will be reduced by at least a factor of 4.

d. Chemical generation of the copper vapor is the only approach capable of producing an overall electrical efficiency of ~10 percent in a flowing CVL.

Chemical generation has the additional advantages of more efficient storage (in terms of weight and volume) and of a very rapid startup time.

Solid-fuel propellants seeded with powdered copper have been examined in this study as an example of chemical generation of the copper vapor. The approach taken was to ignite a solid-fuel propellant in a separate burning chamber called the gas generator. The burning propellant generates copper vapor along with combustion gas products. The evolved gases transport the copper vapor into the laser cavity where a pulsed electrical discharge provides the excitation of the copper upper laser level. The optical axis of the laser cavity is transverse to the gas flow; however, the electric field can be along or transverse to the gas flow axis. A throat is provided between the generator and laser chamber to permit the propellant to burn at a higher pressure than that required for optimum laser operation.

One major concern of the solid-fuel propellant approach was the effect of the combustion product gases on the performance of the CVL. Small amounts of N_2, H_2 and CO_2 had previously been introduced into a static CVL without extinguishing the laser action. However, a more thorough investigation of the effect of these and other potential product gases was required to guide the propellant selection. The gas effects tests were carried out in a static (nonflowing) CVL at PIB and are described in Section III. Except for argon, all of the additive gases examined degraded the laser's output power. The severity of the degradation increased in the following order: N_2, CO_2, CO, H_2 and H_2O.

The second major task was the selection of a propellant which would burn smoothly under low enough pressures and evolve only acceptable gases to provide laser action. Selection and testing of the propellant was carried out at the same time as the gas effects tests. The propellant development and design and testing of the generator are described in Section IV. Homogeneity measurements were carried out in a Michelson interferometer constructed at ARC for this purpose. This work is described in Section V.

CVL operation was obtained under simulated conditions of the solid-fuel propellant. Tank gases were used to generate the expected mixture of combustion product gases which then flowed over molten copper upstream of the laser cavity in the modified PIB apparatus. This is described in Section VI. Tolerance of the gas mixture is poor. Above a total cavity pressure of 4 torr, laser performance is seriously degraded, and at pressures greater than 6 torr, efficiency is reduced by at least an order of magnitude. The propellant-generated flow tests, described in Section VII, were unsuccessful partly because of this tolerance of the gas mixture, and partly because of insufficient vaporization of the copper seed particles.

Finally, Section VIII reviews the results in terms of conclusions and recommendations for future work.

SECTION II

BACKGROUND

I. INTRODUCTION

Efficiency plays a dominant role in the development of high-power lasers. The problems of handling the excess heat as well as the size and weight of the power supply are relieved by an improvement in efficiency. Although in the far infrared, carbon dioxide lasers have operated with electrical conversion efficiencies as high as 30 percent, the electrical conversion efficiency of visible lasers has been less than 1 percent and usually on the order of 0.1 percent.

The first source of inefficiency is inherent in the energy-level structure of the active medium. When the upper laser level is many electron volts above the ground level, as it is in the helium-neon laser or the argon ion laser (Figure II-1), the quantum efficiency is very low. The energy of a laser photon is only a small fraction of the excitation energy – the energy of the upper laser level. A second source of inefficiency occurs when the cross section for electron excitation of the upper laser level does not dominate over the sum of excitation cross sections of all other levels combined. The third limitation in the case of the rare gas visible lasers is the radiative relaxation process – namely, spontaneous emission to a metastable or radiation-trapped level. This is the controlling process which limits the power extraction rate from the rare-gas visible lasers.

In 1966 Walter, et al., (Ref 4) described a class of efficient, pulsed gas-discharge lasers which were called cyclic lasers – cyclic because the excitation and relaxation processes function sequentially or cyclically instead of simultaneously. The active media proposed were the vapors of certain metals with attractive, low-lying energy-level structures. The energy-level structure of certain metals are attractive for two reasons. First, the energy levels lie closer to the ground level than in the rare gases; so, unlike the rare-gas lasers, the quantum defect can be made very small. In copper, for example as indicated in Figure II-2, the energy returned by the green laser photon is 64 percent of the energy required to excite the upper laser level. Second, the cross section for excitation of the upper laser level can dominate over excitation of all other levels since the upper laser level is the resonance level of the atom. In copper the f numbers for excitation of the doublet resonance level total 0.475 while the sum of the other lines terminating on the ground level for which measurements have been made total only 0.054. The measured f and A values by Corliss and Bozman (Ref 5) for copper are indicated on energy level diagrams in Figures II-2 and II-3 to illustrate this point. While there are a number of lines to higher-lying copper levels whose f numbers have not been measured, individually each will be small; and collectively they will not substantially change the picture just presented here. Since the excitation cross sections are proportional to the f number, the dominant excitation is that of the upper laser levels – again a more efficient situation than that occurring in the visible rare-gas lasers.

Cyclic metal-vapor lasers such as the copper vapor laser have the same efficient low-lying energy-level structure as the CO_2 laser; however, the lower laser level is 1.5 eV instead of 0.1 eV above the ground level. Therefore, a copper vapor laser can tolerate a substantial rise in temperature; in fact, high temperatures are required to bring the copper into the discharge in a fully vaporized state. Operation at an elevated temperature also has the advantage of allowing radiative cooling processes to be utilized to carry off the wasted input energy instead of having to depend on the slower convective cooling processes.

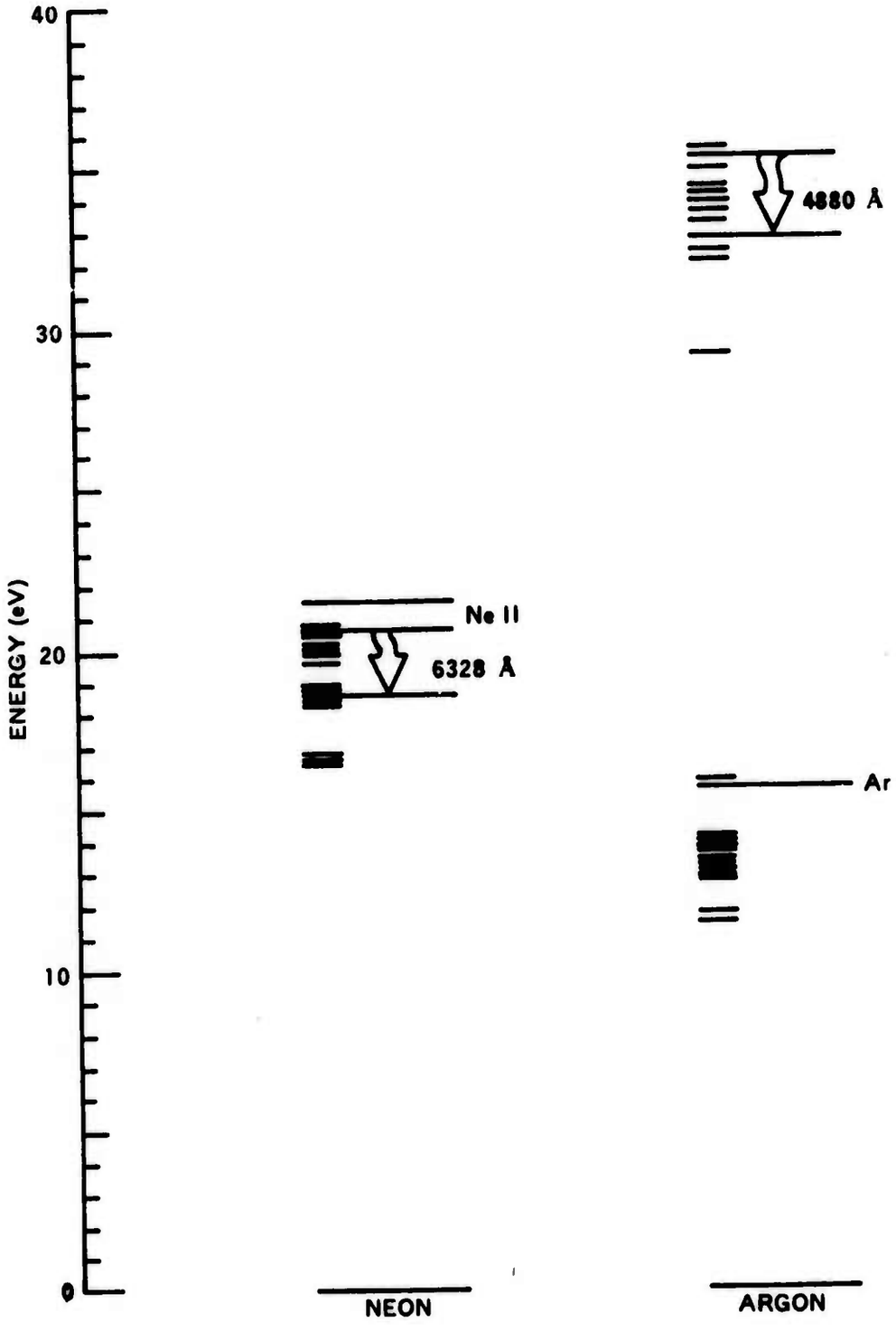

Figure II-1. Energy Level Structure of Hellum - Neon and Argon - Ion Lasers.

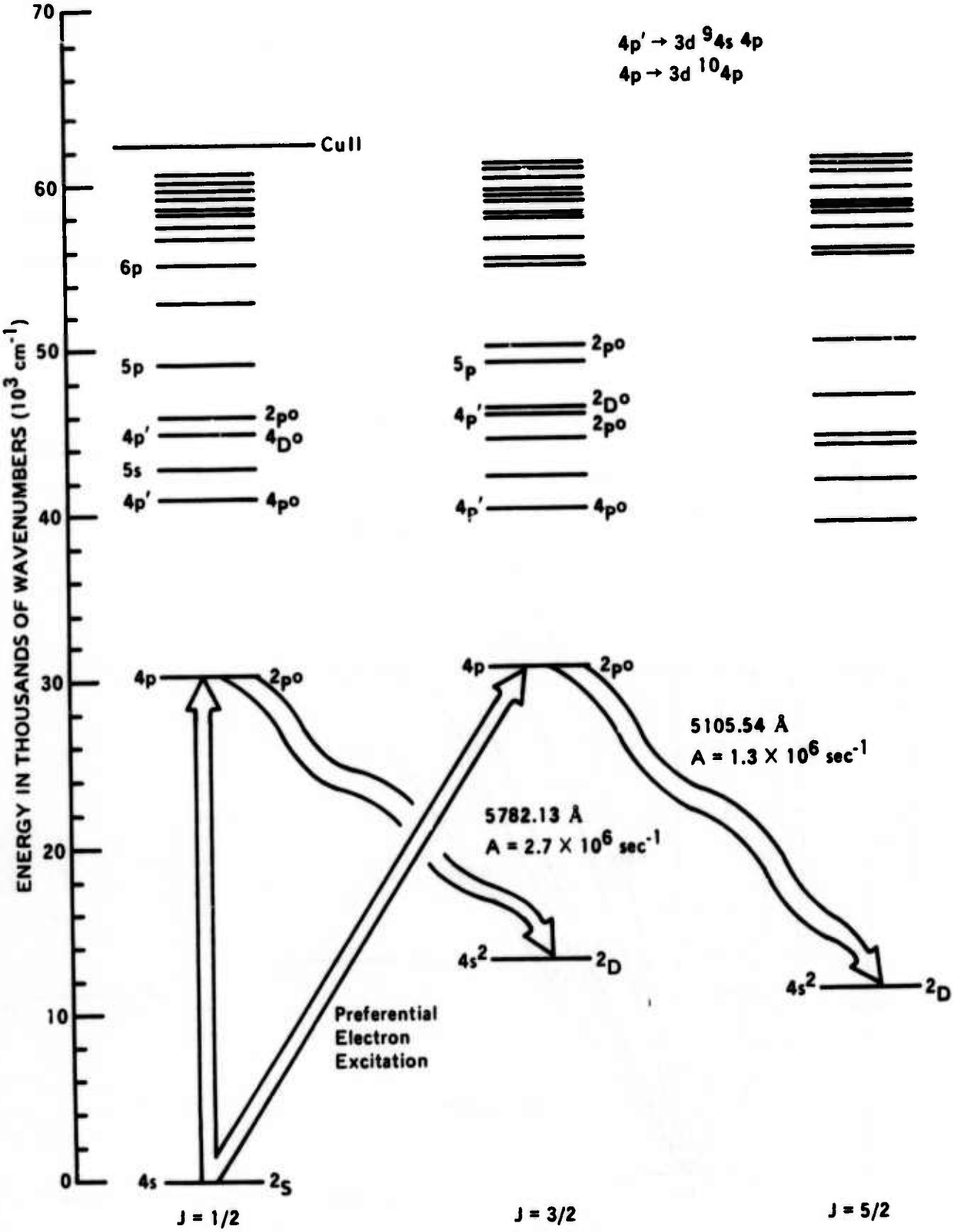

Figure II-2. Copper Laser Processes Indicated on the Copper Energy Levels.

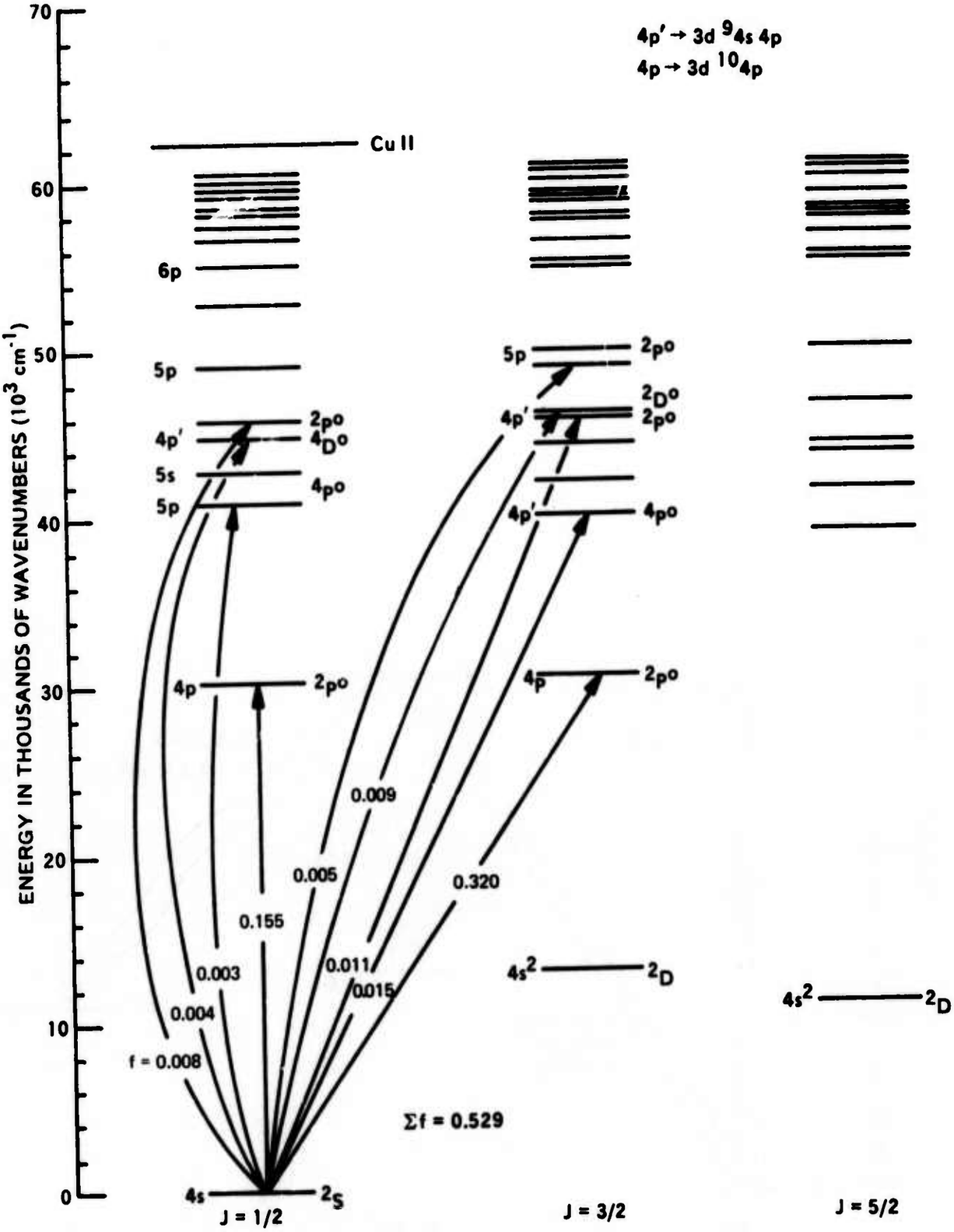

Figure II-3. Excitation Values Indicated on the Copper Energy Levels.

A further distinction and advantage in many applications is that the laser output is in the green portion of the visible spectrum, instead of in the far infrared, permitting corresponding reductions in the size and weight of optics and tracking equipment (and allowing some transmission through water).

2. THE CYCLIC COPPER VAPOR LASER

The copper vapor laser (CVL) is one of a class of efficient, pulsed gas-discharge lasers which operates by means of cyclic excitation and relaxation in an atomic vapor discharge. The cyclic laser (Ref 4) (shown in Figure II-4) is a three-level system in which the upper laser level is a resonance level of the atom, while the lower laser level is a metastable level between the ground and resonance levels. Transient population inversions are efficiently produced by the preferential electron excitation of those atomic energy levels which are both close to and optically connected with the ground level. These inversions are inherently transient because of the metastability of the lower laser level. Collisional relaxation of the lower laser level will determine the repetition rate of the laser pulses in a static or low flow velocity system. In fast flowing systems ($>10^3$ cm/sec) the pulse repetition rate may be increased by transporting the metastable copper atoms from the interaction region.

In addition to having the ground level, metastable level and resonance energy level structure, the most efficient members of the class of cyclic lasers will satisfy additional restrictions on the A value of the laser transition and the spacing of the metastable level above the ground level as indicated in Figure II-4. Furthermore, the branching ratio into the laser transition should be $\simeq 1$. Thus the metal vapor density must be high enough to suitably trap the resonance radiation, and the laser A value should dominate over the A values of any other transitions out of the upper laser level. At present, flowing CVL systems and copper generation from compounds have had great difficulty in meeting this requirement.

Three different metal vapor energy level structures are shown in Figure II-5 – mercury, thallium and copper. Each has a metastable level between the ground level and the resonance level. However, the 10^{-1} sec^{-1} A value of the indicated 5μ transition between the fine structure levels in mercury is so small that an unattainable inversion density is required for adequate gain. In thallium, on the other hand, the 10^8 sec^{-1} A value of the 5350 Å transition is so fast that it is difficult to make the risetime of the excitation current pulse shorter than the reciprocal of the A value. Spontaneous emission can drain the upper laser level before a sufficient population inversion is achieved. Even when fast risetime pulses can be produced, because of the large A value the gain becomes large enough at low inversion densities that superradiance occurs and limits the output energy of the laser pulse. The situation in copper is more nearly ideal. Because the A value of the laser transition is 10^6 sec^{-1}, it is relatively easy to produce excitation pulses with risetimes $<1/A$. This favorable situation occurs because the laser transition is a two-electron transition as indicated in Figure II-2.

The copper vapor laser is the most efficient of the cyclic lasers investigated thus far. The excitation and laser processes are indicated on the energy level diagram in Figure II-4. Because the resonance and metastable levels are doublets, there are two laser transitions inn copper – a green transition at 5106 Å (in the region of maximum water transmission) and a yellow transition at 5782 Å.

The advantages of the cyclic copper vapor laser are readily apparent from the location of the energy levels. First, two-thirds of the excitation energy is returned by the laser photon. Second, the structure is remarkably free of other levels and their possible parasitic influence. The first two excited levels in copper are the lower and upper laser levels. The next copper energy level is already 1 eV above the upper laser level and requires 27 percent more energetic electrons for threshold excitation.

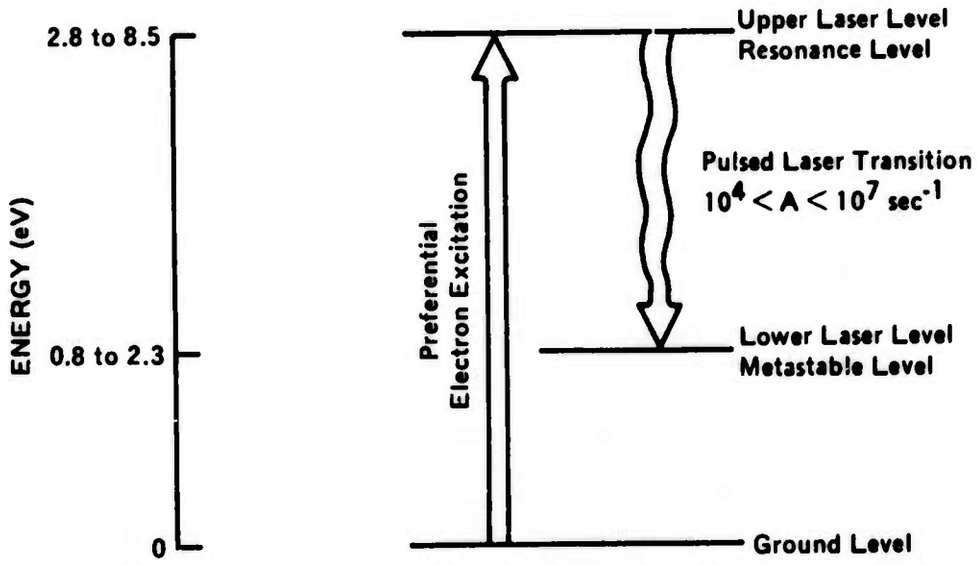

Figure II-4. Cyclic Laser Efficient, Pulsed Discharge Laser.

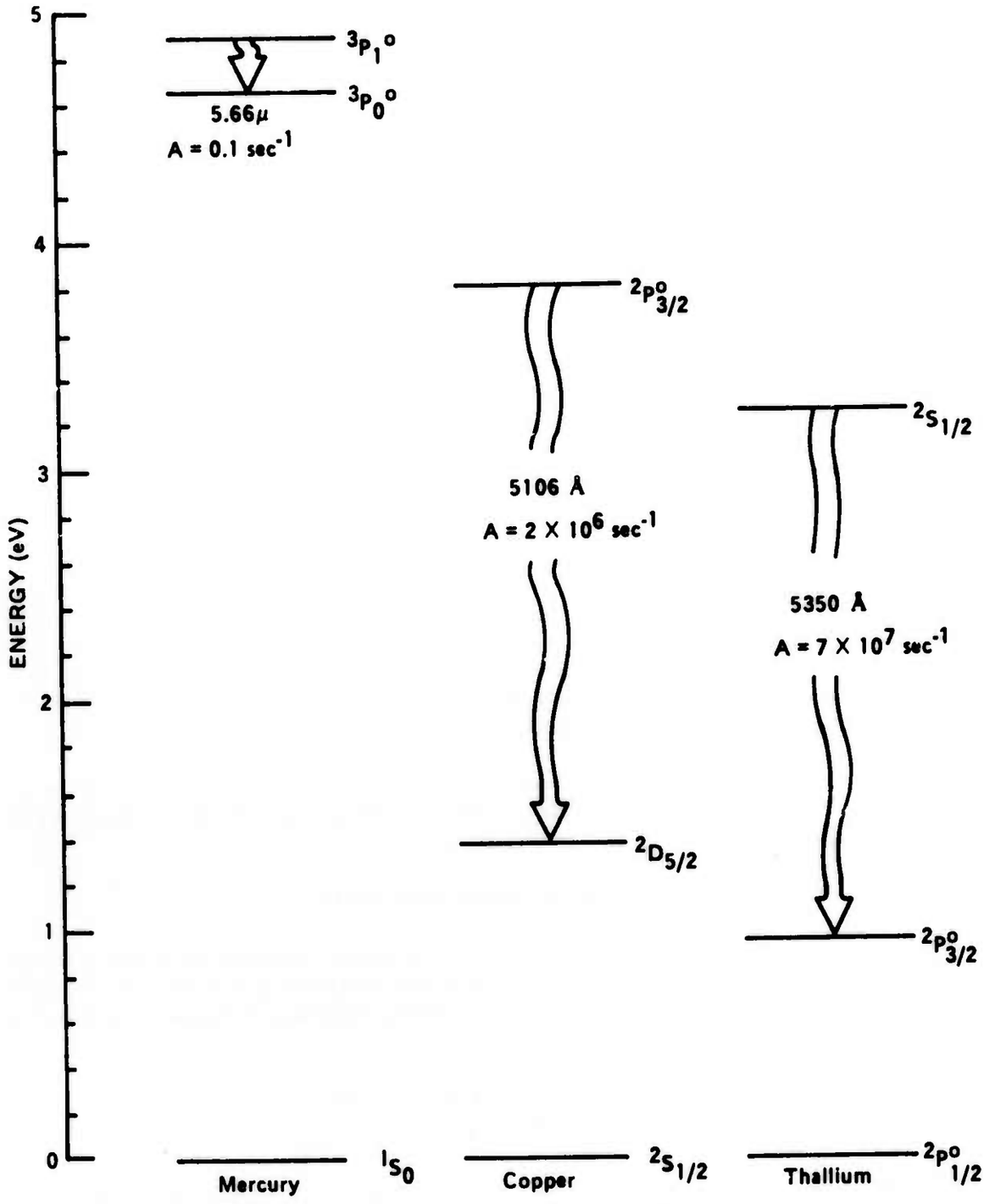

Figure II-5. Low-Lying Energy Levels of Mercury, Copper and Thallium.

The attractiveness of the low-lying energy levels of the copper atom is indicated in Figure II-6 where a comparison is made between the level structure of the copper vapor laser and the CO_2 laser, which has been the most efficient gas laser, and the argon ion laser, which has produced the highest average power in the visible. Relative energy is plotted on the ordinate scale. The fraction of the energy of the excitation returned by the laser photon may be directly compared. It is 41 percent in CO_2, 64 percent in copper and 7 percent in ionized argon.

An upper limit to the efficiency achievable in copper may be estimated by considering three factors: the quatum defect, the statistical weights of the laser levels, and the efficiency with which the input energy can be channeled into exciting the upper laser level. First, 36 percent of the excitation energy must be lost in relaxing the lower laser levels. Second, a fraction of the excited atoms which is at least equal to $g_u/(g_u + g\ell)$ will remain in the upper level when the oscillation terminates. The g's represent the statistical weights of the upper and lower laser levels. Therefore, the theoretical limiting efficiency is $g\ell E_{laser}/(g_u + g\ell)E_{excitation}$ or 38 percent for the pulsed copper vapor laser. The third factor is the fraction of input power which is effective in exciting the upper laser levels (ϕ). Mercury resonance levels in a fluorescent lamp are excited typically with an efficiency: $\phi \sim 60$ percent. Using this as a maximum value, the practical limiting efficiency

$$\epsilon = \frac{g\ell}{g_u + g\ell} \frac{E_{laser}}{E_{excitation}/\phi}$$

would be about 23 percent; so actual operating efficiencies of 10 percent seem to be a reasonable goal if the resonance levels in copper can be excited as efficiently as in mercury. This may be an optimistic assumption, however, since efficient coupling to the copper vapor may be very difficult. Fast risetime current pulses must be generated. Besides minimizing circuit inductances (coaxial transmission line), one should try to optimize the matching between the line characteristic impedance and the load (discharge) impedance at least during the time period of the current risetime in order to maximize the energy transfer (and laser efficiency).

The highest electrical conversion efficiency achieved thus far is 1.7 percent measured during this program in a static copper vapor apparatus developed at PIB. This efficiency has been calculated by dividing the energy of a laser pulse by the total energy stored on the input capacitor, $1/2\ CV^2$.

3. EFFECT OF METASTABILITY OF THE LOWER LASER LEVEL

Relaxation of the metastable lower laser level is the fundamental limiting process in the copper vapor laser. In a static or nonflowing apparatus, the metastable copper atoms must diffuse to the walls of the tube to relax back to the ground level. The diffusion time is equal to the number of collisions squared (because it is a random walk process) multiplied by the mean time between collisions.

$$\tau_{diffusion} \sim \left(\frac{D}{\lambda}\right)^2 \cdot \frac{\lambda}{v} = \frac{D^2}{\lambda v}$$

where D is the tube diameter, λ is the mean free path, and v is the average velocity of a copper atom. Therefore, the diffusion time is proportional to the tube diameter squared.

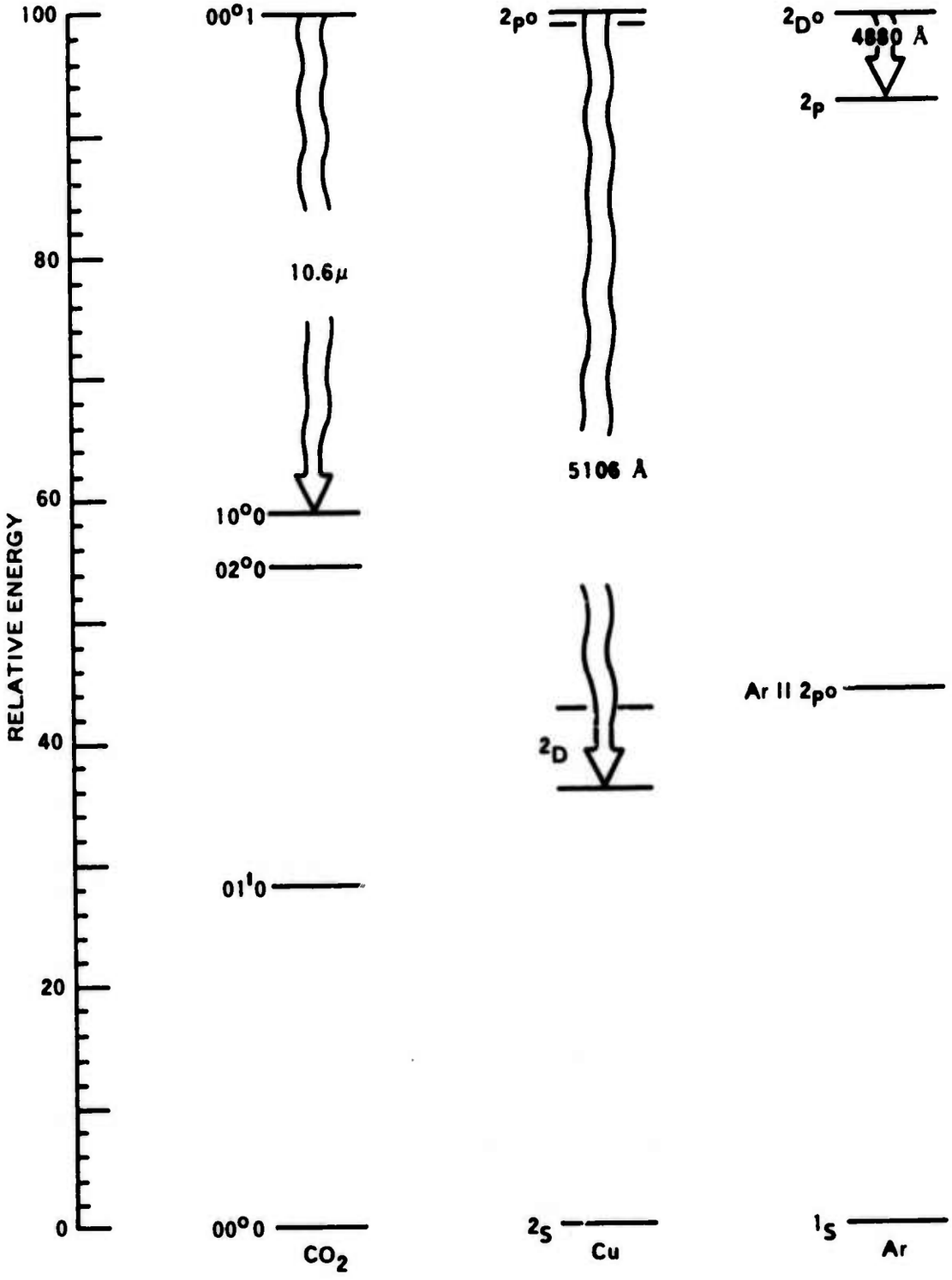

Figure II-6. Energy Level Structure Comparison of CO_2, Copper and Argon Lasers.

In Figure II-7 the relaxation time between pulses, namely the reciprocal of the laser pulse repetition frequency (PRF) which maximized the average power output of the laser, is plotted as a function of the tube diameter for the four tube diameters tested. If the relaxation time is determined by the diffusion of metastable copper atoms to the walls, then $\tau \sim D^2$. Scatter in the data prevents us from distinguishing between a first or second power dependence on the tube diameter. If, however, diffusion is the limiting relaxation process, so the power output per unit volume $\sim D^{-2}$ while the tube volume $\sim D^2$, then the average power output should be independent of the diameter of the tube. In fact, we obtained 1.2 watts from the 1.5 cm diameter, 1.0 watts from the 2.4 cm diameter, 1.1 watts from the 3.2 cm diameter and 1.3 watts from the 4.4 cm diameter tubes. The average power output was essentially independent of diameter, as expected for diffusion-limited relaxation.

Two methods of increasing the relaxation rate beyond the limit imposed by diffusion are (1) volumetric quenching and (2) high-speed flow. A volumetric quenching agent should quench the lower laser level in a time $<10^{-4}$ sec without interfering with the excitation process. A high-speed flow should sweep the metastable copper atoms out of the interaction region in a time $<10^{-4}$ sec. Both approaches would enable the laser to operate at higher PRF and therefore generate higher average powers.

For the lower level quenching rate to exceed 10^4 sec^{-1}, $n_Q v_Q \sigma_{QL} > 10^4$ sec^{-1} where n_Q is the density of the quenching species and σ_{QL} is the quenching cross section for a copper atom in the lower laser level to the ground level. Since velocities at the operating temperature of the laser will be $\sim 10^5$ cm/sec,

$$n_Q \sigma_{QL} > 10^{-1} \text{ cm}^{-1}.$$

This indicates that $\sigma_{QL} > 10^{-17}$ cm^2 for 1 torr pressure or $> 10^{-18}$ cm^2 for 10 torr pressure of the quenching species. Although quenching cross sections of 10^{-16} cm^2 or larger have been measured, these have usually been for optically allowed transitions such as the alkali resonance levels. Quenching cross sections of metastable levels, in mercury and thallium for example, are generally 10^{-16} cm^2 at most. A further concern is the possible quenching of the copper upper laser level, the resonance level, by the quenching species. It has already been pointed out that the quenching species must not interfere with the optimum discharge conditions by modifying the electron temperature distribution and degrading the direct electron excitation number of the upper laser level. The quenching species must also not quench the upper laser level during the excitation and laser portion of the cycle, $\sim 10^{-7}$ sec. Thus $n_Q v_Q \sigma_{QU} < 10^7$ sec^{-1} or

$$n_Q \sigma_{QU} < 10^2 \text{ cm}^{-1}$$

where σ_{QU} is the quenching cross section of the copper upper laser level. This indicates that $\sigma_{QU} < 10^{-14}$ cm^2 for 1 torr pressure or $< 10^{-15}$ cm^2 for 10 torr pressure of the quenching species.

These restrictions imply that the quenching cross section of the upper laser level, which is a resonance level, cannot exceed the quenching cross section of the metastable, lower laser level by more than 10^3.

$$\sigma_{QU} < 10^3 \, \sigma_{QL}$$

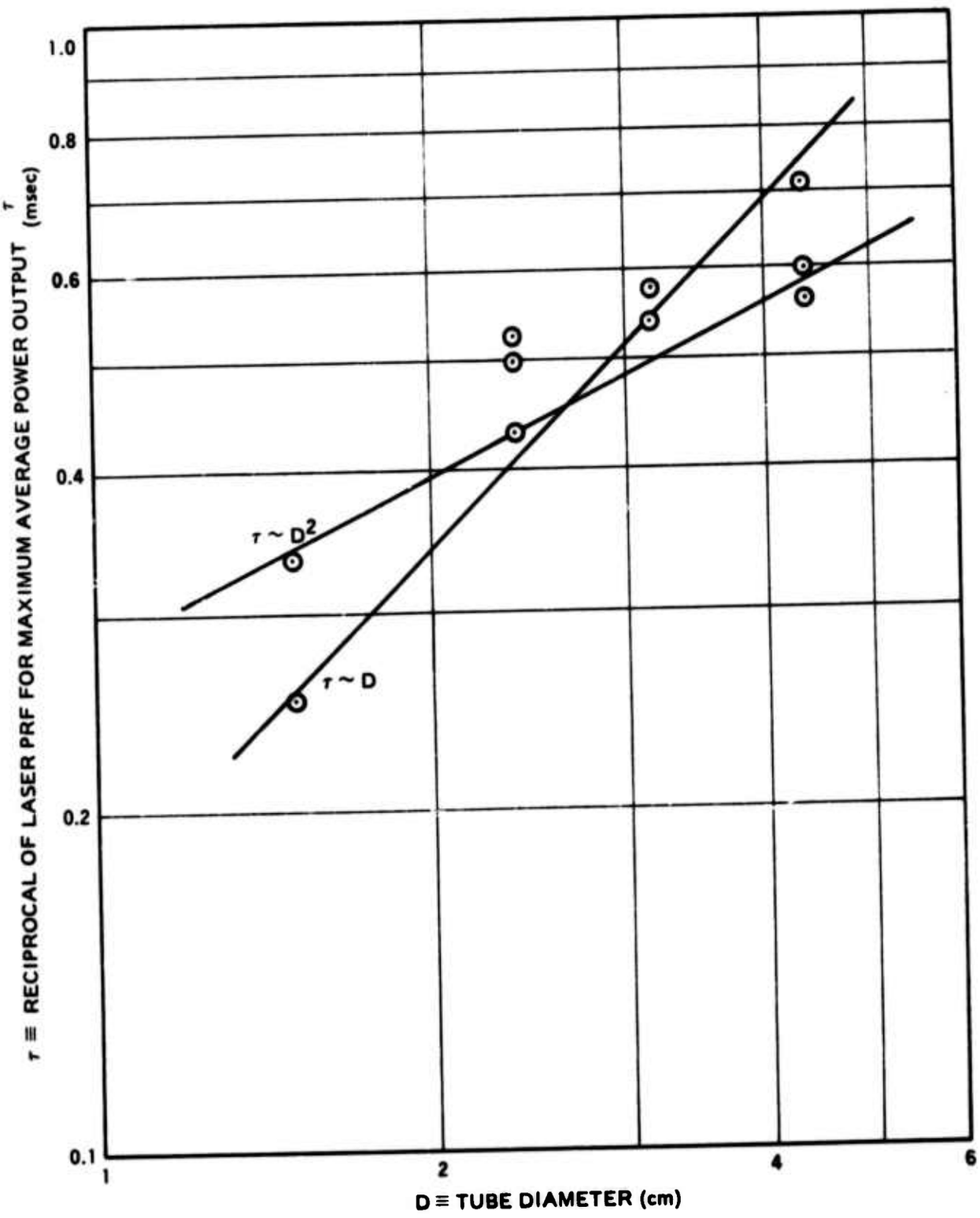

Figure II-7. Effect of Tube Diameter on Laser Pulse Repetition Frequency for Maximum Average Power Output.

Satisfaction of this condition is not automatically assured. The quenching cross section of N_2, for example, for the resonance $3P_1$ level of mercury or $2S_{1/2}$ level of thallium in each case is at least 10^4 times larger than the quenching cross section of the lower metastable $3P_0$ level in H_g or $2P_{3/2}$ level in Tl. Some selectivity is therefore required in the quenching ability of the additive quenching species.

A molecule with an electronic energy level resonant with the copper lower laser level and not with the upper laser level would be expected to provide this selective quenching ability. The only common molecule that appears to satisfy this requirement is oxygen. Oxygen, however, is too chemically reactive with copper to serve as a quenching agent in a static system. The vibrational levels of the groun; electronic levels of common diatomic molecules including N_2, H_2, CO, NO, etc., have been examined for levels resonant with the copper metastable-to-ground level spacing. Molecules with low-energy defects for this spacing also have low energy defects for the copper upper-to-lower laser level or upper-to-ground level spacings. In Section III the results of the preliminary testing of the common gases, N_2, O_2, CO, CO_2, H_2 and H_2O, will be described. No indication of the selective quenching required for increased PRF operation and increased average power output has been observed. At this stage of investigation the possibility of finding a volumetric quenching agent should not be written off. Although the more common gases do not appear promising, there are some other more complex possibilities still to be pursued.

A high-speed flow is a second method to increase the laser PRF and hence the average power output. High-speed flows have been very successfully used in the CO_2 laser to remove excess heat and prevent a buildup in the gas temperature which can provide thermal population of the lower laser level. High-speed flows have also been successfully used to increase the PRF and average power output in a pulsed N_2 laser by rapidly removing the metastable lower-laser level molecules and providing a supply of unheated N_2. It seems reasonable, therefore, to consider similar high-speed flows for the copper vapor laser. The difference in the situations is that while CO_2 and N_2 are gases at room temperature, copper is a solid which requires some 3.86 eV per copper atom to generate it at 1800°K in the vapor phase.

Furthermore, not every atom can be excited to the upper laser level before flowing out of the optical cavity. Leonard's analysis (Ref 6) indicates that the dominant electron processes are excitations of the upper laser level (R_{02}) and deexcitation of the upper to lower laser level (R_{21}). If all other processes are neglected compared to these two during the excitation portion of the cyclic laser before laser action begins,

$$\frac{dn}{dt} = (N - n) R_{02} - nR_{21}$$

where n is the density in the upper laser level and N is the total copper atom density. If f is defined as the fraction of copper atoms which can be excited to the upper laser level, then

$$f \equiv \frac{n}{N} \leq \frac{R_{02}}{R_{02} + R_{21}}$$

According to Leonard's analysis $R_{21} > R_{02}$. The collisional deexcitation rate varies from 20 times larger at an electron temperature, T_e = 2 eV (where the electron excitation rate of the upper laser level just exceeds that of the lower laser level) to 4 times larger at T_e = 10 eV which is greater than the 7.7 eV ionization potential of copper. Therefore, f is limited to 20 percent at 10 eV and decreases to 5 percent at threshold. Even if an electron temperature of 10 eV is assumed throughout the excitation period, the maximum fraction of copper atoms which can be excited to the upper laser level is at most 20 percent. This estimate is probably optimistic. The maximum that has been achieved in a static system thus fas is ~5 percent.

The total efficiency ϵ is given by:

$$\epsilon = \frac{g_\ell}{g_u + g_\ell} \cdot \frac{E_{laser}}{3.86/f + E_{excitation}/\phi} = \frac{1.4566f}{3.86 + 3.8167f/\phi}$$

where ϕ is the fraction of input discharge energy which is effective in exciting the upper laser level and 1.4566 eV = $g_\ell E_{laser}/(g_u + g_\ell)$. If ϕ = 60 percent, again from the analogy with the efficient mercury discharge lamp, and f = 0.2, then the limiting practical efficiency for a flowing system is 5.7 percent compared with 23 percent in a static system in which each atom can be cycled through the laser process many times before it escapes from the hot zone or the optical cavity. Therefore, the practical limiting efficiency has been reduced by a factor of 4. Whereas we may expect an attainable operating efficiency of 10 percent in the static system, 2 percent is the corresponding figure for a high-speed flow system. This limitation cannot be overcome by increasing the PRF (i.e., making the PRF > flow velocity/optical cavity dimension along the flow). Unless a volumetric quenching agent is discovered and employed, those copper atoms which contributed to the previous laser pulse will still be found in the lower laser level.

The situation for a high-speed flow copper vapor laser is therefore equivalent to lowering the ground level of the copper atom by 3.86/f eV to a virtual ground level. This lowering is at least 19 eV. It has the effect of converting the attractive energy level structure of the copper atom to a much less attractive, rare gas type of level structure as indicated in Figure II-8.

If the energy required to generate the copper vapor can be supplied chemically instead of electrically, then although the total energy efficiency remains limited to 5.8 percent; the limitation on the total electrical efficiency is increased to 23 percent.

Another method of reducing the 3.86 eV energy required to generate a copper atom in the vapor phase at 1800°K starting from metallic copper at room temperature is to utilize a more-volatile molecule which contains copper and dissociates at moderate temperatures. The difficulties with this scheme are low atomic copper density, association in the vapor phase; that is, formation of Cu_2 or higher complexes and condensation of the copper, and production of electronegative species. The presence of these species and other fragments of the original molecule can lower the electron temperature and change the discharge conditions so that the appropriate laser excitation conditions are no longer satisfied. None of the several attempts to produce a copper vapor laser in this fashion have been successful. Recently Weaver, et al., (Refs 7,8) have reported gain in a copper iodide system but no laser oscillation. Therefore, of all of the high-speed flow approaches, chemical generation of the copper vapor appears to offer the greatest potential of achieving an overall efficiency of 10 percent.

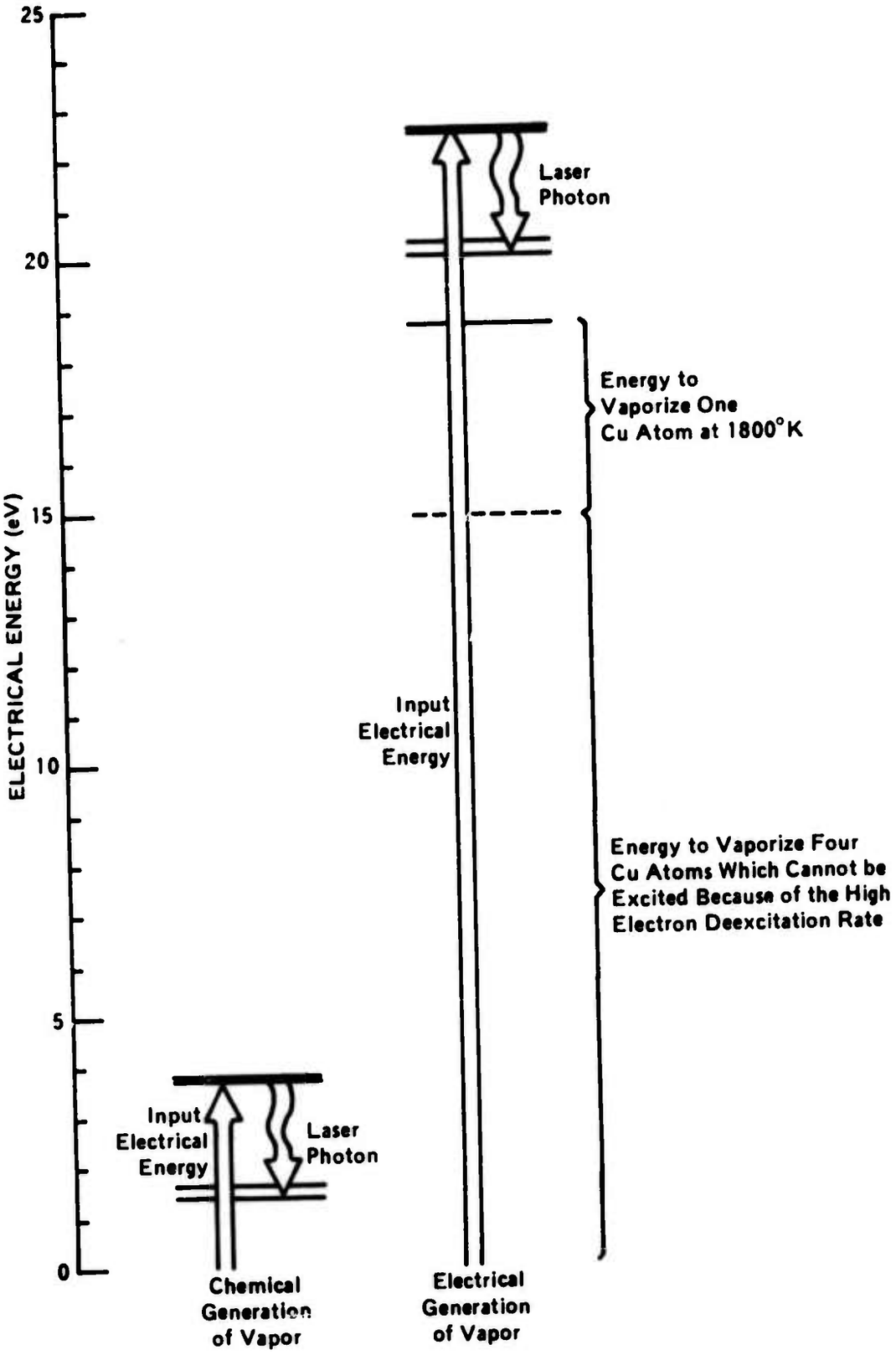

Figure II-8. Comparison of Chemical and Electrical Generation of Copper Vapor in Flowing CVL Systems.

4. COMPARISON OF PREVIOUS CVL RESULTS

The first copper vapor laser was constructed by Walter, et al., (Refs 4,9) in 1965. It had a hot zone 1 cm in diameter X 80 cm long and produced a peak power output of 2 kW with a pulse half width of 20 nsec. The second CVL (Refs 1,2) was constructed with the tube diameter scaled up by a factor of 5 to 5 cm. The peak power produced was 40 to 50 kW which suggests that up to 5 cm diameter the peak power scales as the cross sectional area of the tube. The energy conversion efficiency was 1.2 percent – that is, the energy of a laser pulse divided by 1/2 CV^2.

A static CVL apparatus is schematically shown in Figure II-9. Ceramic aluminum oxide tubes are used to contain the copper vapor because of the high temperature involved. Laser action begins about 1300°C where the equilibrium copper vapor pressure is 10^{-2} torr. The output power continues to increase up to 1600°C at least, where the equilibrium copper vapor pressure is 1 torr. Copper is placed in the apparatus by distributing metallic copper in several piles inside the inner alumina tube. Only the central segment of the discharge tube is heated to produce the copper vapor. The windows and electrodes at each end remain close to room temperature. High-temperature metal-to-ceramic seals are avoided in this design.

Several torr of a buffer gas, such as helium or argon, are added to confine the metal vapor by lengthening the diffusion time of the metallic vapor from the central hot zone. The buffer gas also carries the discharge from the electrodes to the region of the copper vapor. Usually the apparatus is operated in a flushing mode so that outgas products can be removed. Buffer gas is admitted and evacuated at each end of the tube, however, the flow rates are adjusted so there is no net flow from one end to the other. Gases which enter the discharge tube because of outgassing or because of the increased porosity of the tube at high temperatures, diffuse to the end regions where they are flushed out. The electrical excitation is provided by a thyratron which acts as a fast switch and suddenly applies a charged capacitor longitudinally, breaking down the gas between the electrodes at each end of the tube.

In the improved copper vapor laser which is shown in Figure II-9, a graphite heating element has replaced the earlier platinum-rhodium heating element and a hydrogen thyratron replaced the original air spark gap. The hot zone of the graphite furnace is 10 to 15 cm long. The tube diameter can be varied from 1.5 to 4.4 cm by means of a nesting set of alumina liners. Four tube diameters – 1.5, 2.4, 3.2 and 4.4 cm – have been tested. An average power output in excess of 1 watt has been obtained from each of these tubes (Ref 10). The volume of the active medium was only 12 cm^3 for the smallest tube diameter. This corresponds to an average power generation density of 0.1 W/cm^3 which compares favorably with other nonflowing high-power lasers and indicates the attractiveness of the copper vapor laser.

The heater power required to bring tubes of this size to operating temperatures can be 1 to 2 kW. If this power were supplied from wasted discharge energy, then 10 to 20 watts of average power could be produced assuming that the energy conversion efficiency remained at 1 percent. An active volume of 100-200 cm^3 would be required if the 0.1 W/cm^3 average power generation density can be maintained. Petrash's (Refs 11,12) group at Lebedev Institute have recently demonstrated such a self-heated copper vapor laser and generated 15 W with a total efficiency of 1 percent.

Asmus and Moncur (Ref 13) of Gulf General Atomic (GGA) in 1968 were the first to apply a high-speed flow to the copper vapor laser. They used an exploding wire generator shown in Figure II-10 to produce the flowing

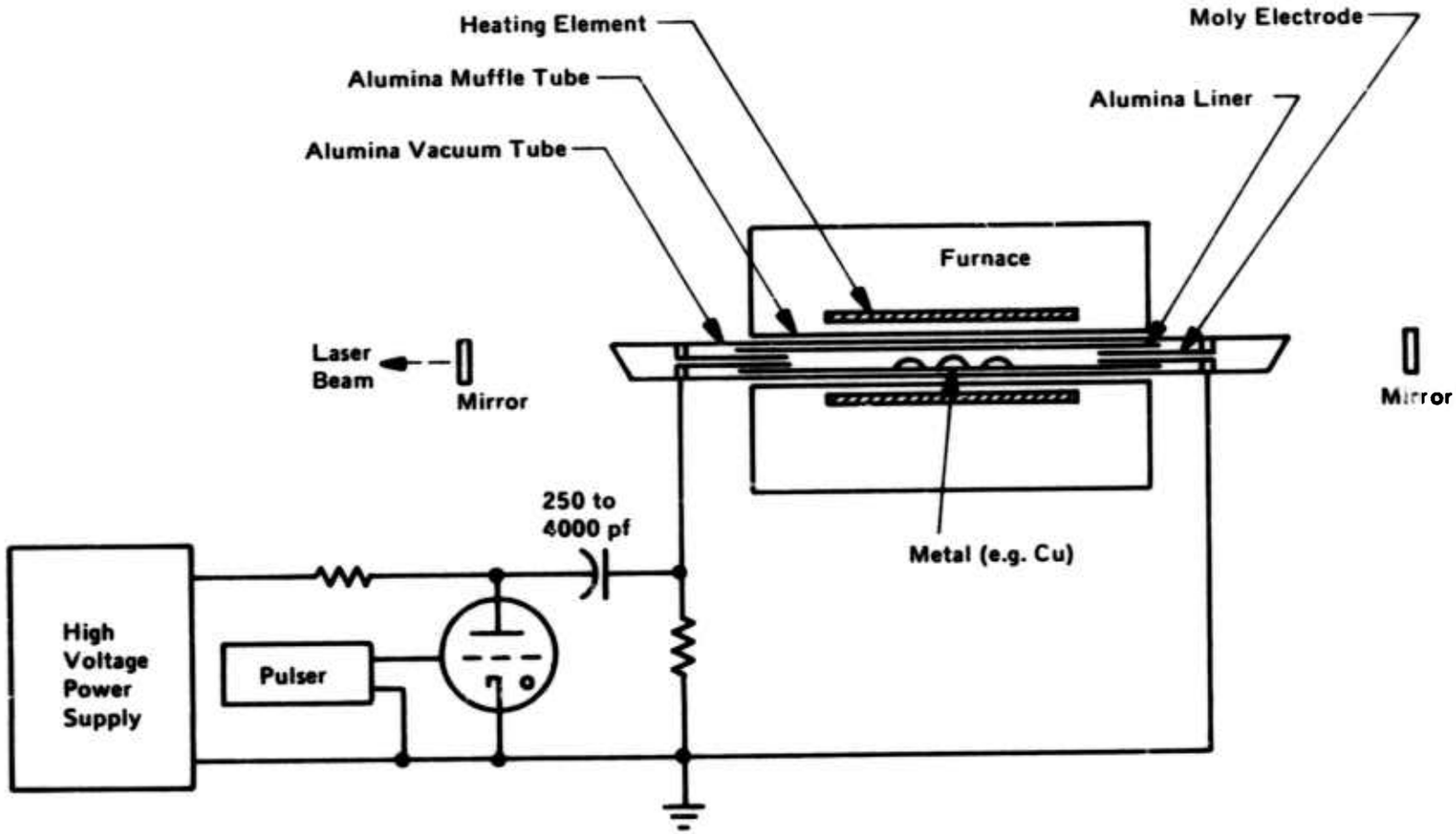

Figure II-9. Static Copper Vapor Laser Apparatus.

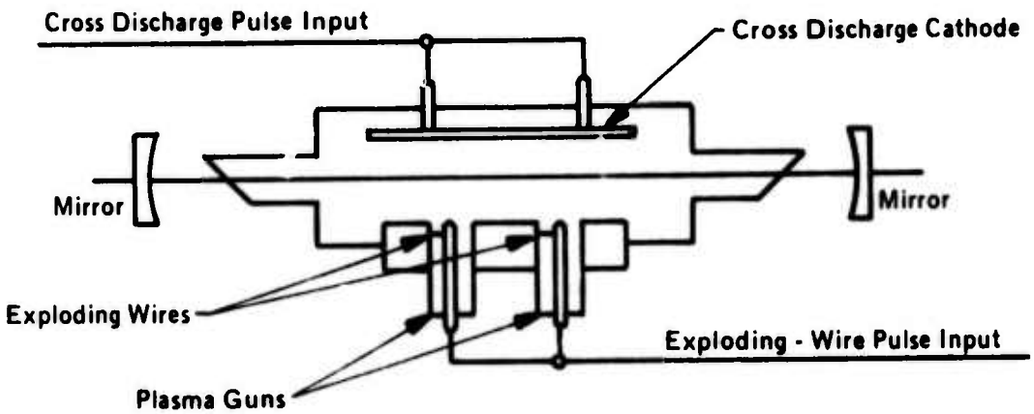

Figure II-10. Exploding - Wire Copper Vapor Laser.

copper vapor. Approximately 100 joules (J) was delivered to each plasma gun to explode 12 m-microns (μ) diameter copper wires. Several microseconds later 20 kV was applied across the laser channel to produce the population inversion. The width of a laser pulse increased from 15 to 65 nsec as the copper wire size was changed to increase the plasma velocity. Similar changes in the laser pulse width were observed at PIB as the copper density is lowered from 5×10^{15} cm^{-3} at our normal operating conditions to 10^{14} cm^{-3} at the laser threshold. Hence, an observed change in the pulse width cannot be unambiguously attributed to the increase in plasma velocity until it is established that the copper density has not changed. Asmus and Moncur measured a peak power of only 30 W which suggests that their conditions were just above the threshold for laser action. The output pulse was 2 μJ, while the input pulse energy was 1200 J. (Up to 12 plasma guns were used in parallel.) The total efficiency was 10^{-9}.

In 1970 Leonard (Ref 14) at AVCO used a flow of heated helium gas to transport evaporating copper atoms into the laser cavity. The flow rate was subsonic, 1350 cm/sec. A peak power of 13 kW was obtained from a 20 cm^3 volume. The pulse energy generation density was 8 μJ/cm^3 which represents a factor of 16 improvement over the first static laser systems. Since 19 kW of heater power was required, the energy conversion efficiency was $< 7 \times 10^{-4}$. The laser would have to operate at 10 kHz to attain a 7×10^{-4} energy conversion efficiency.

Three new forms of flowing copper vapor lasers have recently been reported. Russell, Nerheim, and Pivirotto (Ref 15) at Jet Propulsion Laboratories (JPL) have developed a copper vapor laser, shown in Figure II-11, in which the flow rate was supersonic (Mach number 2.5). An argon-helium arc heater supplied the energy to vaporize powdered copper. The argon-helium-copper vapor mixture was expanded through a supersonic nozzle and then excited in a cross-field discharge. The 1.4 kW peak power and 2.5 μJ/cm^3 energy density and the 3×10^{-5} energy conversion efficiency measured are very low compared with the prior systems probably because of low copper densities.

Karras, et al., (Ref 16) at General Electric (GE) have developed a copper vapor generator which utilizes supersonic expansion from a liquid copper surface through a set of nozzles. The input power was supplied by passing an electrical current through a thin liquid copper layer (0.005 inch thickk $\times$ 1 cm wide) sandwiched between a carbide layer on the top and a graphite film on the bottom. Copper wets the carbide (a mixture of tantalum and tungsten carbide) and is drawn into the evaporating region. Copper does not wet the graphite which has an array of holes that function as the nozzles. Because of the small surface area which is heated, only 2 kW of electrical heater power was required to generate copper atom densities of 4×10^{14} cm^{-3}. This electrical input power is considerably less than that required for prior flowing systems (GGA, AVCO, and JPL). However, thus far, CVL operation has been obtained only with a buffer gas in the system.

The presence of a buffer gas diminishes the copper flow velocity, spreads the copper vapor jet by diffusion and lowers the copper density. Output powers have been very low; 72 W peak and 0.3 mW average. This partially reflects the small active volume, but is largely a result of the low copper densities and the difficulties in obtaining and operating discharges in higher copper densities. The figures which were reported (Ref 16) were experimental values multiplied by 33.3 because the transmission of the output reflector was 3 percent. A more realistic estimate on the maximum power output, that could have been obtained in their system with optimum mirror transparency is about 5 times the experimentally measured quantity, based on the following logic. The power output at optimum coupling is proportional to T/(T + L) not to T where T is the fractional output coupling and L is the sum of the dissipative losses within the optical cavity (Ref 17). Karras, et al., (Ref 16) reported that 3.3 times more power output was obtained with 10 percent fractional output coupling but only 5 times more with 50 percent

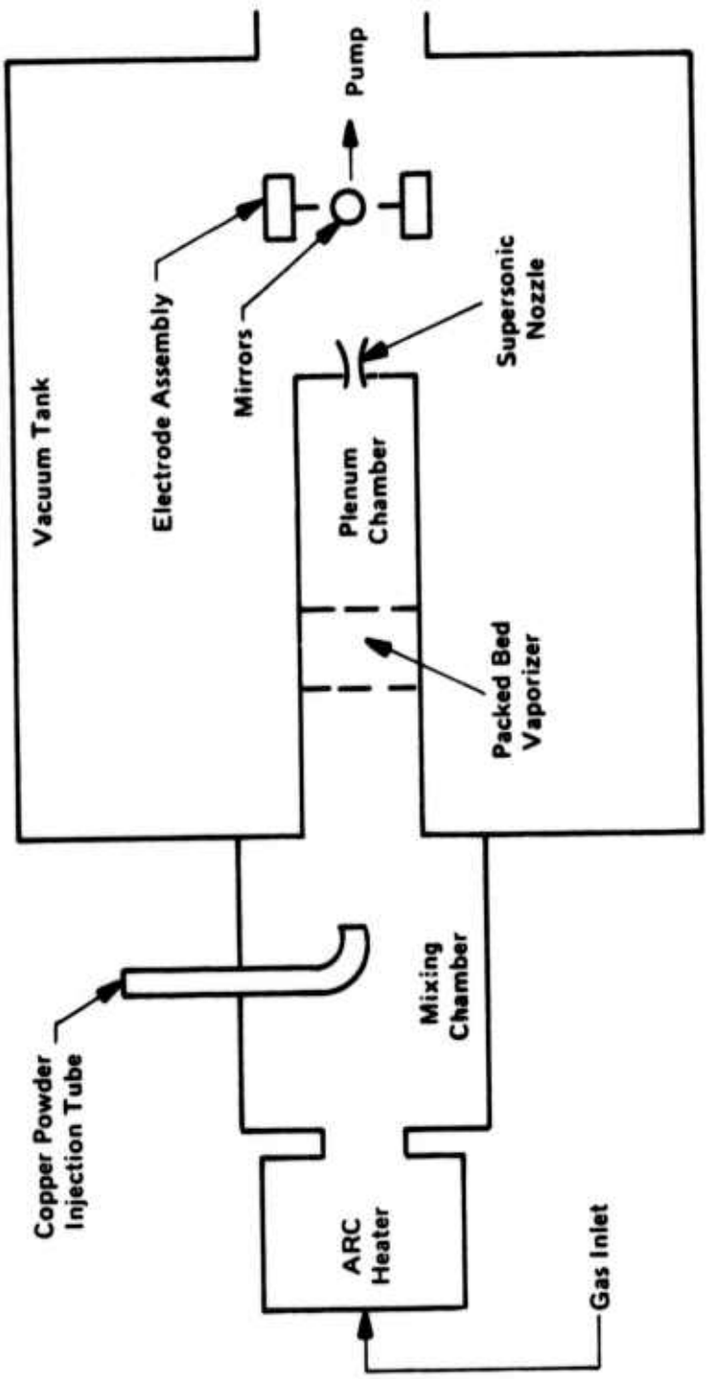

Figure II-11. Supersonic-Flowing Copper Vapor Laser.

fractional output coupling. This indicates that cavity losses were 10 to 15 percent, and justifies an extrapolation only to 5 times the measured values. In Table II-1 the measured values are given with the extrapolated values for optimum coupling (5 times experimental) given in parentheses. At PIB observations have been made which show little difference in the power output with a 61 percent or a 96 percent transmitting reflector, indicating that the power output does not appear to be a sharply peaked function of the output coupling. The extrapolated values of Karras (Ref 16) at GE are comparable to the earlier results of Leonard (Ref 14) at AVCO, but are not as high as the static laser results.

Ferrar (Ref 18) at United Aircraft has developed a CVL with a closed-cycle transverse vapor flow. Copper atoms evaporate from a boiler, flow at thermal velocities across the transverse discharge and laser channel to a condensing surface. Gravity then returns the liquid condensate to the boiler. Only approximate numbers have been reported. As indicated in Table II-1, these results are similar to the measured GE results and somewhat lower than the other flowing CVL results.

A summary of the demonstrated copper vapor laser system is given in Table II-1. A steady improvement in the significant parameters is apparent. The maximum pulse energy generation density is 25 $\mu J/cm^3$. The maximum average power generation density is 0.1 W/cm^3. The maximum energy conversion and total efficiencies are 1 percent. These values have all been obtained only in static systems thus far.

Table II-1. Demonstrated Copper Vapor Laser Systems.

	1966 TRG/PIB[4,9]	1967 TRG/PIB[1,2]	1968 GCA[13]	1970 AVCO[14]	1971 PIB[10]	1972 LEBEDEV[11]	1972 JPL[15]	1973 GE[16]	1973 UA[18]
Hot Zone - Gain Region									
Length, cm	80	80	–	1.3	10	70	20	4	2-3
Diameter, cm	1	5	1.2	4.4	1.2	1.5	2	0.64	1-2
Volume, cm^3	60	1600	–	20	12	125	63	1.3	~2
Cu Density, cm^{-3}	$2x10^{15}$	$2x10^{15}$	–	$5x10^{15}$	$5x10^{15}$	$2x10^{15}$	$<3.5x10^{14}$	$<4x10^{14}$	–
Flow velocity, cm/sec	0	0	–	1350	0	0	$11x10^4$	$<6x10^4$	$8x10^4$
Electrical									
Capacitance, nf	1.8	1.8	–	1.8	1.8	0.57	100	2.5	0.5
Voltage, kV	7.7	7.7	20	18	15	18	10	3	20
Laser Pulse									
Width - FWHM. nsec	20	16	65	12	20	5	120	30	25
PRF, kHz	0.66	1.0	0.001	0.001	4	18	0.001	3	10(50)
Peak Output Power, kW	2	40	0.03	13	15	170	1.3	0.072 (0.36)	~0.12
Generation density, kW/cm^3	0.03	0.03	–	0.65	1.3	1.4	0.02	0.055(0.28)	0.06
Pulse Energy									
Generation density, $\mu J/cm^3$	0.5	0.4	–	8	25	6.8	2.5	1.66(8.3)	~1.5
Average Power, W	0.02	0.5	–	–	1.2	15	–	0.033(0.15)	0.03(0.15)
Generation density, W/cm^3	0.0003	0.002	–	–	0.1	0.12	–	0.002(0.12)	0.015(0.75)
Input Heater Power, kW	2	5	1200/pulse	19	5	0	40	2	–
Efficiency									
Discharge conversion, percent	0.07	1.2	–	0.05	0.15	1.0	0.003	0.19(0.096)	0.003
Total, percent	0.0001	0.006	10^{-7}	<0.007	0.24	1.0	>0.003	0.0003(0.0016)	–

Numbers in parentheses are extrapolated values.

SECTION III

EFFECT OF ADDITIVE GASES ON CVL PERFORMANCE

1. INTRODUCTION

Crucial to the success of chemical generation of flowing copper vapor is the absence of undesirable species. Knowledge of the effects of various additive or carrier gases on the performance of the CVL is required to choose intelligently among a number of possible fuel ingredients which will generate the energy required to vaporize the copper and at the same time produce acceptable carrier gases.

In the course of earlier investigations at PIB (Refs 19,20) of additive gases to selectively quench the ^2D metastable lower laser levels, several tank gases including N_2, H_2, O_2 as well as the rare gases He and Ar were added to a CVL. Some of the results are shown in Figure III-1. The static CVL apparatus shown in Figure II-9 was used. The hot zone was 2.2 cm in diameter and 10 to 15 cm long. The laser output was measured for increasing pressures* of various additive gases. The temperatures indicated on the three graphs in Figure III-1 - namely 1330°C, 1425°C and 1560°C - correspond to partial copper pressures of 0.03, 0.1 and 0.6 torr. At the lowest temperature helium was the additive gas which produced the highest output power. Laser oscillation at 1330°C was visually observed with nitrogen or hydrogen at partial pressures of 1 torr; however, the peak powers were less than 2 W which was the minimum detectable power.

As the temperature and therefore the copper density increased, three effects can be noticed in comparing the upper graph in Figure III-1 with the middle and then the lower graphs:

a. Argon becomes the additive gas producing the highest output power as the copper density increases.

b. The optimum additive gas pressure increases as the copper density increases.

c. The relative performance of N_2 and H_2 improves as the copper density increases.

For these experiments the peak discharge current was adjusted at each measurement to be a constant 100 A.

Effects b and c are of particularly great significance to future work since improved performance can only be achieved at higher copper vapor densities. At these conditions, the detrimental effects of diluent gases are expected to be reduced. Also, the higher cavity total pressures will make the difficulty of stably and predictably burning solid fuels less severe.

---

*The pressures indicated in Figure III-1 are 2 to 3 times lower than the pressure in the CVL because the pressure gauge was located close to the vacuum pump. This situation was corrected for subsequent measurements in Figures III-2 through III-4 for which the pressure monitoring location was the input to the CVL gain tube.

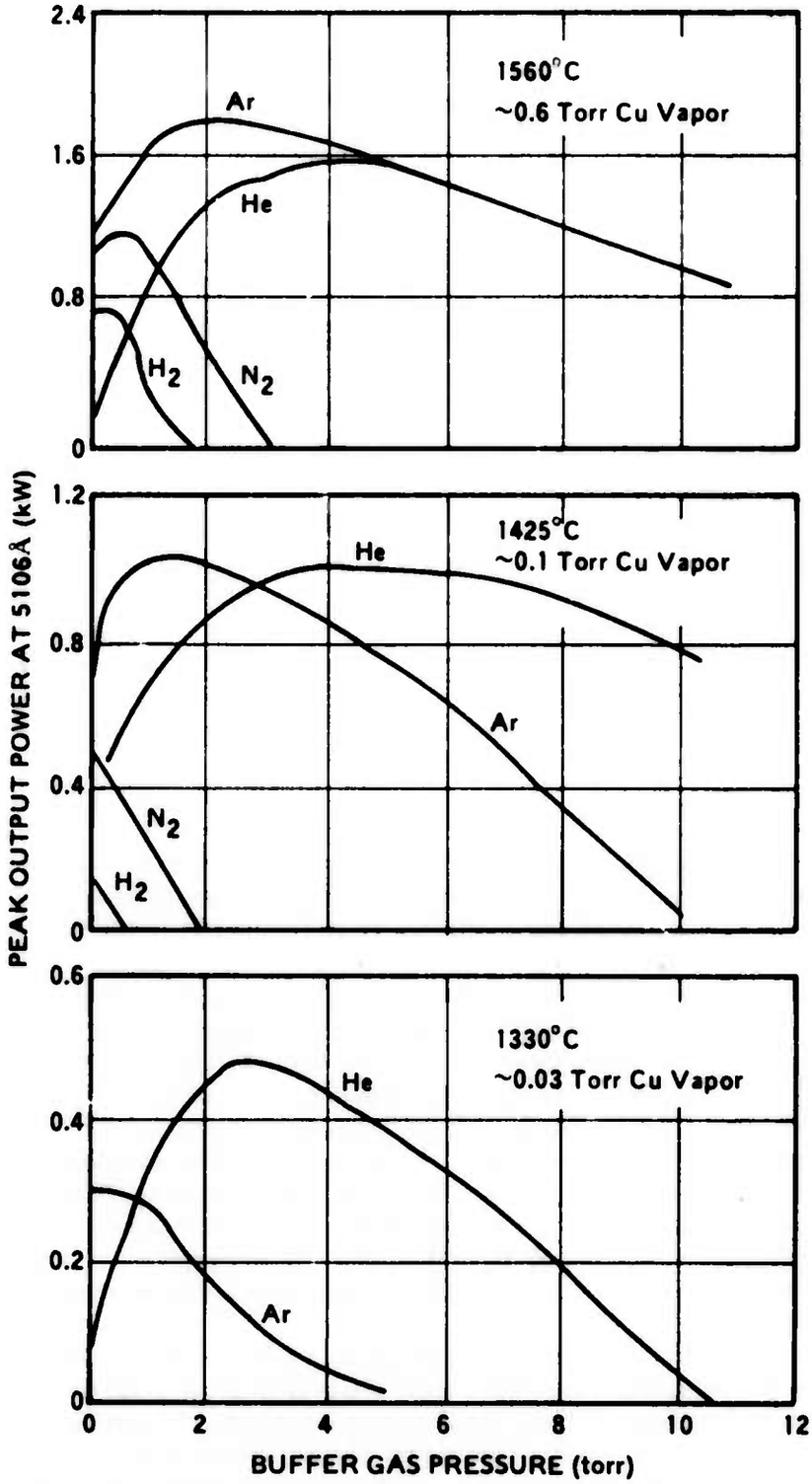

Figure III-1. Peak Output Powar of tha Copper Vapor Laser as a Function of the Prassure of Savaral Additiva Gases.

The effect of oxygen as an additive gas was dramatic and clearly detrimental to the CVL performance. Upon introduction of oxygen, laser action quickly ceased. Copper oxide was formed. The convex meniscuses of the molten copper piles disappeared, and the copper oxide formed a solid solution with the aluminum oxide containing tube.

The static CVL (Figure II-9) was modified to allow controlled introduction of individual gases or of combinations of up to five different gases (N_2, CO_2, CO, H_2 and H_2O). The other gases were bubbled through H_2O in a mixing chamber to obtain high enough partial pressures of H_2O.

2. ADDITIVE GAS TEST RESULTS

Of all the gases tested thus far, argon gives the best results and yields the highest output powers. Figure III-2 shows the dependence of the average output power of the copper vapor laser on the charging voltage of the capacitor for various additive gases. The threshold voltage for laser action is lowest with 7.8 torr of argon than it is for a similar pressure of any of the other gases. As the charging voltage is increased, the threshold voltages with N_2, CO, and CO_2 are reached and then finally H_2 and H_2O. At voltages above the threshold, the ordering of the additive gases in terms of maximum average power laser output remains the same except for CO_2 which surpasses CO and N_2 at higher capacitor charging voltages. The rate of increase of the average power output with charging voltage (given by the slope of the curves) is larger for argon than it is for any of the other gases. Furthermore, at the highest voltages tested there appears to be a flattening or saturation for all of the gases except argon.

The upper curve in Figure III-2 shows the electrical conversion efficiency with argon as the additive gas. The input power has been taken as $1/2\ CV^2$ times the pulse repetition rate. The efficiency peaks at 1.7 percent at a 5 kV charging voltage. Although the output power continues to increase, perhaps linearly with voltage, the input energy increases quadratically, so that the electrical conversion efficiency drops as shown. The 1.7 percent energy conversion efficiency is believed to be the highest efficiency reported for the CVL or indeed for any visible gas laser.

The charging voltage was then set at 6 kV since the efficiency peaks in this vicinity, and the effect of varying the pressure of the various additive gases was explored. This is shown in Figure III-3 at somewhat lower copper density than in the previous figure. The pressure range over which the laser will operate at 6 kV is much more restricted for all the other gases than it is for argon. The other gases are operating closer to their voltage threshold. Only the argon curve, however, has a positive slope at low additive gas pressures. Up to ~8 torr an increase in the pressure of argon improves the average power output. This may be due to either an optimization of the discharge conditions and electron temperature for excitation of the copper resonance levels or to a decrease in the diffusion length which effectively raises the density of copper atoms in the hot zone of the discharge tube. In either case such an increase is not observed for N_2, CO_2, CO, H_2 or H_2O. Each of these curves has a negative slope, even at the lowest pressures. Each behaves as if the minimum amount of these gases would yield the maximum laser output.

The sequence in which the various gases were tested is indicated in the legend on Figures III-2 through III-4. The method of data taking was to add a high pressure of each gas ($\gtrsim$ 20 torr) and then reduce the pressure by 0.5-2 torr increments to approximately 2 torr. The pressure was measured at room temperature just outside the furnace. Additional data points were taken by increasing the additive gas pressure back to 20 torr. The difference between the data points taken while decreasing or increasing the additive gas pressure is not significant as can be seen on the individual curves in Figure III-1. Argon was repeated as the last as well as the first additive gas tested. Again there is only a minor difference between these two sets of data points.

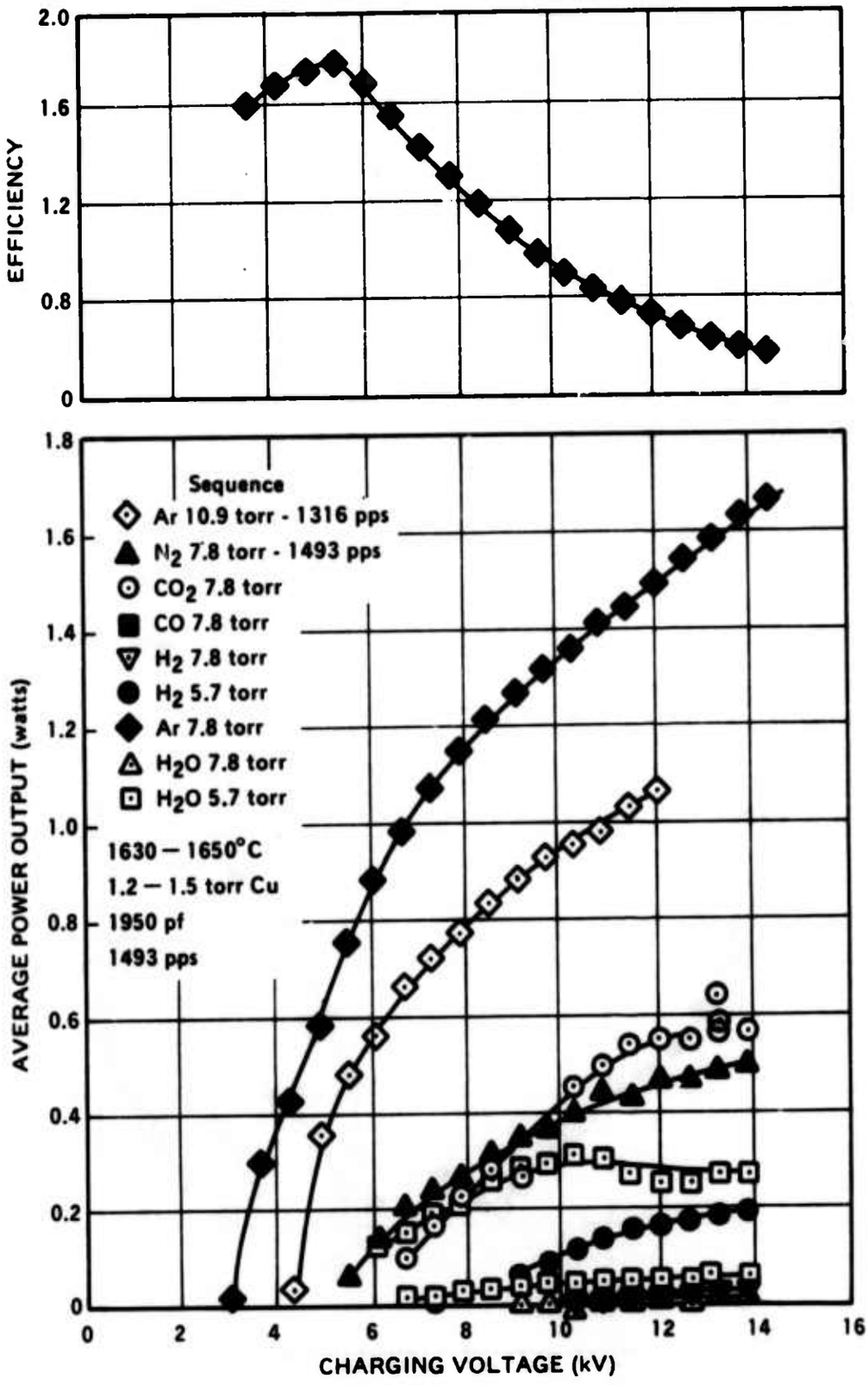

Figure III-2. Dependence of CVL Average Power on Changing Voltage for Various Additive Gases.

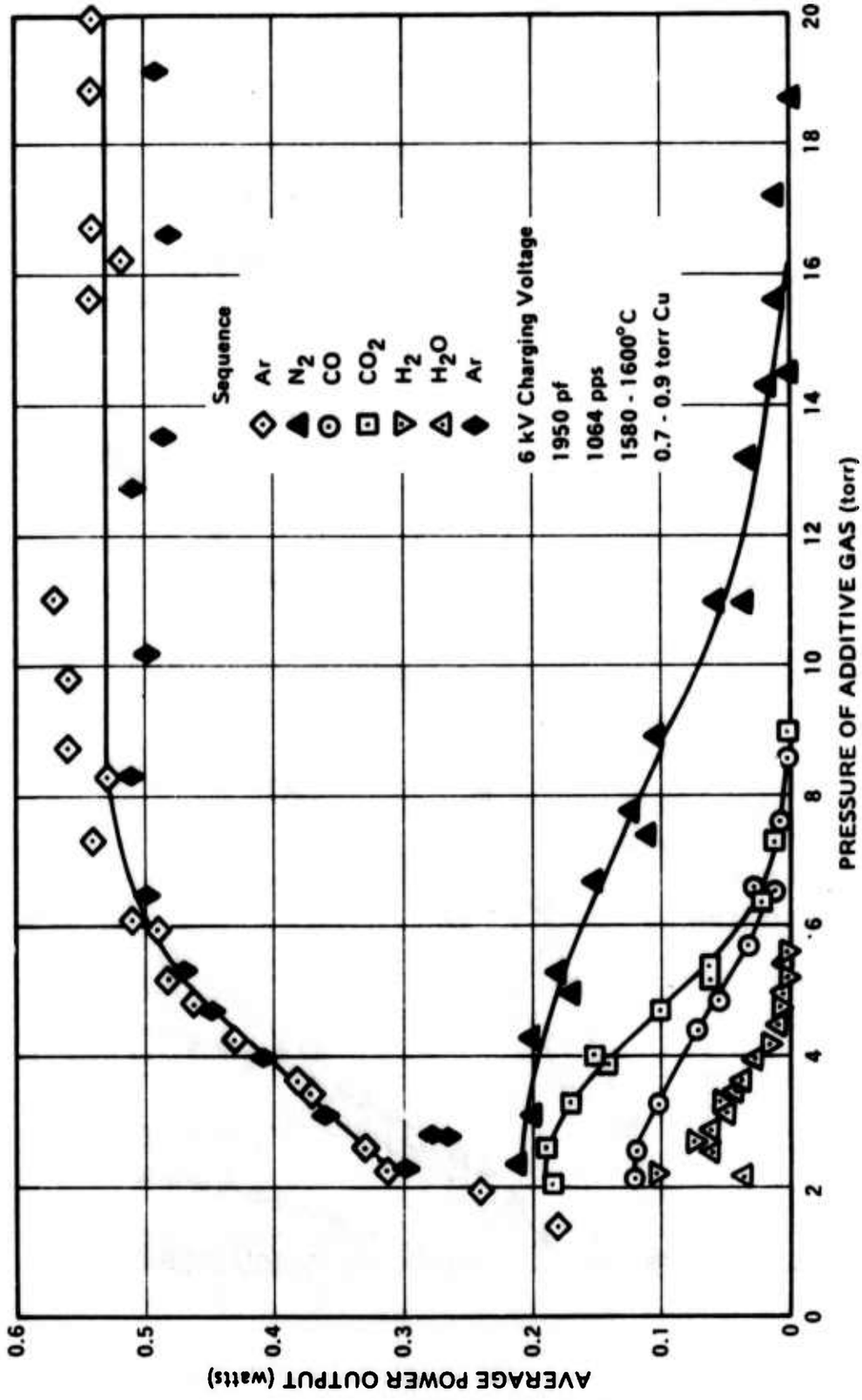

Figure III-3. Effect of Pressure of Additive Gases on CVL Power Output.

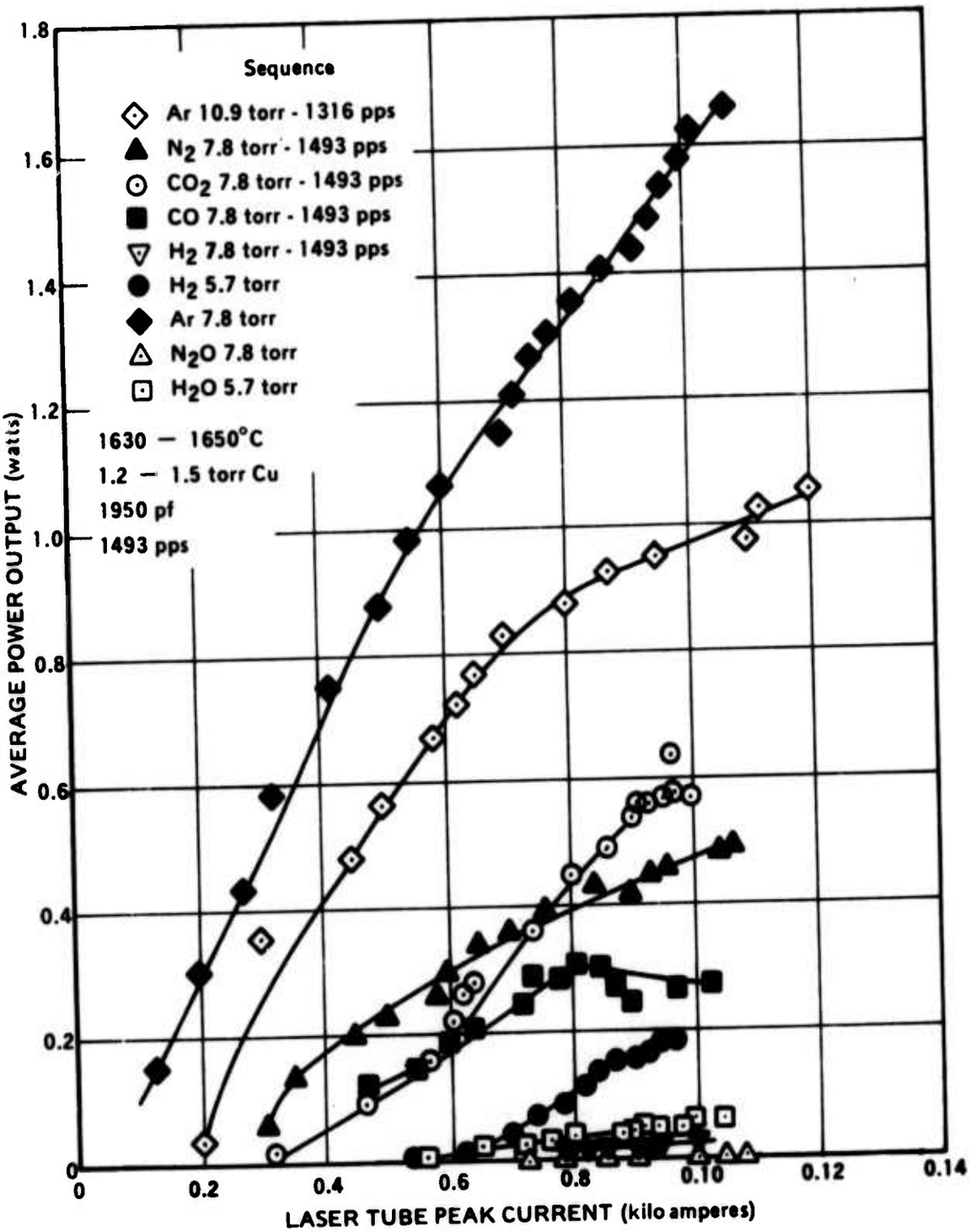

Figure III-4. Dependence of Copper Vapor Laser Average Power Output on Peak Excitation Current for Various Additive Gases.

Figure III-4 shows the dependence of the copper vapor laser output power on the peak excitation current for the various additive gases. The ordering and qualitative results are similar to those already discussed for Figures III-2 and III-3. It is encouraging to note that with argon as the additive gas, no saturation in the average output power was observed up to 1 kA of peak current through the 3.8-cm-diameter tube.

The general conclusion is that argon is the best additive gas. The other gases tested degrade the output power. The severity of the degradation increases in the following order N_2, CO_2, CO, H_2 and H_2O. With argon as the additive gas, an average output power of 1.7 W has been measured. The electrical conversion efficiency maximized at 1.7 percent at one-third of this power output.

The ordering of the gases tested, Ar, N_2, CO_2, and H_2O, is not in agreement with the quenching cross sections (Ref 21) that have been measured for the upper laser level which are: $Ar \rightarrow 0.8$, $N_2 \rightarrow 19$, $H_2 \rightarrow 23$ and $CO_2 \rightarrow 36 \times 10^{-16}$ cm^2. Therefore quenching of the upper laser level alone cannot account for our results. On the basis of quenching alone, we would have expected the addition of CO_2 to be more severe than that of H_2. The additive gases must also affect the electron temperature and discharge conditions thereby degrading the excitation process.

A conventional double-based propellant such as 60 percent BTTN + 40 percent NC would be expected to produce the following mixture of combustion gas products: 42 percent CO, 19 percent H_2O, 16 percent N_2, 12 percent H_2 and 10 percent CO_2 (see Section IV-2). Because of the detrimental effect of the presence of H_2 and H_2O on the performance of the CVL as described in Section III-2 and Figures III-2 through III-4, hydrogen-free propellant systems were considered as an alternative to the conventional double-base systems. As described in Section IV-2, a hydrogen-free propellant system could be produced by utilizing alkali metal salts, particularly the perchlorates, for the oxidizer. Such systems, however would produce alkali halide vapors, such as KCl or LiCl as gaseous combustion products. To evaluate these systems, it was necessary first to test the effect of alkali halide vapors on CVL performance.

The vapor pressures of alkali halides are very low at room temperature ($\ll 10^{-11}$ torr). Temperatures of ~900°C are required to obtain ~10 torr of vapor pressure. As indicated in Figure III-5, the furnace temperature profile is very steep in the vicinity of 900°C when the center of the furnace has been set to give a copper vapor of 1 torr (1610°C). It would be difficult to control the temperature and hence the vapor pressure of several grams of an alkali halide inserted at the expected location for a temperature ~900°C. What is required to test the effect of vapors of alkali halides, on the CVL performance is a furnace temperature profile with two flat zones; one at ~1600°C for the copper and a second at ~900°C for the alkali halide. It was decided to use heat pipes within the furnace to provide the desired temperature profile which would permit the evaluation of the effect of alkali halide vapors as possible gaseous combustion products. It was found that KCl could not be used as an effective working fluid in a heat pipe because it sublimes. LiCl does not sublime, so its effect on laser performance could have been tested by using the heat pipe, if sufficient time and funds had been available. Since they were not, no halide data was gathered and that particular propellant approach was left to future efforts. The development of heat pipes within an operating CVL is described in the next section.

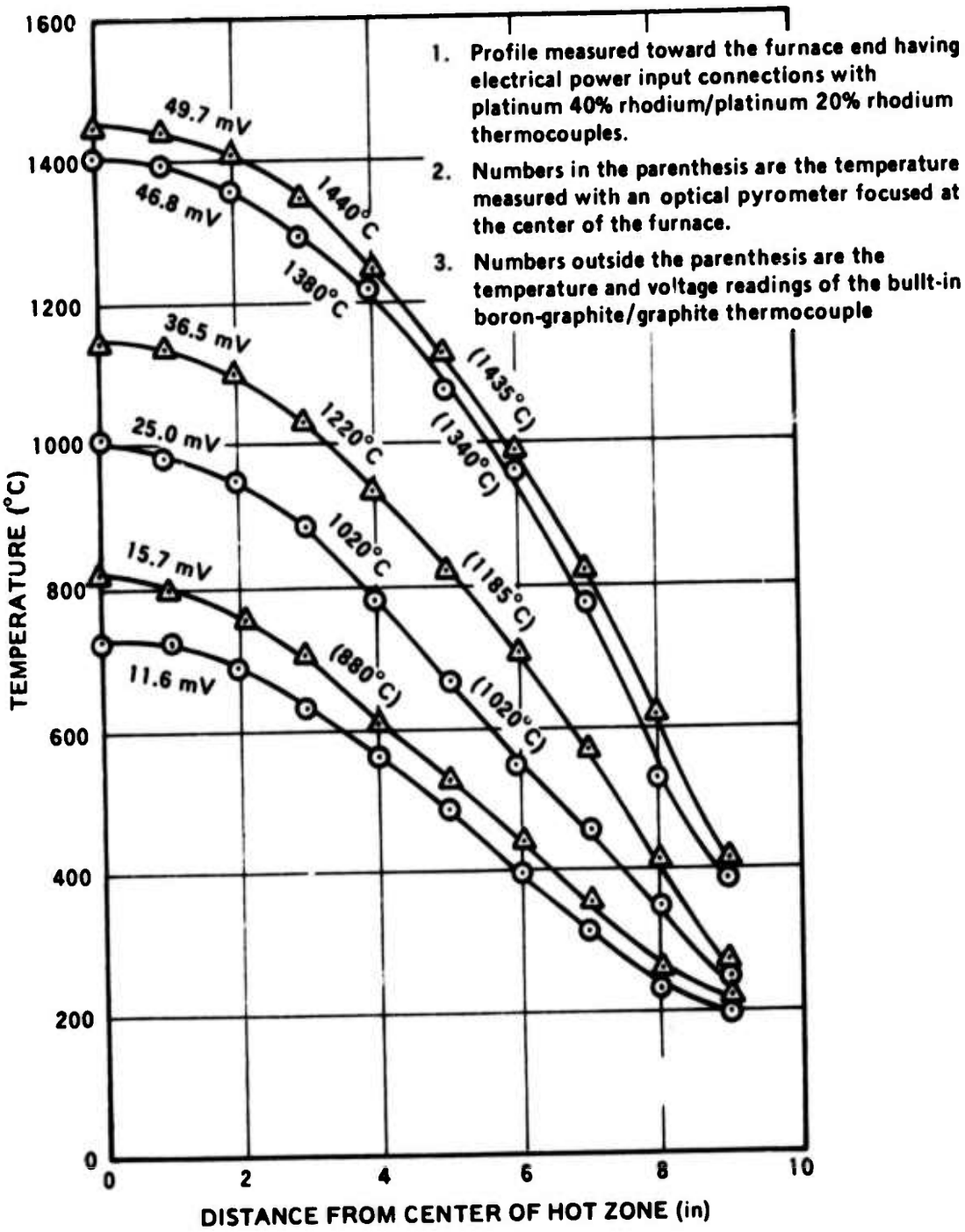

Figure III-5. Temperature Profile of Static CVL Furnace.

3. COPPER VAPOR LASER WITH A HEAT-PIPE DISCHARGE TUBE

Greatly increased thermal conductivity was the characteristics of heat pipes which received the most attention when the first heat pipe was demonstrated by Grover, et al., (Ref 22) in 1964. Subsequently, Vidal and Cooper (Ref 23) used the uniform temperature resulting from the accelerated thermal transport cycle to create a "heat-pipe oven" which could generate homogeneous, pure metal vapors with well defined pressure, temperature and optical path length. The heat pipe itself usually consists of a number of layers of a fine mesh which would be wetted by the liquid phase of the vapor of interest. The mesh acts like a wick to draw the liquid back by capillary action into the hot zone of the furnace. The heat-pipe oven was an important development for quantitative spectroscopy. Sorokin and Lankard, (Ref 24) for example, used it to investigate laser action in the vapors of alkali metals irradiated by beams from various giant pulse lasers. We wanted to carry out a similar investigation with the vapor of alkali halides – except that we also had to be able to create an electrical discharge in the vapor. The ability to impose a discharge is a severe additional requirement because the heat pipe can provide a good electrical short circuit for the discharge.

One solution to this problem was recently proposed by Dr. R.T. Hodgson (Ref 25) of IBM; namely, the use of separate heat pipes at each end of a vapor laser to confine and recirculate the material vaporized. In the case of metal vapors, Hodgson suggested that the heat pipes can also serve as electrodes for a discharge between the separated heat pipes. Sorokin and Lankard (Ref 26) have used Hodgson's suggestion to construct an alkali metal discharge tube with heat-pipe electrodes.

There are two ways in which a separated heat-pipe configuration could aid copper vapor laser research:

a. As a means of introducing a known pressure of an alkali halide to determine its effect on copper vapor laser performance, as already suggested at the end of Section III-2.

b. For the copper vapor laser itself as a means of confining the copper vapor, preventing its loss by diffusion, and perhaps also serving as the electrodes.

The adaptation of the PIB static metal-vapor laser facility to a separated heat-pipe configuration is shown in Figure III-6. This novel geometry has several important advantages. First, extended operating times and therefore higher copper pressures can be achieved because the liquid copper will recirculate from the outer regions of the tube to the central region. This results from the capillary action of the mesh which acts as a wick. Second, the purely diluent gas portions of the discharge present now can be eliminated because the electrodes will extend into the region where copper is present in the vapor. This should result in an improvement in efficiency. Third, purely copper vapor discharges may be compared with copper-plus-diluent-gas discharges by setting the diluent gas pressure P_0 to be equal to or greater than the copper vapor pressure P_1. Finally, heat-pipe electrodes permit an extension of the coaxial geometry both in a transverse as well as a longitudinal configuration. This should result in an improvement in the risetime of the excitation current pulse.

The PIB metal vapor laser furnace was modified to include separate heat pipes at each end as indicated in Figure III-6. This heat-pipe copper vapor laser was expected to operate in the following way: The tube would be filled with a buffer gas such as argon to the same pressure P_0 as that desired of the metal vapor. Then the temperature of the furnace would be increased until T_1 is the appropriate temperature to generate a vapor pressure of the metal, P_1, which is equal to the buffer gas pressure, P_0. The heat pipe at each end would then operate as a

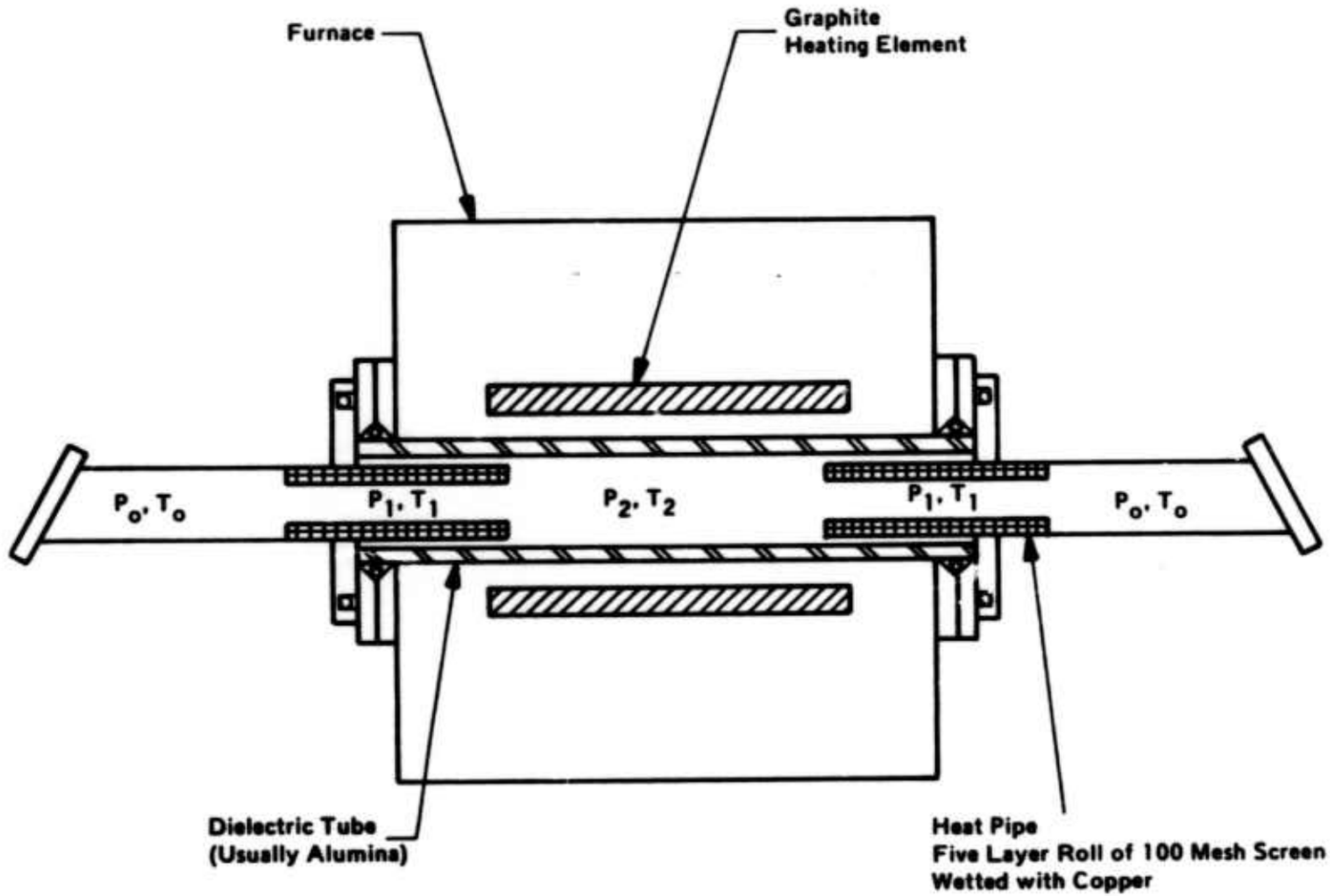

Figure III-6. Heat - Pipe Copper Vapor Laser.

diffusion pump and pump the buffer gas and any impurities outside of the hot zone within the furnace. The gases will then have separated so that the P_0 region consists entirely of buffer gas while the P_1 and P_2 regions consist entirely of the metal vapor. In this manner discharges in pure metallic vapors can be explored. A buffer gas can still be admitted into the hot zone by increasing the buffer gas pressure P_0.

Several wick materials were tested for the two heat-pipe applications mentioned above – copper as the working fluid or KCl as the working fluid. For copper, the wick material should have a melting point (MP) above 1900°C and be readily wet by copper. Molybdenum (MP 2610°C) and tungsten (MP 3410°C) were tested. Copper promptly wet molybdenum mesh (100 mesh, 2-mil wire) under a few torr of argon. When hydrogen was substituted for argon, copper also wet tungsten mesh (100 X 106 mesh, 2-mil wire). At the elevated temperatures required to melt copper (MP 1083°C), hydrogen removes the surface oxidation enabling a more intimate contact between working fluid and the wick material. Hydrogen was not sufficient for tungsten. The successful technique involved an initial plating of Cu on the tungsten immediately after a chemical cleaning. Successful copper heat pipes were constructed with both wick materials, molybdenum and tungsten. Tungsten mesh has an economic advantage, being half as expensive as molybdenum.

For KCl (MP 790°C) as the working fluid, meshes of copper (MP 1083°C), nickel (MP 1452°C) and 304 stainless steel (MP 1420°C) were tested for suitability as the wick material. T_1 temperatures of 820 to 1020°C would be required to generate P_1 = 1 to 20 torr of KCl vapor pressure. A crucible containing KCl was heated in air until the KCl melted. Samples of copper, nickel and 304 stainless steel mesh were inserted into the liquid KCl. The KCl wet each of the meshes. Stainless steel (100 mesh, 4-mil wire) was selected as the wick material. All attempts to produce heat pipes using KCl as the working fluid were unsuccessful, however. The KCl deposited all over the cooler regions of the apparatus. Further investigation revealed that KCl sublimes and therefore would not serve as an effective working fluid in a heat pipe. Therefore a controlled measurement of KCl vapor on CVL performance could not be carried out as originally intended through the use of heat pipes. LiCl does not sublime; so it may be possible to use heat pipes to test the effect of this alkali halide on CVL performance. Unfortunately, due to shortness of available time, the effect of the presence of LiCl vapor in the discharge on CV laser performance could not be tested.

Tests of the copper heat pipe were more successful. A heat-pipe CVL was assembled as shown in Figure III-6. Heat pipes at each end were constructed from molybdenum mesh and also served as the electrodes. The furnace was taken up to 1600°C. The discharge appeared very uniform. The output of the laser was the one watt which is usually obtained at this temperature. The average power maximized at a higher pulse repetition rate (4 kHz instead of the usual 2 kHz) and a higher argon pressure (14 torr instead of 7 torr) than previously. The most serious difficulty was a buckling of the electrodes which resulted in a partial obscuration of the output beam. The buckling may have been due to a mechanical constraint on the mesh. A subsequent design did produce less buckling but was not completely free of this effect.

Three additive gases were examined; Ar, N_2 and H_2. The effect on the CVL output power of 1 to 20 torr of each additive gas differs from previous results (Figure III-3) in several respects. The Ar curve increases to a maximum at much higher pressures and is more sharply peaked than the curve shown in Figure III-3. The effect of the addition of N_2 is more severe and the double-peaked character of the curve is quite peculiar. There are a number of possibilities to be considered to account for the different behavior:

a. The heat-pipe electrodes may lower the temperature so that the actual Cu temperature and pressure may be lower than indicated by the thermocouple temperature outside the center of the tube.

h. In addition to the Cu placed on the electrodes, Cu was also placed in the center of the tube. The Cu pressure may not have been in equilibrium at the temperature of the electrodes. Higher pressures of Ar may have slowed the Cu diffusion and effectively increased the Cu density.

c. The effect of the presence of grade A boron nitride (BN) which is discussed below.

d. The influence of molybdenum nitride which is said to form above 1500°C.

e. The performance of the CVL and the effects of variables such as gas composition were clearly affected by changing electrode geometry and discharge configuration. The nature and size of these effects on performance must be determined. This area has not been addressed in this effort and must be included in future work.

A similar heat-pipe CVL apparatus was constructed using tungsten mesh heat pipes at each end which also served as electrodes. No excess of Cu was placed in the center. Only ~50 mW average power was obtained from this configuration. The copper containment and electrode functions were then separated by inserting molybdenum wires at each end to serve as the electrodes. Then 0.5 W of output power was obtained. We had been considering the use of heat-pipe transverse electrodes in the flow apparatus (Figure VII-1), however, at this point we decided to use molybdenum wire electrodes and halted further heat-pipe work.

In summary, a heat-pipe CVL was demonstrated with a power output within a factor of 2 of that produced by the static CVL. A greatly extended operating time was demonstrated compared with the tens of hours of operating time from a static CVL. Further work is required to sort out the influence of the several factors mentioned above, but clearly this could be a very practical form for CVL systems with average output powers up to 100 W.

As it was discussed earlier in this Section, experiments verified that higher operating temperatures require higher background pressure for optimizing laser output. It is of great interest to explore operating conditions under which increased background pressure optimizes laser performance since this facilitates the generation of copper vapor from combustion processes. The PIB system was limited by a maximum temperature of approximately 1650°C. Above this temperature the alumina muffle tube began to loose its mechanical strength. At temperatures above 1650°C, additional consideration should be given to the selection of the dielectric tube material. The material must have a high melting point (above 2200°C), a low vapor pressure, a compressive strength above 15 psi, a high electrical resistivity, must reasonably tolerate thermal shock and must not react with copper, the mesh material or with the heating element material (presently graphite but tungsten may be a better choice). There does not appear to be an ideal material so preliminary tests were made of alumina (MP 2050°C but it loses its compressive strength above 1850°C), magnesia (MP 2800°C but poor thermal shock capability and low compressive strength), zirconia (MP 2715°C, poor thermal shock capability and it becomes a conductor at high temperatures), and boron nitride (MP $>$ 2800°C but there is some vapor pressure, BN reacts with carbon, and it is difficult to obtain long tubes). There are the additional possibilities of the use of a combination of materials such as boron nitride inside of an alumina tube. The boron nitride has good compressive strength and could keep the alumina tube from collapsing, and the alumina would shield the boron nitride from reacting with the graphite.

A magnesia and a zirconia tube were tested. The zirconia tube cracked during the initial heatup despite a much slower than usual heatup rate. The very high thermal shock and conductivity at high temperatures appear to

rule out further consideration of zirconia. The magnesia tube was porous. (Dense, vacuum-tight magnesia tubes are not commercially available.) The angle of copper with magnesia is larger than with alumina. Graphite vapor from the heating element did produce some reduction of magnesia to magnesium, posing a safety hazard. Nevertheless, magnesia is a material which warrants further investigation.

We were not able to obtain boron nitride in long enough tubes. Instead sample pieces of grade HP and grade A boron nitride were tested inside alumina tubes at 1380°C. In both cases the CVL operated well, yielding 150 mW of average power under these near-threshold conditions. Grey blisters and fine cracks were noticed on the grade HP material but not on grade A. This is probably due to the stabilizers which are present in the HP material to retard water absorption. After the heat-pipe run at a higher temperature, described above, flakes of a white crystalline material were found in the alumina tube in the vicinity of the grade A BN. The alumina tube appeared etched where contact occurred between BN and alumina. Water vapor can react with BN at a red heat to form boric oxide.

$$3H_2O + 2BN \rightarrow B_2O_3 + 2NH_3$$

The boric oxide may then act as a flux with the alumina to form an aluminum borate glass.

The refractory material with the highest dielectric strength at high temperatures (up to and above 2000°C) is beryllium oxide. BeO also retains its excellent mechanical properties to these temperatures. It has the highest thermal conductivity and resists thermal shocks very well. BeO seems to be the only material beyond 1900°C that can be used as an insulator in a low impedance high temperature coaxial line, which is required to deliver joules of energy in narrow pulses (tens of nanoseconds). However, its dust is toxic. Also at high temperatures (like all other ceramics), it reacts with certain materials, therefore, its incorporation in a high-temperature system requires extreme engineering design care.

SECTION IV

COPPER VAPOR LASER SOLID FUEL GENERATOR

1. INTRODUCTION

A primary objective of the program was the development of a solid propellant system capable of producing desired concentrations of copper vapor as a combustion product. Emphasis was placed on the use of commercially available chemicals and state-of-the-art propellant formulations since the program scope did not permit a more extensive development effort. The propellant formulations considered are comprised of a fuel, oxidizer, and copper metal (or copper compounds). The combustion products consisted of water-gas,* nitrogen and copper vapor. The existing CVL required that the combustion products generated must be delivered to the laser cavity at a temperature of 1800°K and a pressure of less than 10 torr.

These conditions posed several unusual problems for the propellant work. The low flow rates of vapor needed for the laser tests resulted in the need to either burn at cavity conditions or to burn at somewhat higher pressure and expand to cavity conditions. The first was eliminated because it was impossible to burn the propellant at 10 torr. The second alternative still presented the low pressure combustion problem since nozzle throat sizes could not be made too small and the inhomogeneities in the vapor are expected to increase with increasing expansion. The low pressure combustion presents two problems. The first being that the combustion process may not be correctly predicted by thermochemical equilibrium and the second being that low pressure gases provide poor heat transfer to the copper. Finally, there is the problem of heat losses after combustion which tend to further reduce copper concentration. Since these effects are all difficult to predict accurately, it was decided to make the generator and then test for copper vapor density. This was done but the test threshold level failed to identify what later turned out to be a very serious problem in copper density.

Initially a thorough thermochemical screening analysis was conducted for mixtures of copper and selected propellant systems. Calculations were based on adiabatic combustion at various pressure levels, and isentropic expansion to the desired cavity conditions. Several promising candidate propellant systems were selected for further evaluation. These evaluations consisted of laboratory mixing studies, physical properties, combustion properties and safety properties tests. Selected formulations were then processed into test grains for combustion, burning and copper vapor concentration determinations.

Detailed discussion of the development of copper vapor generating systems follows.

2. PROPELLANT SCREENING AND SELECTIONS

Theoretical values of combustion product composition were computed for mixtures of copper and selected propellants. Calculations were based on adiabatic combustion at an assigned pressure, and isentropic expansion to cavity conditions. Nominal cavity conditions used in these calculations were 1800°K and either a cavity pressure of 10 torr or the maximum pressure permitted by Cu saturation, whichever is less. Given below are all compositions of propellants evaluated and the advantages and disadvantages of each in terms of ease of use and applicability for CVL. These compositions are representative of the state of the art of pressed and castable propellants, and all are comprised of commercially available ingredients.

*The term water-gas refers to an equilibrium mixture of $H_2O(g)$, CO_2, CO and H_2.

All of the propellants selected for evaluation are high-energy compositions which yield only gaseous combustion products, and are characterized primarily by high values of flame temperature. The reasons for this selection are: (1) maximization of Cu(g) content in the combustion products and (2) optimization of the combustion pressure. Also versatility in combustion product composition is permitted by judicious selection of propellant ingredients. For (1) the desired mol fraction of Cu(g) in the combustion products, N_{Cu}, is in the range 0.1 to 0.2, and high-energy systems are required to attain these values. For (2), pressures high enough for the propellant to sustain combustion are, of course, necessary and for adiabatic expansion to assigned exhaust (i.e., cavity) conditions it is seen that the required combustion pressure increases with flame temperature (T_f).* Alkali-metal salts (particularly the perchlorates) were evaluated as oxidizers as a method of eliminating hydrogen and water as combustion products. The major alkali-metal combustion product generated by the oxidizer is the chloride, which is gaseous at cavity conditions, and stable relative to Cu(g). Also in this regard, propellant selection was dictated by stoichiometry. In all cases, the compositions stoichiometric to CO were evaluated. Thus, the influence of CO_2 and H_2O on the CVL effect are obviated. Higher-energy compositions for which the ratio CO_2/CO in the combustion products is ~1, which is low enough to prevent the formation of condensed Cu oxides, were also evaluated. For both stoichiometries, a high-energy, low-gas-yield fuel is desired for maximization of T_f and N_{Cu}. The fuel incorporated for theoretical evaluation was tetracyanoethylene (TCE), a stable, readily-available compound having a heat of formation of +150.46 kcal/mol. The use of the compound is particularly valuable in offsetting the inherently low energetics of the CO stoichiometries.

Incremental addition of metallic copper to the compositions as listed below lowers the flame temperature because of the energy required to vaporize the metal. Since condensation of copper is to be avoided, this lowers the maximum permissible cavity pressure (the ratio of the vapor pressure of Cu-0.3765 torr at 1800°K - to the mol fraction of Cu(g) in the combustion products), and therefore lowers the combustion pressure. The yield of Cu(g), expressed as mol fraction, designated N_{Cu}, and the maximum permitted values of combustion pressure (P_c) and cavity pressure (P_s; i.e., the pressure at which the combustion products in the cavity are saturated with Cu) are all parameters of interest to the design of propellants and hardware for CVL systems. Values of these parameters, as a function of copper content in the propellant expressed (on a weight basis) as parts per hundred parts of propellant (php) were determined for all candidate systems. Data derived for the double-base propellant system, type a. is plotted in Figure IV-1. A summary of computed results at $N_{Cu} = 0.1$ for selected propellants is given in Table IV-1. Values of P_s refer to 1800°K, and at other temperatures to 1800°K ± 200°K can be computed (in torr) from the expression

$$P_{s,T} = \frac{760 \exp(-13698/T)}{N_{Cu}}$$

Combustion pressure is not easily recomputed for values $T_c \neq 1800°K$, because P_c varies with T_f significantly, but is approximately

$$P_{c,T} = P_{s,T}(P_c/P_s)\,(T/1800)^4$$

Branches of the curves for combustion pressure marked B refer to values for $P_s = 10$ torr.

*For adiabatic expansion, $Tc/Te = (P_c/P_e)^{\gamma/\gamma-1}$, where T, P, and γ are temperature, pressure, and the ratio of specific heats, and the subscripts c and e refer to combustion and exhaust (i.e., cavity) conditions.

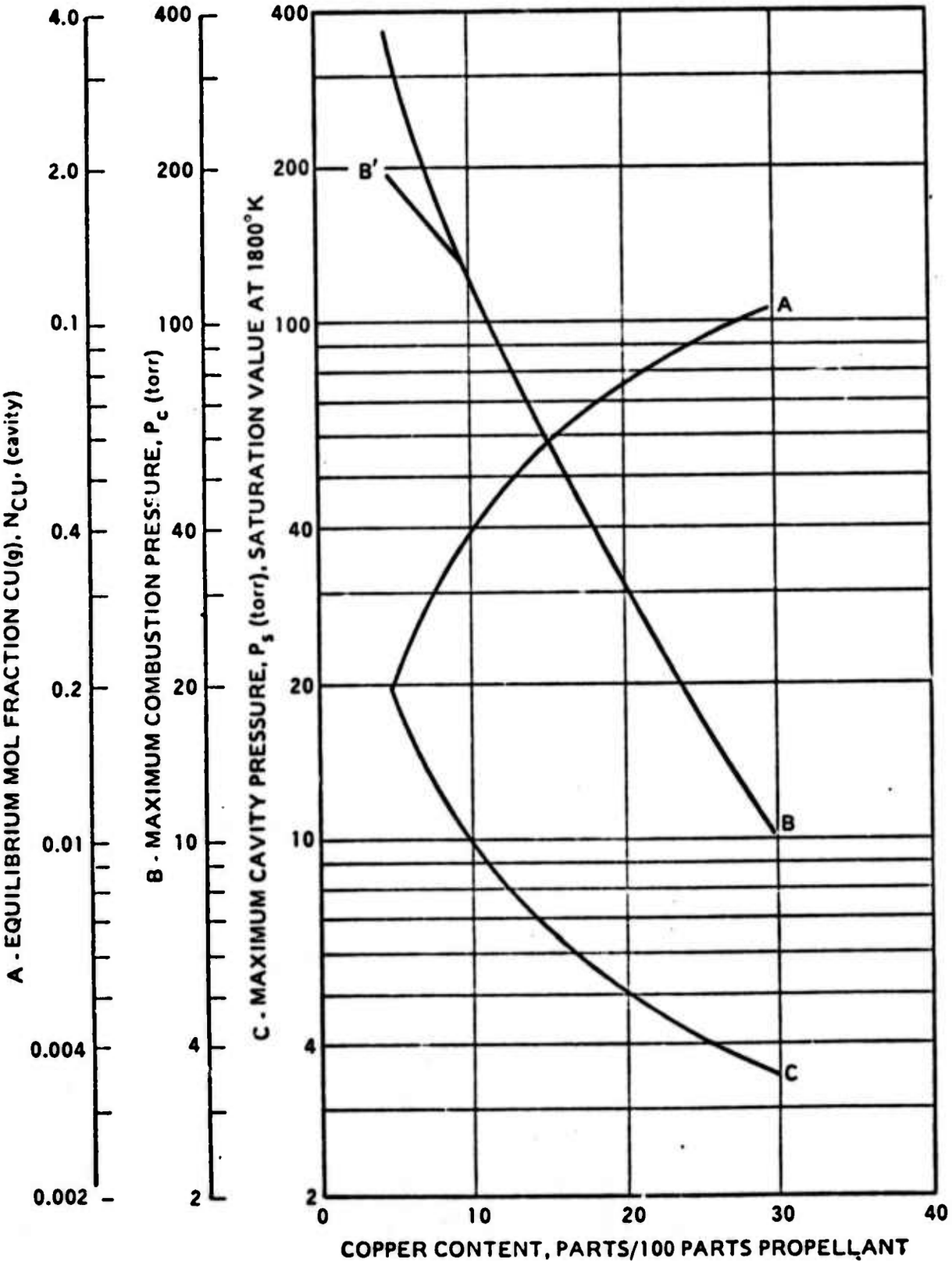

Figure IV-1. Equilibrium N_{cu} P_c and P_s - 40 percent NC + 60 percent BTTN.

Table IV-1. Computed Values of Combustion Pressure, Cavity Pressure, and Combustion Product Composition at Cavity Conditions for Propellant Compositions Yielding 10% by Volume Cu(g) at 1800°K.

1. Composition ID	IA	IIA	IIIA	IIIB	IVA	IVC	IVD
2. Propellant Composition Weight	60% BTTN 40% NC	100% RDX	68% TNM 32% TCE	56.744% TNM 43.256% TCE	70% $KClO_4$ 30% TCE	65% $LiClO_4$ 35% TCE	55.473% $LiClO_4$ 44.527% TCE
3. Metallic Copper Content parts/100 parts propellant	28	29	21.5	25.5	19.5	20.5	25
4. Combustion Pressure, torr	12.5	19	400	28	38	70	7.5
5. Cavity Pressure, torr	3.7	3.8	3.7	3.7	3.7	3.8	3.3
6. Cavity Temperature, °K	1800	1800	1800	1800	1800	1700	1800
7. Combustion Product Composition, mol %							
Cu	10	10	10	10	10	10	10
CO	25	20	27	58	29	27	56
CO_2	18	10	28	0	23	26	0
H_2O	24	20	0	0	0	0	0
H_2	9	10	0	0	0	0	0
N_2	13	30	35	32	17	18	19
H + OH + CuH + CuO + Cu_2	1	<1			18 KCl	19 LiCl	14

7. Cont.	IA	IIA	IIIA	IIIB	IVA	VA	VB
CuO + Cu_2 + NO			<1		1.2K	Li + CuCl + etc <1	Li + CuCl + etc = 1
Cu_2				<1	1.2 CuCl		
CuO + Cu_2 + Cl + K_2Cl_2					<1		

Candidate Propellant Compositions

Double-Base Propellants

1. Compositions

   a. 60% BTTN + 40% NC (by weight)

   b. 43.231% BTTN + 28.821% NC + 27.948% TCE

   c. 80% NIBTN + 20% NC

2. Comments

These are castable compositions yielding water-gas and N_2 as combustion products. Composition b. is stoichiometric to CO, while a. is oxygen-rich of this stoichiometry. The major advantage of the compositions is ease of reduction to practice; the major disadvantage is the yield of CO, H_2, H_2O (the latter two absent from the products of h.) which is detrimental to the CVL effect.

RDX Propellants

1. Compositions

   a. 100% RDX

   b. 77.619% RDX + 22.381% TCE

2. Comments

These are pressed propellants yielding water-gas and N_2 as combustion products, although Composition b. is stoichiometric to CO and yields only CO, H_2, and N_2. The advantages/disadvantages are the same as those of double-base.

TNM/TCE Propellants

1. Compositions

   a. 68% TNM + 32% TCE

   b. 56.744% TNM + 43.256% TCE

2. Comments

These are pressed hydrogen-free compositions. Composition a. yields N_2 and an equimolar mixture of CO_2 and CO, while Composition b. is stoichiometric to CO and yields only CO and N_2 as combustion products. The

major disadvantage of the compositions is the low melting point of TNM (13°C) which would require refrigeration for storage and use. The major advantage is the removal of H_2 and H_2O as combustion products.

Propellants Containing Alkali-Metal Oxidizers and TCE

1. Compositions

   a. 70% $KClO_4$ + 30% TCE

   b. 61.864% $KClO_4$ + 38.137% TCE (stoichiometric to CO)

   c. 65% $LiClO_4$ + 35% TCE

   d. 55.473% $LiClO_4$ + 44.527% TCE (stoichiometric to CO)

   e. Others

      (1) 75% $KClO_3$ + TCE

      (2) 65.677% $KClO_3$ + 34.323% TCE (stoichiometric to CO)

      (3) 68% $LiClO_3$ + 32% TCE

      (4) 58.528% $LiClO_3$ + 41.472% TCE (stoichiometric to CO)

      (5) 57.542% KNO_3 + 22.458% HCE + 20% TCE

      (6) 51.194% KNO_3 + 19.980% HCE + 28.820% TCE (stoichiometric to CO)

      (7) 64.138% KNO_3 + 15.862% TFE + 20% TCE

      (8) 56.332% KNO_3 + 13.931% TFE + 29.737% TCE (stoichiometric to CO)

      (9) 47.968% $LiNO_3$ + 27.302% HCE + 25% TCE

      (10) 41.698% $LiNO_3$ + 23.867% HCE + 34.435% TCE (stoichiometric to CO)

      (11) 55.037% $LiNO_3$ + 19.963% TFE + 25% TCE

      (12) 46.796% $LiNO_3$ + 16.974% TFE + 36.230% TCE (stoichiometric to CO)

      (13) 68% $NaClO_4$ + 32% TCE

      (14) 58.91% $NaClO_4$ + 41.087 TCE

(15) 71% $NaClO_3$ + 29% TCE

(16) 62.43% $NaClO_3$ + 37.566% TCE

(17) 80% $CsClO_4$ + 20% TCE

(18) 73.125% $CsClO_4$ + 26.875% TCE

Glossary of Abbreviations

BTTN	Butane trioltrinitrate, a plasticizer
NC	Nitrocellulose, 12.6% N, a resin
TCE	Tetrocyanoethylene, a high-energy hydrogen-free fuel
RDX	Hexahydro-1, 3, 5-trinitro-s-triazine
HCE	Hexachloroethane
TFE	Teflon
TNM	Tetra-nitro-methane
NIBTN	Nitroisobutanetrioltrinitrate, a plasticizer

Results of the detailed computer studies were weighed against the advantages and disadvantages of each system, i.e., processability, handling, chemical availability, etc. The candidate formulations shown in Table IV-2 were selected for further screening studies. These formulations appeared to offer the best balance between theoretical and practical considerations.

The compositions of BTTN/NC/Cu and NIBTN/NC/Cu were selected for evaluation for reasons of practicality. Reduction of the H_2, H_2O content of compositions, without using TNM, can be done by the use of hydrogen-free fuels. Metal fuels were not considered due to the formation of condensed metal oxides as combustion products. Addition of graphite to 40 NC/60 BTTN reduces hydrogen content by dilution and reduces H_2O and CO_2 content by reduction,

$$C + H_2O \text{ or } CO_2 \rightarrow CO + H_2 \text{ or } 2\,CO$$

These reactions consume 31 and 41 kcal/mol of H_2O or CO_2 reached, respectively, and also cause an increase in gas yield. The endothermic reactions reduce the energy available to vaporize Cu, and the increased gas production reduces the mol fraction of Cu in the combustion products for any given level of Cu in the propellant. Both are undesirable results. The beneficial effect of increased combustion pressure (because cavity pressure is increased at

Table IV-2. Selected Candidate Propellant Systems.

Composition Number	Composition (by weight)	Note
I-A	47.244% BTTN + 31.496% NC + 21.26% Cu	High Cu content
I-B	66.6% NIBTN + 16.7% NC + 16.7% Cu	
I-A	52.174% BTTN + 34.783% NC + 13.044% Cu	Low Cu content

saturation conditions) via reduced Cu mol fraction is more than offset by the reduced energy, and the resultant effect of graphite addition is reduction of P_c. What was needed is a fuel with higher energy than graphite. Organic azides cannot be considered because of the presence of Cu. The next best on the scale are nitriles, such as TCE. The reactions

$$TCE + H_2O \text{ or } CO_2 \rightarrow H_2 + CO \text{ or } 2\,CO$$

consume 6 and 16 kcal/mol of H_2O or CO_2 consumed, respectively, which are significantly lower than the graphite heats, but still endothermic. These reactions also increase the gas yield, more so than does graphite (per mole of CO_2 reduced) because of the N_2-yield of TCE. Thus, TCE also causes a reduction in energy, mol fraction of Cu, and P_c just like graphite, but not as great (per mol of CO_2 reduced). Consequently from the standpoint of performance, it was considered best to use no fuel.

The change needed is energetic hydrogen-free organics that contain enough oxygen (and preferably no other element) to yield CO_2 or at least mixtures of CO and CO_2 upon self-combustion. Aside from things like TNM, HNE, and PNA, such compounds are not known. The H_2/H_2O yield of double-base propellants can be reduced slightly by decreasing plasticizer/resin ratio, but, as above, at the expense of energy, Cu mol fraction and P_c. The latter three increase with increasing plasticizer/resin but at the expense of increase H_2, H_2O content.

The alternate approach, that of using metal halide producers instead of hydrogen producers could not be evaluated because of the failure to gain data on the effect of these compounds on laser operation. Future work should reexamine this possibility.

3. EXPERIMENTAL TESTING OF HARDWARE

The pressure requirements for sustained propellant burn and for laser cavity operation are conflicting. The CVL operation is optimum at a maximum of a few tens of torr. Typical chamber pressures for burning propellants are from one to several hundred atmospheres. Therefore, expansion to low pressure after combustion is a necessity. A supersonic flow would cause shock waves throughout the laser cavity region. Therefore the flow was allowed to shock down to subsonic flow to avoid inhomogeneities which would degrade the optical beam quality.

The combination of these conditions led to the design of a low mass flow, low chamber pressure (subatmospheric) gas generator. The difficulties inherent in this type of design are excess heat loss and difficulty in achieving ignition and sustaining burning.

Given the experimentally determined burn rate data (see Figures IV-2, 3 and 4) and the desired mass flow as determined by the subsonic flow condition, the nozzle throat area is determined via the conservation of mass equation

$$\dot{m} = P_c C_d A_t = S\dot{r}\rho$$

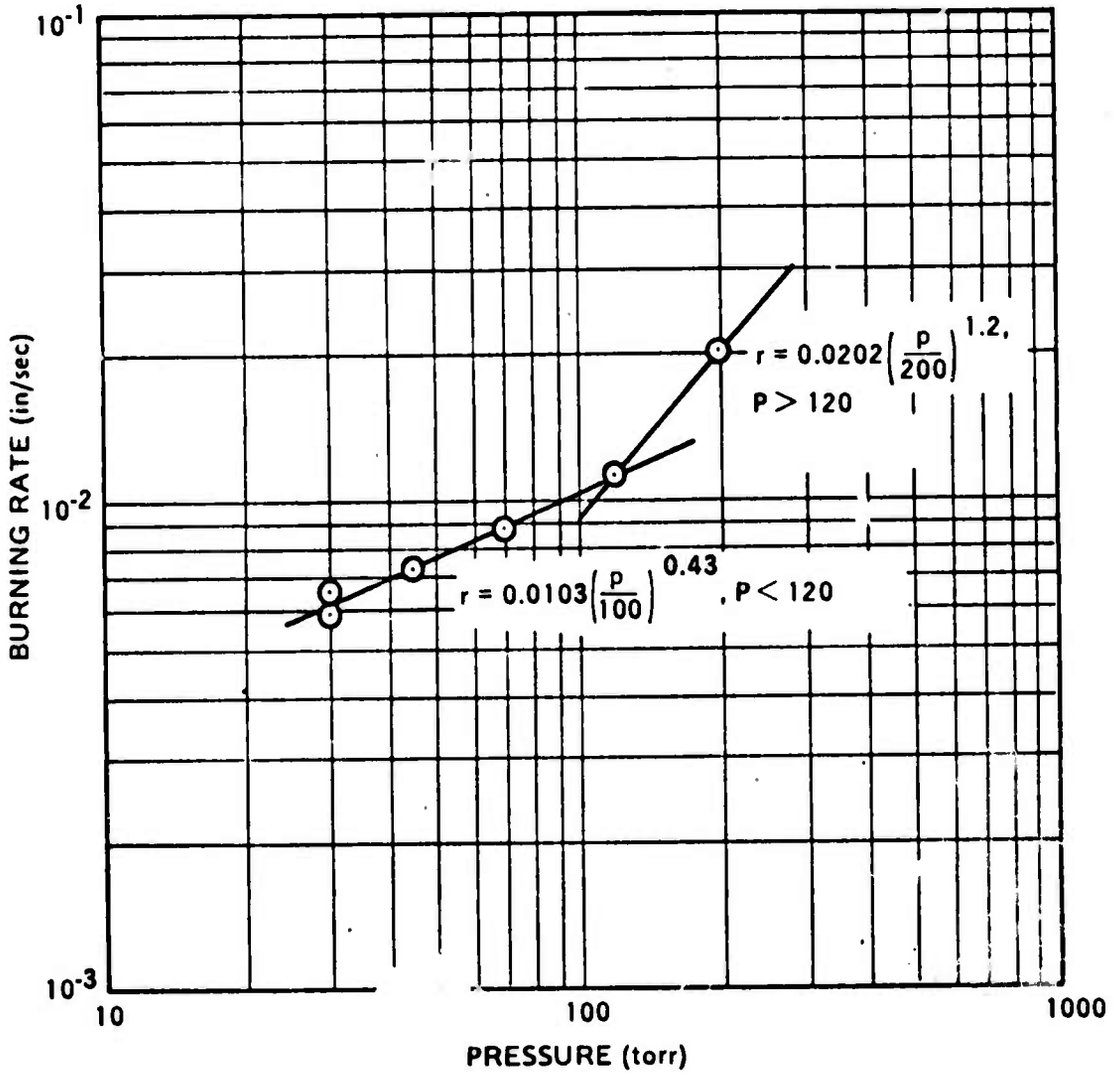

Figure IV-2. Burning Rate Versus Pressure: 31.5 percent NC + 47.2 percent BTTN + 21.3 percent CU.

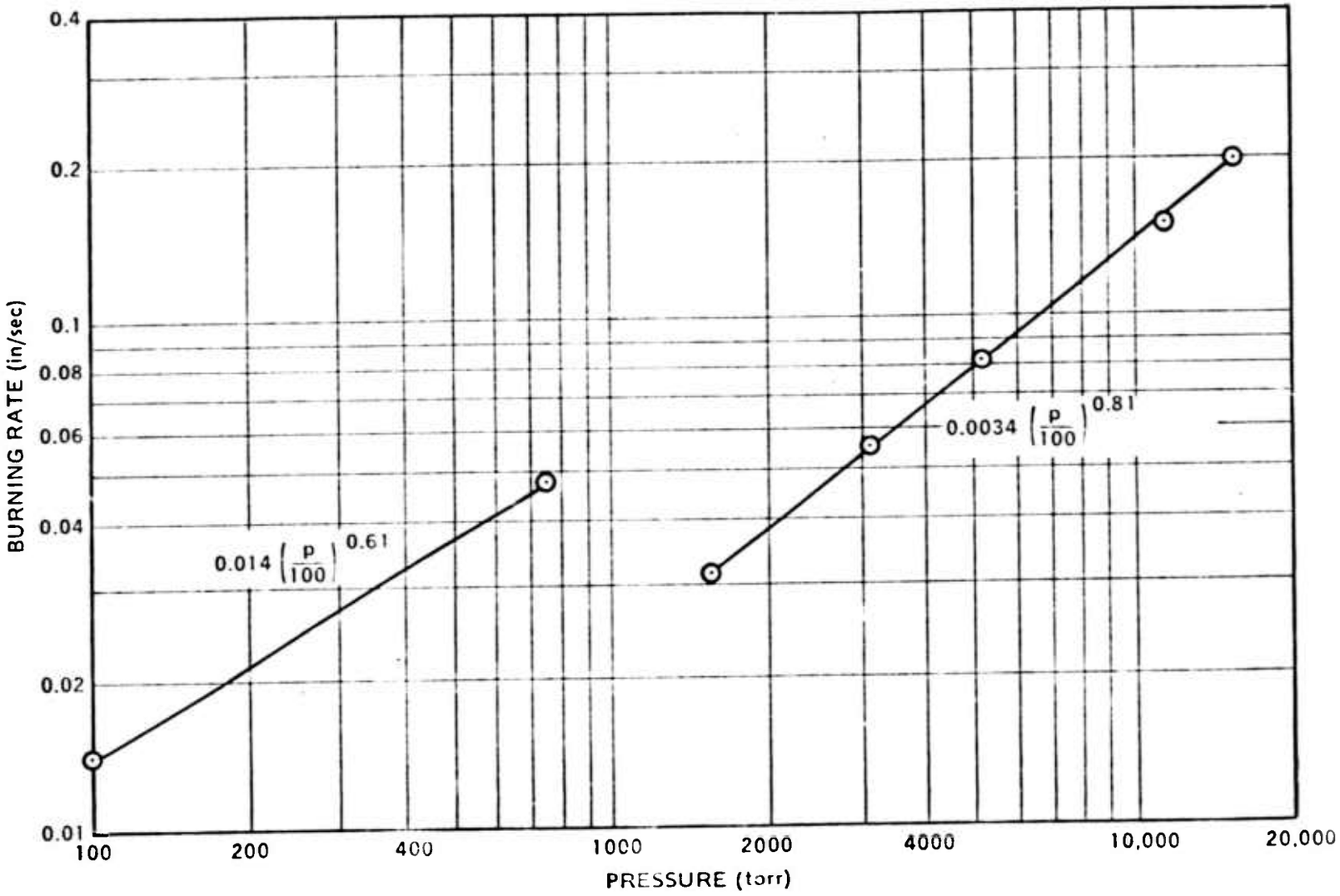

Figure IV-3. Burning Rate Versus Pressure: 66.7 percent NIBTN + 16.7 percent NC + 16.6 percent CU.

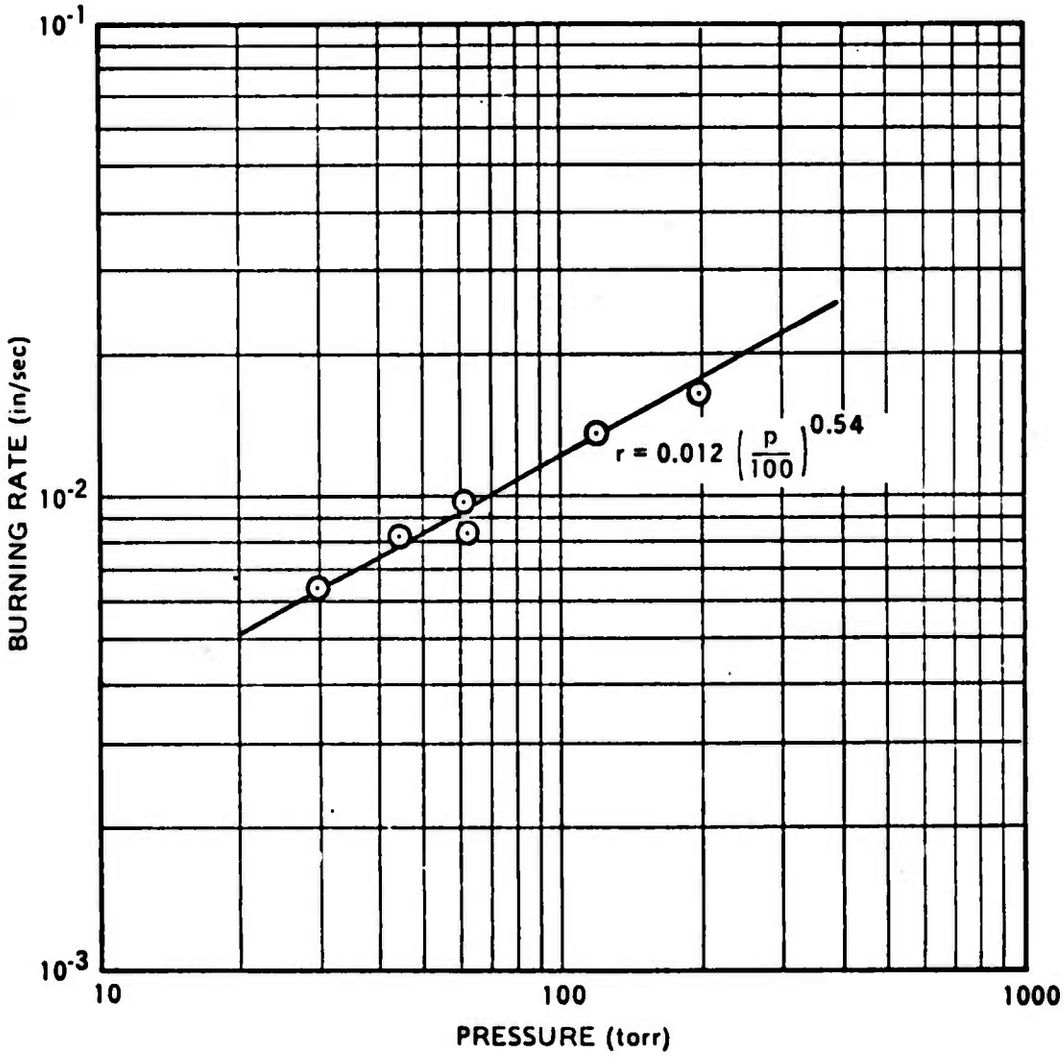

Figure IV-4. Burning Rate Versus Pressure: 34.8 percent NC + 52.2 percent BTTN + 13.0 percent CU.

where

P_c = chamber pressure

C_d = discharge coefficient

A_t = throat area

S = burning surface area

$\bar{r}$ = burn rate = $F(P_c)$

$\dot{m}$ = mass flow

ρ = propellant density

Using these parameters, an initial estimate for the throat diameter of the expansion nozzle was determined. This value was then modified experimentally until proper burn characteristics were achieved.

The grain was a toroidal-shaped cylinder with dimensions: 1-inch I.D. X 2-inch O.D. X 2 inches high. The burn was initiated on the inside diameter and continued to burn radially outward. Under typical operating conditions, with a throat diameter of 0.35 inch, the chamber pressure was ~6 psi, the burn duration was ~20 seconds, and the mass flow was ~5 gm/sec. A typical chamber pressure versus time trace is shown in Figure VII-2.

The hardware initially used to form the chamber was an existing 1/4 pound hardware. (The maximum safe load is 1/4 pound of propellant material.) The hardware was modified for low heat loss by adding Fibrefrax insulation on the inner diameter. The nozzle insert was modified from all graphite to graphite plus phenolic, the latter having greater insulating properties at the critical throat area (see Figure IV-5).

Chamber pressure was monitored with the use of a strain-gauge pressure transducer.

In order to simulate the operating conditions when the motor is to be used in conjunction with the laser apparatus, the tests were performed in a vacuum chamber.

In the following paragraphs a brief summary is given of the hardware and igniter development.

The burn rate of the NIBTN formulation was experimentally determined to be

$$\bar{r} = 0.14 \left[\frac{P_c}{100}\right]^{0.61} \text{ in/sec}$$

where P_c is the chamber pressure measured in torr. Using this value for $\bar{r}$ in the conservation of mass Equation, an initial value for the throat diameter of 0.540 inch was determined. This value of throat diameter was then experimentally varied from test to test until proper burn conditions are achieved. The throat diameter in the final configuration was 0.350 inch.

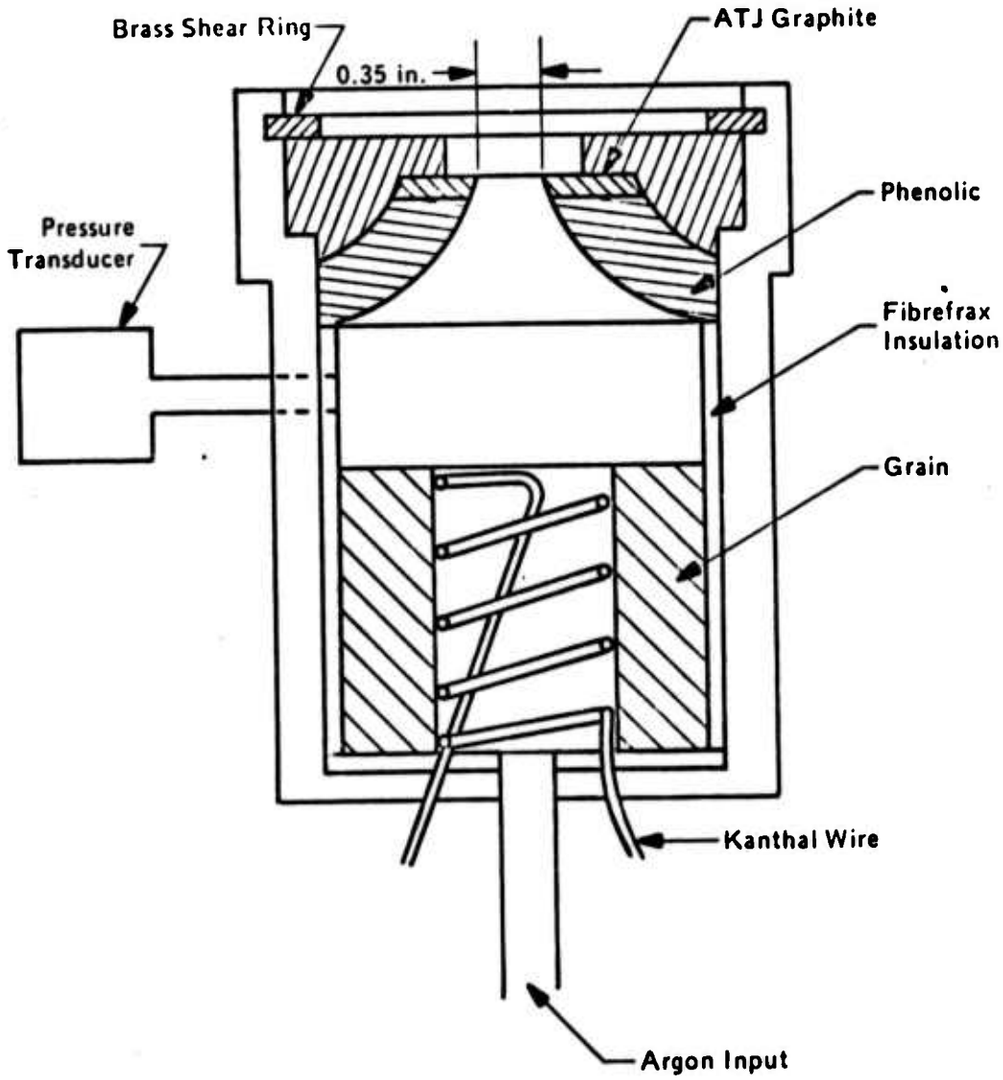

Figure IV-5. Gas Generator Hardware Assembly.

Initial ignition attempts using a pyrogen igniter, igniter pellets, squibs, and other standard techniques failed. It was determined that the only successful ignition system required the use of an electrically heated hot wire (Kanthal Al) wound in a spiral on the I.D. of the grain.

Typically, Kanthal wire would melt halfway into the burn, but the burn sustained itself. The conclusion is that the NIBTN formulation at these low pressures (<1 atmosphere) needs heat applied for a long period of time, (greater than 3 seconds), in order to achieve ignition.

In the initial tests the burns were initiated in vacuum. This was necessary to duplicate operation with a laser in which the system is pumped down prior to ignition. The motor incorporated a 0.005-inch-thick scored copper blowout disc which would allow P_c to increase until ignition whereupon the disc blows out.

The combustion was not stable and the decision was made to pressurize the motor chamber with preheated argon, a particularly good diluent gas. The argon flow initially pressurized the motor to about 50 torr and after ignition could be readjusted. For example, during the tests at PIB, the argon was turned off halfway during the burn to afford the maximum amount of information in one burn.

Since the presence of hardware reduces the thermochemically predicted value of temperature at 6 psia, a reduced temperature computer calculation (using an artifically low ingredient enthalpy to simulate heat loss) was made. At a temperature of 2200°K the byproducts are listed in Table IV-3, where it is observed that the partial pressure of O_2 is 0.05 percent and Cu 5 percent. This can be compared with the equilibrium values where the p.p. of O_2 is 2 percent and Cu, 7 percent at a temperature of 2628°K (see Table IV-4). This abundance of oxygen for the latter case would be disturbing in that the static tests for laser action indicate that oxygen rapidly degrades laser output.

4. MEASUREMENT OF THE DENSITY OF COPPER VAPOR

For several reasons it is likely that the copper density is below its equilibrium value determined by the flame temperature. Possible causes are: (1) nonequilibrium burning resulting in reduced flame temperature, (2) insufficient residence time of the copper particles in the flame, (3) heat loss to the hardware resulting in reduced flame temperature, and (4) condensation of Cu vapor on cold surfaces. For these reasons it was important to measure the density of copper vapor after expansion to the low pressure region.

Of the different methods to measure the number density of copper atoms the one that required the simplest instrumentation also appeared to be able to cover the range of densities (about 5 decades, from 10^8 to 10^{14} cm^{-3}) with immediate interest.

The method used required measuring absorption of monochromatic light at the center of the resonance transition from the ground state to the upper laser levels $^2P_{3/2}$ (λ = 3247 Å) and $^2P_{1/2}$ (λ = 3274 Å) by using emission from a hollow cathode copper lamp. In general, the absorption coefficient is

$$\alpha(\nu) = \left(N_1 \frac{g_2}{g_1} - N_2\right) \frac{\lambda^2}{8\pi_{spont.}} g(\nu-\nu_o)$$

Table IV-3. Analytically Predicted By-Products at Reduced Temperature (T = 2200°K) to Simulate Hardware Heat Loss.

H	C	N	O	CU										
6.000	4.000	4.000	11.000	0.0	0.0	0.0	0.0	0.0	0.0	0.0	0.0	80.000	-363.	1.6400
7.550	6.000	2.450	9.900	0.0	0.0	0.0	0.0	0.0	0.0	0.0	0.0	20.000	-625.	1.0000
0.0	0.0	0.0	0.0	1.000	0.0	0.0	0.0	0.0	0.0	0.0	0.0	20.000	0.	8.9200

AMOUNTS FOR PROPELLANT WEIGHT OF 120.000 PROPELLANT ENTHALPY -41520.4 DENS(G/CC) 1.690 #/IN3 0.06105

(C)	(N)	(O)	(CU)
1.558990	1.298331	3.802617	0.314733

ISP	IVAC	P(PSIA)	TEMP.(K)	ENTHALPY	ENTROPY	HT. CAP	MOLS GAS	VELOC	AE/M	C*
		6.0000	2200.0	-9372).	253.583	41.782	3.5378			

	CHAMBER	THROAT	EXHAUST		CHAMBER	THROAT	EXHAUST		CHAMBER	THROAT	EXHAUST
	0.00000	0.0	0.0	CH	0.00000	0.0	0.0	CH2	0.00000	0.0	0.0
	0.00000	0.0	0.0	CH4	0.00000	0.0	0.0	CN	0.00000	0.0	0.0
	0.38352	0.0	0.0	CO2	1.17545	0.0	0.0	CU	0.18991	0.0	0.0
	0.00417	0.0	0.0	CUO	0.00926	0.0	0.0	CU2	0.00158	0.0	0.0
	0.00000	0.0	0.0	C2H2	0.00000	0.0	0.0	C3	0.00000	0.0	0.0
	0.00422	0.0	0.0	HCN	0.00000	0.0	0.0	HCO	0.00000	0.0	0.0
	0.00000	0.0	0.0	H2	0.06519	0.0	0.0	H20	1.04193	0.0	0.0
	0.00000	0.0	0.0	N	0.00000	0.0	0.0	NH	0.00000	0.0	0.0
	0.00000	0.0	0.0	NH3	0.00000	0.0	0.0	NO	0.00142	0.0	0.0
	0.00000	0.0	0.0	N2	0.64846	0.0	0.0	N20	0.00000	0.0	0.0
	0.00042	0.0	0.0	OH	0.00937	0.0	0.0	02	0.00288	0.0	0.0
	0.00000	0.0	0.0	CCUN$	0.00000	0.0	0.0	CU$	0.00000	0.0	0.0
	0.00000	0.0	0.0	CU02H2$	0.00000	0.0	0.0	CU20$	0.00000	0.0	0.0
	0.10423	0.0	0.0	CU20*	0.00000	0.0	0.0				

Table IV-4. Analytically Predicted By-Products at a Temperature of 2628°K.

H	C	N	O	CU									
6.000	4.000	4.000	11.000	0.0	0.0	0.0	0.0	0.0	0.0	0.0	0.0	80.000	-363.	1.6400
7.550	6.000	2.450	9.900	0.0	0.0	0.0	0.0	0.0	0.0	0.0	0.0	20.000	-625.	1.0000
0.0	0.0	0.0	0.0	1.000	0.0	0.0	0.0	0.0	0.0	0.0	0.0	20.000	0.	8.9200

AMOUNTS FOR PROPELLANT WEIGHT OF 120.000 PROPELLANT ENTHALPY -41520.4 DENS(G/CC) 1.690 #/IN3 0.06105

(C)	(N)	(O)	(CU)
1.558990	1.298331	3.802617	0.314733

ISP	IVAC	P(PSIA)	TEMP.(K)	ENTHALPY	ENTROPY	MT. CAP	MOLS GAS	VELOC	AE/M	C*
		6.0000	2628.5	-41520.	275.251	42.285	3.8373			

	CHAMBER	THROAT	EXHAUST		CHAMBER	THROAT	EXHAUST		CHAMBER	THROAT	EXHAUST
	0.00000	0.0	0.0	CH	0.00000	0.0	0.0	CH2	0.00000	0.0	0.0
	0.00000	0.0	0.0	CH4	0.00000	0.0	0.0	CN	0.00000	0.0	0.0
	0.63611	0.0	0.0	CO2	0.92887	0.0	0.0	CU	0.27610	0.0	0.0
	0.00401	0.0	0.0	CUO	0.03359	0.0	0.0	CU2	0.00052	0.0	0.0
	0.00000	0.0	0.0	C2H2	0.00000	0.0	0.0	C3	0.00000	0.0	0.0
	0.04156	0.0	0.0	HCN	0.00000	0.0	0.0	HCO	0.00000	0.0	0.0
	0.00000	0.0	0.0	H2	0.00996	0.0	0.0	H2O	0.94623	0.0	0.0
	0.00000	0.0	0.0	N	0.00000	0.0	0.0	NH	0.00000	0.0	0.0
	0.00000	0.0	0.0	NH3	0.00000	0.0	0.0	NO	0.01842	0.0	0.0
	0.00000	0.0	0.0	N2	0.63995	0.0	0.0	N2O	0.00000	0.0	0.0
	0.02529	0.0	0.0	O	0.00406	0.0	0.0	O2	0.00858	0.0	0.0
	0.00000	0.0	0.0	CCUN$	0.00000	0.0	0.0	CU$	0.00000	0.0	0.0
	0.00000	0.0	0.0	CUO2H2$	0.00000	0.0	0.0	CU2O$	0.00000	0.0	0.0
	0.00000	0.0	0.0	CU2O*	0.00000	0.0	0.0				

where

$\alpha(\nu)$ = the frequency (wavelength) dependent absorption coefficient

N_1 = ground level population (i.e., number density)

g_2/g_1 = ratio of degeneracies of upper and ground levels i.e., $g_2/g_1 = 2$ ($\lambda = 3247$ Å); $g_2/g_1 = 1$ ($\lambda = 3274$ Å)

N_2 = upper laser level population (~ 0)

λ = wavelength of transition

t_{spont} = $A^{-1} = 1.05 \times 10^{-8}$ sec at $\lambda = 3274$ Å ($= 0.976 \times 10^{-8}$ sec at $\lambda = 3247$ Å)

and

$$g(\nu - \nu_o) = \frac{2\sqrt{\ell n\, 2}}{\sqrt{\pi}\,\Delta\nu} \exp\left[-4\,\ell n\, 2\left[\frac{\nu - \nu_o}{\Delta\nu}\right]^2\right] = \frac{0.93944}{\Delta\nu} \exp\left[-\left(\frac{1.6651(\nu - \nu_o)}{\Delta\nu}\right)^2\right]$$

and

$$g(\nu = \nu_o) = \frac{0.93944}{\Delta\nu}$$

where for Doppler broadened lines

$$\Delta\nu \frac{2\sqrt{2\,\ell n\, 2}}{\lambda}\sqrt{\frac{kT}{M}}$$

where

$k = 1.38 \times 10^{-16}$ erg/°C

$T = 1800°$ (in our experiments)

$M = 63.54$ atomic weight (for atomic copper)

$= 1.0549 \times 10^{-22}$ gram

$\lambda = 3.274 \times 10^{-5}$ cm (in our experiments)

Since

$$\Delta\nu = 3.49 \times 10^{8} \text{ cps}$$

and

$$g(\nu=\nu_o) = 2.692 \times 10^{-10}$$

the absorption coefficient is:

$$\alpha = 1.0934 \times 10^{-12} \times N$$

or

$$N_1 = 9.146 \times 10^{11} \times \alpha$$

Assuming a dynamic range of 3 decades and a resolution of 1:1000 for the absorption measuring instrumentation, a measured optical density of 3 (0.1 percent transmission) means that $\alpha_o L = 6.9$ or $\alpha_o = 6.9$ ($N = 6.3 \times 10^{12}$ copper atoms per cm^3) for L = 1 cm. At the other extreme of the measurable density range; an almost completely transparent medium at λ = 3274 Å with a 0.1 percent absorption, means that $\alpha = 0.001$ for L = 1 cm which means a copper number density of $N = 9.146 \times 10^{8}$ parts per cm^3.

By reducing the optical path length the measurable number density range can be extended to about 10^{14} cm^{-3}, beyond which the lack of knowledge of exact path length destroys the accuracy of measured values.

Other methods, such as measuring the absorption line broadening or to measure excited state absorption allow measuring number densities of copper all the way to 10^{17} - 10^{18} parts per cm^3. These methods were not implemented due to requirements of more involved instrumentation, such as the use of a Cu vapor laser in conjunction with strong dependence of the results on temperature.

The method as described above was used to measure the copper density in the flow. A schematic of the absorption measurement is illustrated in Figure IV-6. Here the Cu lamp output is collimated and passed through the plume. The collimated beam was carefully aligned with the rest of the hardware and the generated copper vapor column, that no spillover of beam occurred. The attenuated beam is directed toward a beam splitter and detected by two monochromators fitted with RCA/1P28 phototubes. One monochromator is tuned to the 3274 Å resonance copper line and the other instrument to one of the nearby neon lines. (The hollow cathode lamp uses neon as a carrier gas.) This precaution is taken so that particle scattering is not mistaken for resonance absorption. For the former, both lines would be attenuated, and for the latter, only the 3274 Å line would be attenuated.

Using this technique, the copper density was monitored for various parameters. A case, where complete absorption takes place is shown in Figure IV-7. A chopper rotating at one cycle per second periodically interrupts the hollow cathode lamp so that a zero reference is maintained.

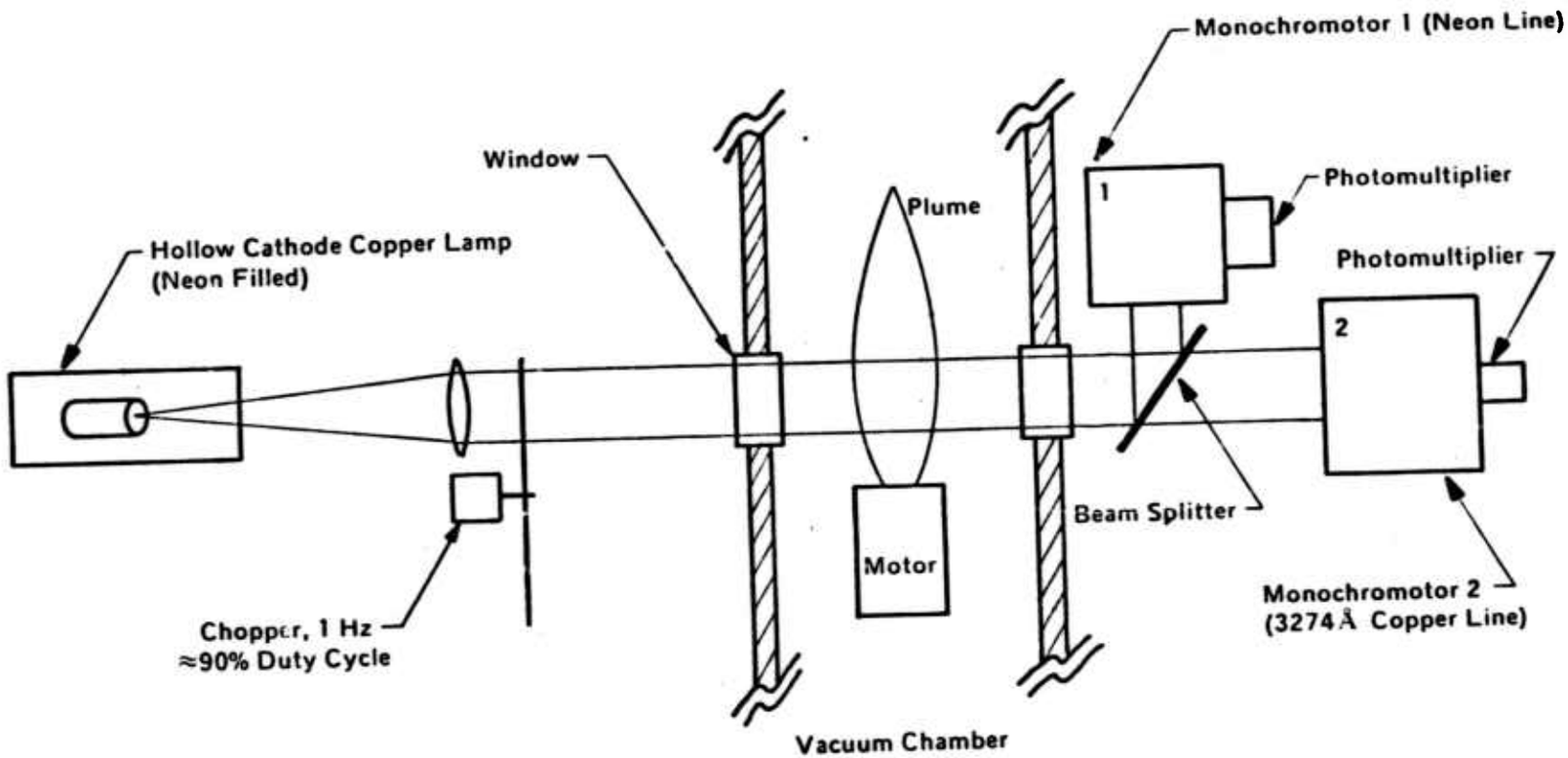

Figure IV-6. Copper Vapor Absorption Experimental Set-Up.

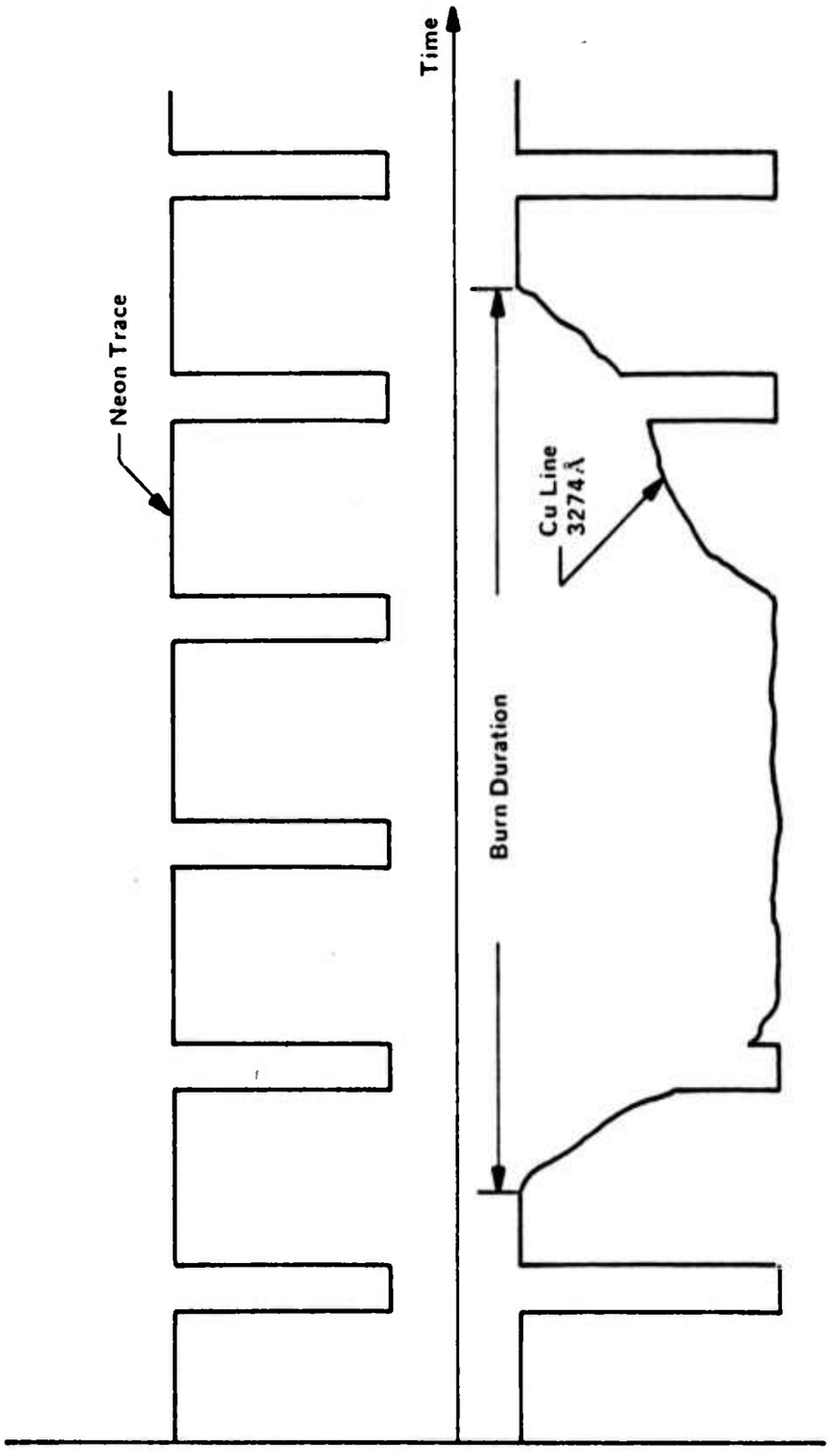

Figure IV-7. Copper Vapor Attenuation Versus Time.

The interpretation of these results indicate that the gas generator produced at least enough copper vapor density to render the medium opaque at $\lambda = 3274$ Å. For the path length used in the experiments ($L \geq 1$ cm) this implies that $N \geq 10^{12}$ copper atoms per cm^3 immediately above the throat of the generator.

SECTION V

HOMOGENEITY MEASUREMENTS

1. INTRODUCTION

The optical quality of the output beam depends on the homogeneity of the laser medium. A measure of beam quality may be defined in terms of the energy delivered in the far field in relation to the energy delivered by a diffraction limited, Gaussian beam. Near-field parameters can be used to predict the far-field behavior. In turn, the near-field parameters are determined in part by the degree of homogeneity of both the real and imaginary parts of the refractive index of the medium.

There are variations in the value of the complex refractive index both in time and space. In both cases, we are concerned primarily with gradients transverse to the optical axis of power extraction. If variations in the cross-sectional plane are simple enough geometrically, and steady in time, at least in principle they can be corrected by appropriate correction optics elements. We must be concerned, however, with unpredictable, unsteady variations and their characteristics.

Characteristics of variation in the optical gain profile in the cross-sectional plane relate to the inhomogeneity of the electrical discharge mechanism, which to a great degree relate to the electrode configuration and the external circuitry. The portion of gain variations that is caused by inhomogeneities of the copper and buffer gas densities also shows up in terms of inhomogeneities of the real part of the refractive index.

Allowable uncorrected variations in $\Delta\rho/\rho$, the percentage mass density variation, for a specified beam quality scale directly with the laser wavelength. Based on this factor alone, the requirement on homogeneity is about 20 times more severe in the case of the CVL compared to requirements for CO_2 lasers for example.

There are several factors, however, that ease these restrictions on the homogeneity requirement of the copper vapor medium, when considered in relation to other high power, high pressure electrical discharge laser media. The influence of a fixed amount of mass density fluctuation percentage of the medium on the refractive index homogeneity is linearly proportional to the pressure and inversely proportional to the absolute temperature of the medium. In a copper vapor laser medium, which consists mostly of buffer gases, typical operating pressures are in the order of 1/10 atmosphere or less. Temperatures of the laser medium is up to 5 or 6 times that of other high power (molecular) electrical discharge lasers. Furthermore, given velocities of the working fluid can be produced at relatively low Mach numbers. This is important because $\frac{d\rho}{\rho}$ is proportional to $\frac{dp}{p} \cdot (\gamma M^2)^{-1}$ across a gas dynamic discontinuity, where p is the pressure, M is the Mach number, and γ is the ratio of the specific heats at constant pressure and volume. By far the biggest factor in reducing the degrading effects of laser medium inhomogeneity on the output beam quality is associated with the high optical gains (and therefore, short optical paths) of the CVL compared with CO_2 systems. This is a favorable effect by a factor of approximately 30. Since the reduction in far-field brightness due to phase front distortions is proportional to $\exp(-\Delta\phi^2)$ and since $\Delta\phi$ is proportional to L, this latter factor is most important. Here $\Delta\phi$ represents the phase front distortion, and L is the length of the laser medium.

Work in the optical homogeneity studies of copper vapor generator exhaust gases progressed through three phases. The first task was that of problem definition. In this first phase of the work the homogeneity requirements for the medium of a high-power laser was reviewed. These requirements were translated into measurable quantities in a typical interferometric setup. Using flow geometry and other parameters of the solid-fueled copper vapor generator hardware that was used in all the other tests of Cu vapor generation, an experimental arrangement was devised that allowed real-time monitoring, recording and measurement of the dynamic optical homogeneity characteristics of the medium.

In the second phase of work in this area an ARC-built Michelson interferometer was refurbished and interfaced with the copper vapor generator. Custom-built pneumatically dampened legs were added for vibration isolation, and the whole system (with nearly 6-foot long arms, over 1000 pounds in weight) was mounted inside of a large vacuum chamber and tested with an argon ion laser (λ = 5145 Å).

The third phase of work consisted of the actual homogeneity measurements and evaluati experimental data.

In the following, detailed description of the results is given.

2. PROBLEM DEFINITION

The homogeneity requirements for a lasing medium depend on the different parameters of the laser system besides the desired characteristic of the output beam. In qualitative terms, if an ideal plane wavefront traverses through the laser medium (copper vapor and buffer gases in this case), due to the nonzero inhomogeneities in the medium, the plane wavefront is distorted according to the cross-sectional distribution of density variations averaged in the direction ($\vec{z}$) of the plane wave propagation. The optical path in terms of the refractive index n(x,y,z) of the medium is

$$Q(x,y) = \int_0^L n(x,y,z)\, dz = n_{ave}(x,y)\, L$$

Surface imperfections on the mirrors of a laser cavity also affect the wavefront. The reflected portion of a plane wave from a nonperfect laser mirror will carry the imprint of the surface imperfections, magnified by a factor of 2. In most cases, laser mirrors with surface quality of $\lambda/20$ is acceptable. It is reasonable to require a density homogeneity of the laser medium under these conditions to cause an optical path differential in the cross-sectional plane, less than $\lambda/10$, i.e.,

$$\frac{\Delta Q(x,y)}{\lambda} < 0.1$$

The relation between density and refractive index in a gas is described by the Dale-Gladstone Law

$$n = 1 + \Sigma_i K_i \rho_i$$

where the summation is over the different constituents of the buffer gases used and the copper vapor. The value of K is almost constant throughout the visible portion of the spectrum and is 0.226 cm^3/gm. Mass density ρ is related to the particle density N by

$$\rho = N \frac{M}{A_o} \text{ gm cm}^{-3}$$

where

M = molecular (or atomic) weight

A_o = 0.60248×10^{24} molecules/mole, Avogadro's number

$$N = 2.6872 \times 10^{19} \times \frac{P(\text{torr})}{760 \text{ torr}} \times \frac{273}{273 + T} \text{ cm}^{-3}$$

T = temperature in centigrade

In most of the homogeneity tests heated argon gas was injected into the combustion chamber to provide the background pressure for the proper burning rate.

Using two different pressure values and two different temperatures for the exhaust gases to indicate the ranges of the refractive index n, the following values for (n-1) are calculated:

Pressure / Temperature	50 torr	150 torr
1500°C	4.077×10^{-6}	12.23×10^{-6}
500°C	9.354×10^{-6}	28.06×10^{-6}

The phase shift in a Michelson interferometer setup (round trip through the exhaust gases) caused by exhaust gases with the above values of temperature and pressure in terms of the optical wavelength is $\phi = 2L(n-1)/\lambda$.

Pressure / Temperature	50 torr	150 torr
1500°C	0.503	1.509
500°C	1.154	3.463

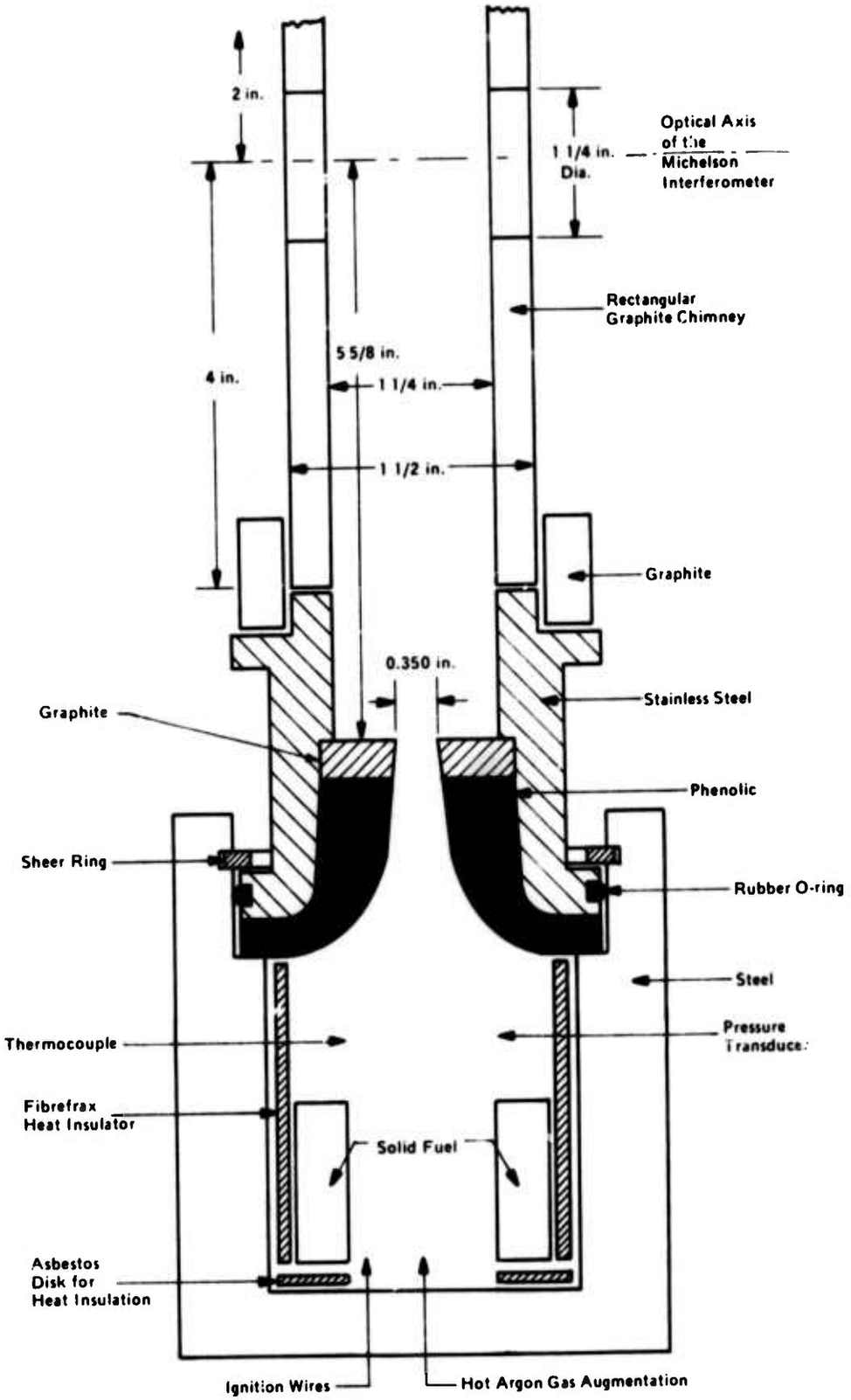

Figure V-1. Copper Vapor Generator with Hardware to Interface with the Michelson Interferometer.

where

$\lambda = 0.5145\mu$

$L = 1.25$ inch $= 3.175$ cm

Ordered medium inhomogeneities have larger overall effect on the electromagnetic field distribution inside the laser cavity.

If a certain feature of the inhomogeneity in the plane normal to the optical axis preserves itself as one traverses through the medium, its effect will dominate over effects due to disordered (random) inhomogeneities. The above table shows the number of fringe shifts in the interferogram obtainable with a Michelson interferometer in the case of 100 percent ordered density inhomogeneity of the medium. Comparing interferograms exposed before, during and after the test, one should be able to resolve a shift of 1/10 of a fringe. (For the conditions listed in the above table a $\Delta\rho/\rho$ value between 2.88 percent to 19.8 percent should be resolvable.) Estimation of accuracy of this method to obtain quantitative data on medium density inhomogeneity is discussed later in Section V-4.

The effect of random or disordered inhomogeneities can be interpreted in terms of a scattering coefficient α, defined as $\alpha = -\frac{dI}{dz}\cdot\frac{1}{I}$. For random inhomogeneities of size ξ where $\frac{2\pi\xi}{\lambda} >> 1$ the parameter controlling the magnitude of the scattering coefficient is $L\xi\,\dot{\mu}^2/\lambda^2$ where $\dot{\mu}^2$ is the mean square value of the refractive index fluctuations. Thus the scattering coefficient α is proportional to $(\rho)^2$, $(\Delta\rho/\rho)^2$, ξ and $1/\lambda^2$ and the far-field intensity reduction is proportional to $\exp(-\alpha L)$. Again the short path and low density of the copper vapor laser medium more than make up for the effect of the short wavelength (compared with CO_2).

3. EXPERIMENTAL APPARATUS

An Atlantic Research Corporation built Michelson interferometer was modified to interface with the copper vapor generator and its operational characteristics. The copper vapor generator has to be operated in partial vacuum in order to be able to control the subatmospheric pressure in the combustion chamber. Also due to large amounts of heat flux generated by the vapor generator it was desirable to place not only the copper vapor generator into a vacuum chamber but also the whole interferometer. Earlier trial runs of burning the copper loaded grains at one atmosphere and bringing the exhaust gases through the "working" arm of the Michelson interferometer, (in other words, performing the homogeneity test out in the open) resulted in a complete obliteration of the fringes, mostly due to the induced air currents throughout the almost 60-inch long arm of the interferometer.

The Michelson interferometer that was used in the homogeneity measurements consists of a "working arm" and a "reference arm" each of which is over 60 inches long. Stability of the structure depends on invar rods which are supported by 3-inch-thick aluminum blocks. The optical axes run through the centers of the arms as shown in Figure V-2. A maximum of 3 inches in diameter clear optical aperture is available in both arms, however, only the center 1-inch-diameter area was utilized in the present measurements. The critical optical component, which also determines the overall system accuracy of the interferometer is the beam splitter which is placed at the junction of the two arms. The beam splitter used in the present experiments is made of fused silica and has a $\lambda/10$ flatness on both sides and 2 arc seconds parallelism or better between its two surfaces. A neutral density 50-50

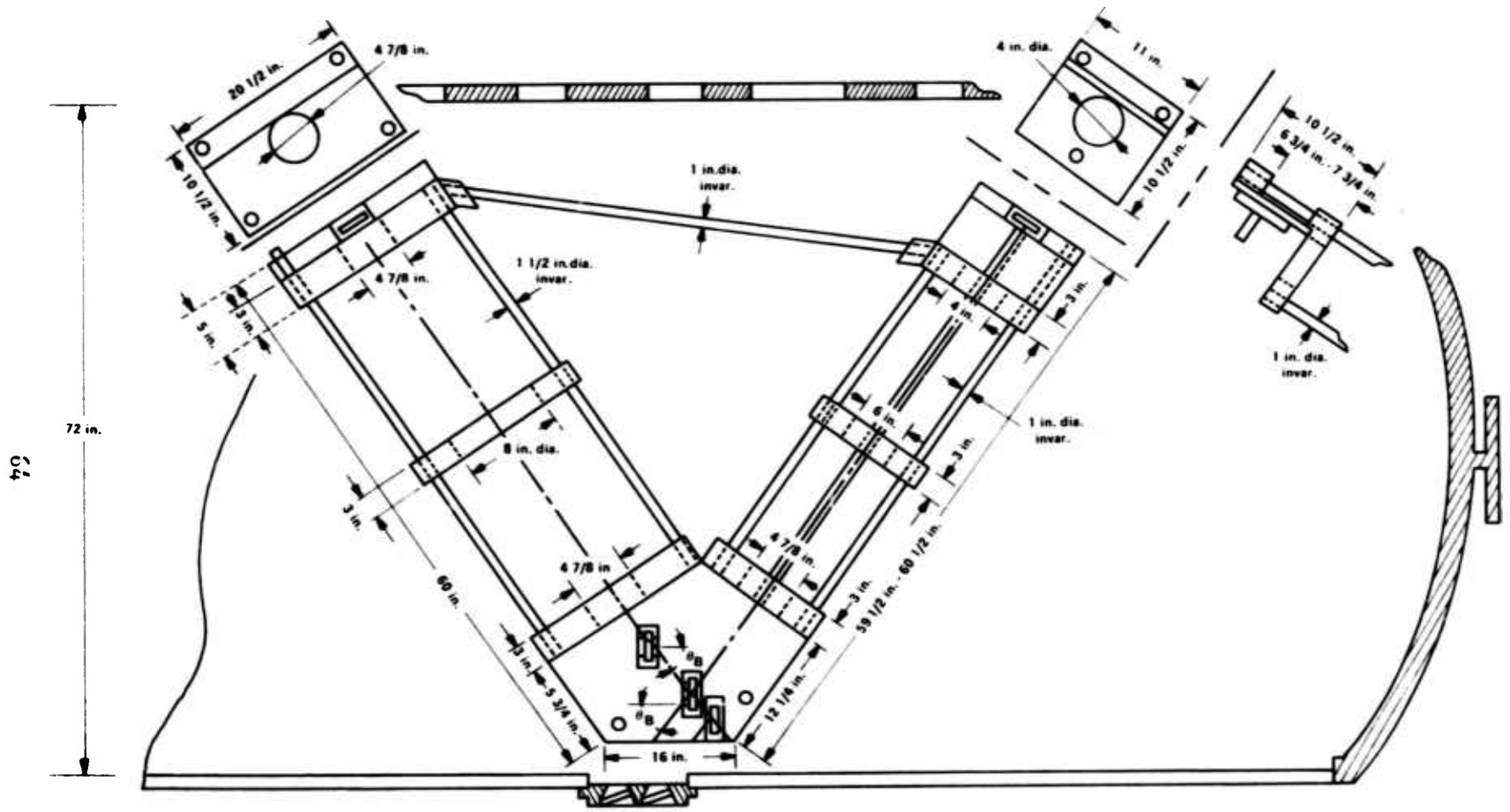

Figure V-2. Michelson Interferometer and its Relationship to the Vacuum Chamber in Which the Copper Vapor Homogeneity Tests were Performed. θ_B = 56 degrees. (Brewster's Angle)

percent coating allows the interferometer to be color insensitive over the visible and part of the near IR range of the spectrum. The interferometer is constructed to take advantage of Brewster's angle of incidence for the purpose of eliminating Fresnel reflection from the second surface of the beam splitter. All optical elements including mirrors and windows are fabricated of fused silica to an accuracy of $\lambda/10$ or better. All optical elements are separately adjustable by having them mounted in angular orientation devices. The length of the reference arm is adjustable over a length of $\pm 1/2$ inch. Other features of the construction are shown in Figure V-2.

From the beginning it was obvious that the very best vibration isolation method that could be obtained was needed to decouple the interferometer from the vibrations of the walls of the vacuum tank (diameter 72 inches) and from the vibrations of the copper vapor combustor. The limited space in the vacuum chamber made it necessary to modify a set of 3 NRC pneumatic vibration isolator legs by shortening them to about 14 inches each, and attaching them to the vacuum chamber through collars that allowed final positioning of the interferometer in both horizontal and vertical directions (see Figure V-4). Pressures in the pneumatic cylinders had to be adjusted to balance under partial vacuum conditions. In equilibrium and under vacuum the optical axes of the interferometer had to line up with the optical port holes mounted in the side of the vacuum chamber ($\lambda/10$ flat, fused silica disks mounted in an orientation to provide Brewster's angle incidence for both incoming and outgoing beams (see Figure V-3).

Three mechanical controls were brought into the vacuum chamber from the outside, for adjusting tilt in two dimensions and position (length of reference arm) of the reference mirror. Initial alignment of the system was made before evacuation; the fine adjustments were made under vacuum just before an experiment. The approximate 1-inch-diameter interference pattern was intercepted and viewed on the outside of the vacuum chamber.

The working arm of the interferometer was originally designed to accept hardware up to 16-1/2 inches in width (space across the 1-1/2-inch-diameter invar rods). This large cross-sectional separation was used to advantage during these measurements, even though the size of the copper vapor generator was less than 6 inches in diameter. The large amount of heat radiated from the combustor toward the invar rods would have severely interfered with the thermomechanical stability of the interferometer if an interferometer structure with much less seperation were used. A part of the empty space between the combustor-chimney arrangement (see Figure V-1) and the structural elements of the interferometer was filled with asbestos layers and metallic heat shield, while carefully avoiding obstruction of the approximately 1-inch-diameter beam. The heat insulating layers were carefully arranged not to get in physical contact with parts of the interferometer.

The portion of the optical instrumentation outside of the vacuum chamber consisted of a 50 mW argon ion laser operating at $\lambda = 5145$ Å mounted on a Gaertner optical bench and aligned with a Glan-Thompson polarizer, a 1-inch beam-expander/spatial filter combination and with the optical axis of the interferometer through one of the optical ports (Figures V-3, V-5). The receiving/recording end of the optical train consisted of an interference filter, its bandpass characteristic centered at $\lambda = 5145$ Å with a half bandwidth of 35 Å, a couple of beam folding optical elements one of which imaged the interference pattern onto the film exposed in the film frame of a 16-mm high-speed D.B. Milliken movie camera. The camera was operated at 400 frames per second with a shutter opening of 72 degrees. This resulted in frame exposure times of 1/2000th of a second. Kodak Tri-X reversal black/white 16-mm movie film was used (ASA 200). Optimum exposure of film under the above mentioned conditions required approximately 50 $\mu W\ cm^{-2}$ at $\lambda = 5145$ Å.

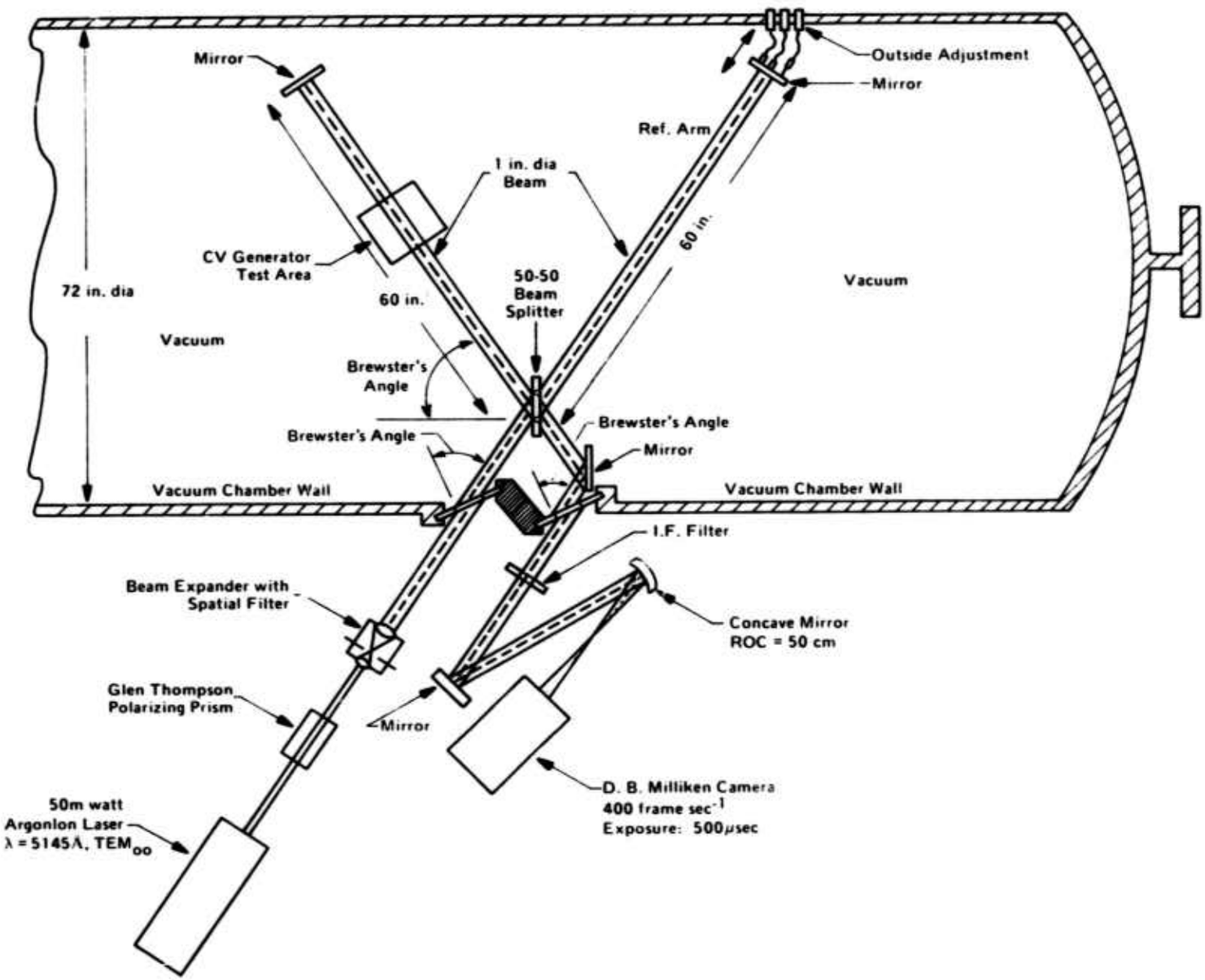

Figure V-3. Block Diagram of Experimental Arrangement of Homogeneity Test.

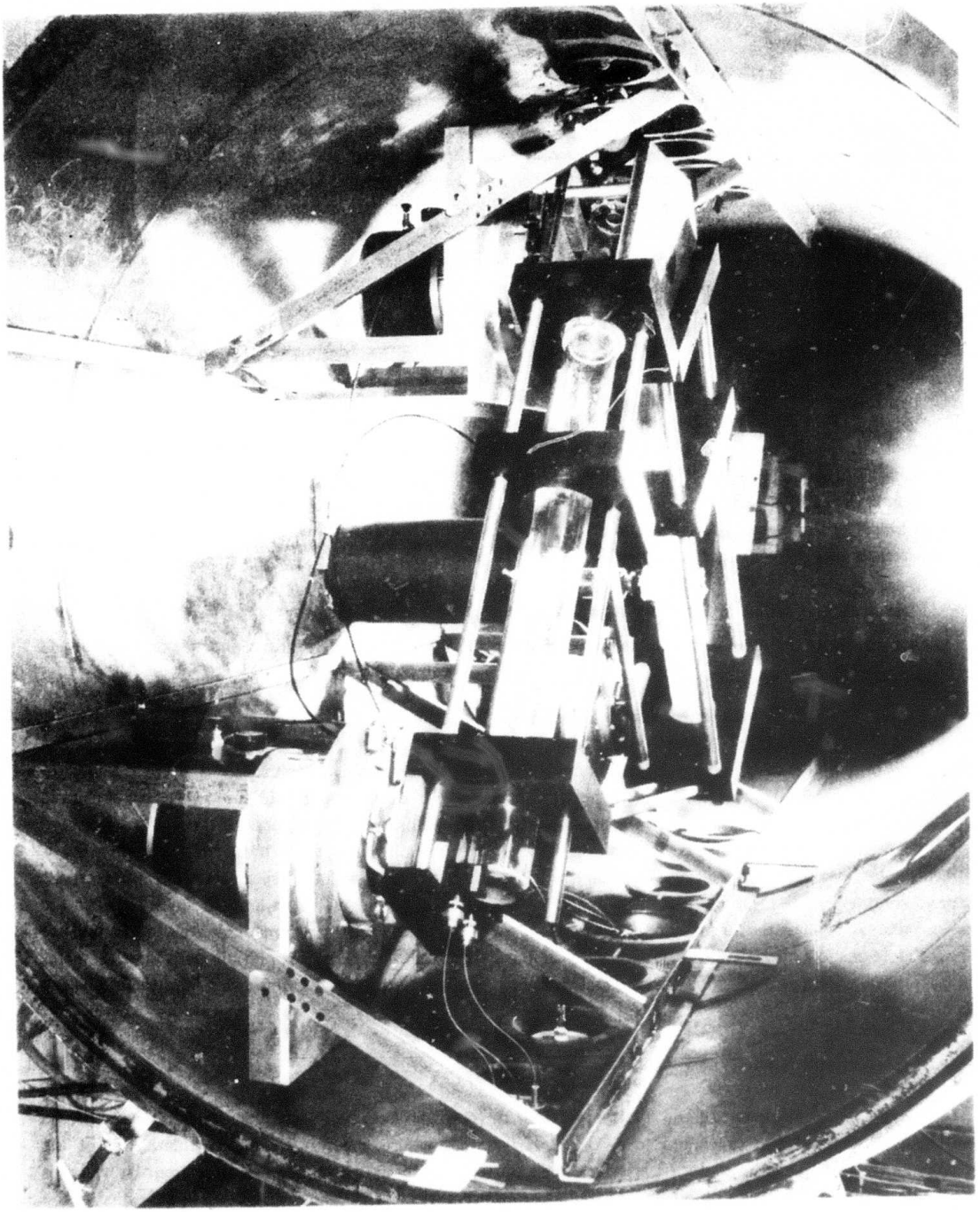

Figure V-4. Photo of Michelson Interferometer in Vacuum Chamber.

4. RESULTS AND DATA ANALYSIS

Due to characteristics of solid-fuel combustion which require pressures that are typically an order of magnitude higher than copper vapor/buffer gas pressures commonly desired and used in copper vapor lasers the combustion chamber must be choked as it is described earlier in Section IV. The main objective of the homogeneity tests then is to determine experimentally the effects of choking and subsequent expansion of gases, and also the effects of developing thermal gradients due to the presence of cold walls, etc. on the density variations of copper vapor/buffer gas mixtures. Since the partial pressure of the buffer gases is about one order of magnitude greater than partial pressure of copper, the recorded inhomogeneity of the medium is basically a measure of the density variation in the buffer gases. Density variations of the different constituents of the gases affect the Michelson interferogram the same way as they affect characteristics of a laser cavity.

The homogeneity measurements were performed over a 1-1/4-inch-diameter rectangular cross-sectional area through the mixture of hot gases and copper vapor approximately 5-1/2 inches above the nozzle of the combustion chamber. The choice of distance of the optical axis from the nozzle was dictated by opposing considerations. Shorter distances to the nozzle would have resulted in excessive turbulence and refractive index gradients due to the sudden expansion of the gases from a throat of 0.35 inch to cover 1 inch in diameter. On the other hand longer distances would have resulted in excessively cooled gases without copper, which would not have been characteristic of a copper vapor laser operation.

As described earlier in this chapter, ordered mass density variations in the range $0.03 < \frac{d\rho}{\rho} < 0.2$ could be detected with the Michelson interferometer depending on the value of ρ which in turn depends on pressure and temperature. In order to achieve the desired resolution of $\frac{d\rho}{\rho} = 0.01$ under all conditions of pressure and temperature one needs at least a 20-inch path length through the flowing medium. The alternate to constructing and testing a copper vapor generator with a 20-inch-wide flow field, i.e., using multiple path interferometry was not experimentally feasible under the present test conditions. Optical components had to be kept at large distances (30 inches in the experiments) away from the copper vapor generator and its flow field for obvious reasons, and stabilizing the long arms even in the case of the Michelson interferometer (only double passage through the medium) proved to be a very difficult problem. Even though the interferometer was built of invar rods, less than 0.2°C temperature change of the structure caused a complete fringe shift, that usually cannot be separated from the effects of medium inhomogeneities. Other difficulties resulting from the long arms include a long air space between the optical surfaces, and unless the air pressure at the arms are much below that of the volume under test, air turbulence may completely mask features of the flow-field inhomogeneities to be measured. A multiple path interferometer would have been even more sensitive to temperature and pressure variations, also vibrations, than the Michelson interferometer.

A typical homogeneity test ran as follows:

After initial alignment of the interferometer with the combustor hardware at atmospheric pressure, the vacuum tank was closed and evacuated to a couple of torr of pressure. Pressure to the pneumatic legs of the interferometer was readjusted to move the interferometer vertically to the proper position. The reference mirror was adjusted with remote controls to obtain the desired interference pattern with fringe visibility of near unity at the

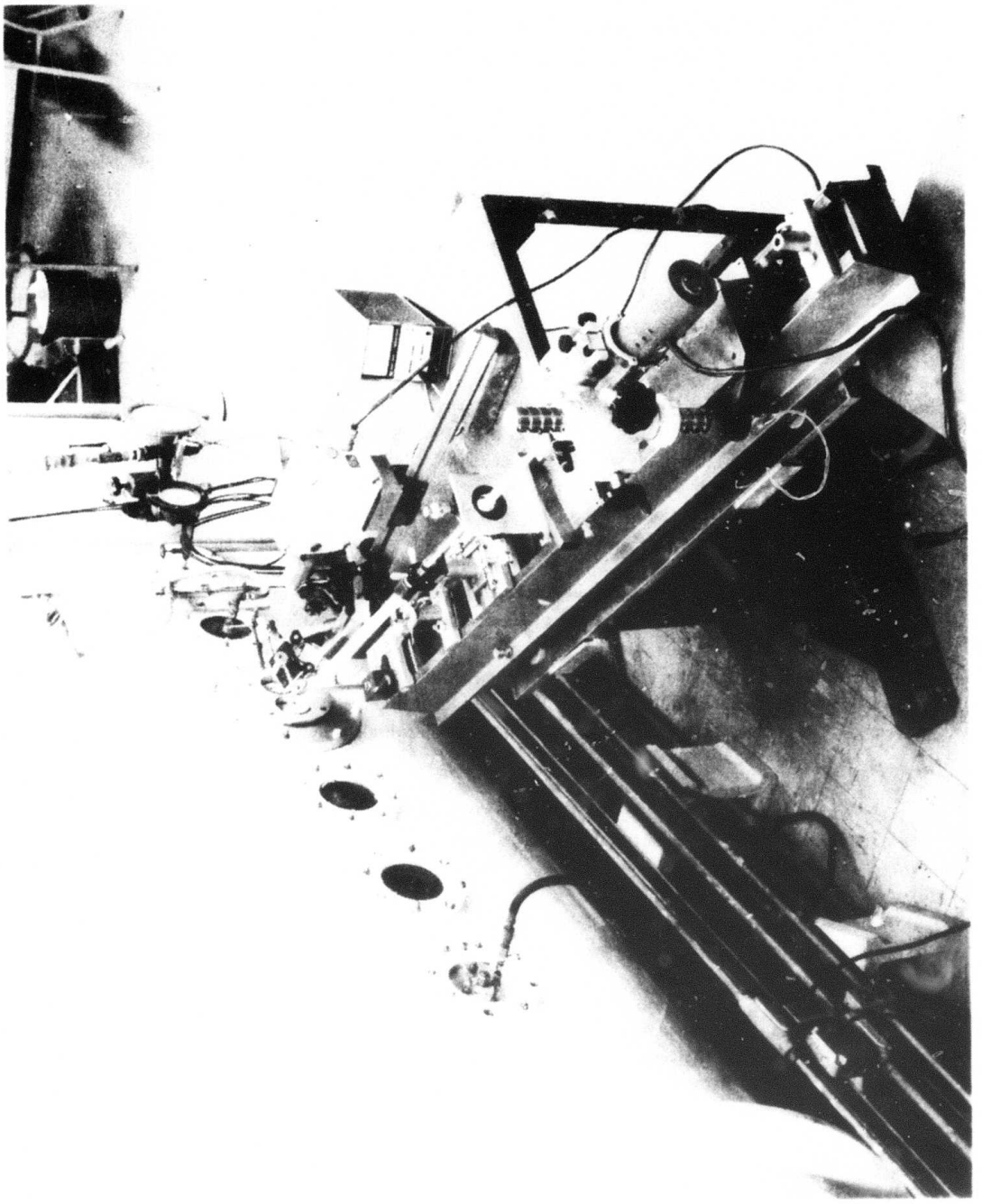

Figure V-5. Photo of Optical Setup Outside of Vacuum Chamber.

output of the optical train. A last check of the degree of vibration isolation is made by observing the stability of the interference pattern as a function of induced mechanical vibration (shock) on the vacuum tank wall. Typically interference pattern stability of ±0.1 fringe over periods of tens of seconds was achieved.

The intensity of the interference pattern at the high-speed movie camera was adjusted to 50 $\mu W\ cm^{-2}$ by using a rotatable Glen-Thompson polarizer on the polarized output of the argon ion laser. This power density was found empirically to give optimum exposure on the 16-mm film used.

The experiment cycle started with a sample exposure of the 16-mm film showing the interference fringes in a "before test" steady-state condition. A strobonar photo flash was used to mark events on the film by blanking one or two frames each time the flash was fired. This flash was used for instance to mark beginnings (or ends) of events such as turning on the hot argon gas, pushing the fire button, time of actual ignition, end of burn, etc.

Typically 200-foot rolls of black and white films were used in recording the time variation of the interference pattern, which at 400 frames per second provided approximately 20 seconds of recording time. Due to the brevity of recording time it was important to synchronize the different events closely so that a significant portion of the available 20 seconds would be spent on recording the homogeneity during burn. Even then several seconds in the beginning of the burn was used up by transients and rapid variations in density throughout the cross-sectional field of observation, which temporarily (for a couple of seconds) reduced the fringe visibility close to zero. (See "time table" on Figure V-6).

About 2 seconds after the camera started recording the steady state, undisturbed fringes, the hot argon gas was turned on (the argon gas heater was previously heated to its maximum temperature in anticipation of the argon flow). Four to five seconds later the grain was ignited electrically. The timing is critical in this arrangement because if the grain is heated too much by the hot gas, it can self ignite. Also, the burning characteristics of the solid fuel is altered as its temperature is raised. On the other hand, the argon gas has to flow long enough to preheat the hardware and to provide the appropriate pressure in the combustion chamber.

About 8 to 10 seconds of recording time is left for recording the interference pattern during actual copper vapor generation. The first 2 to 4 seconds of this time period is used up by thermal and pressure transients which are characteristic of the startup of burning of a grain. (See pressure curve superimposed on the time table in Figure V-6.)

The last 4 to 6 seconds of the recording (about 2000 frames) illustrates typical homogeneity of the beginning of a steady state burn which may last typically between 30 to 60 seconds.

Figure V-7 shows 4 sets of interferograms taken at times as indicated by A, B, C and D in Figure V-6. The interference fringes on inset A characterize the quality of the interferometer itself. The approximately $\pm 0.15\lambda$ variation of the fringes in the center of the field is mostly due to inhomogeneities in the fused silica blank of the beam splitter. (Surface flatness of mirrors, windows and the beam splitter used in the optical train is better than $\pm 0.05\lambda$.)

Secondary fringes, superimposed on the primary fringes (best shown in inset C where the fringe visibility is reduced) are due to Fresnel reflections from the 2 surfaces of the interference bandpass filter which had to be used to reduce to negligible levels the unwanted exposure of the film by the bright flame of the copper vapor generator.

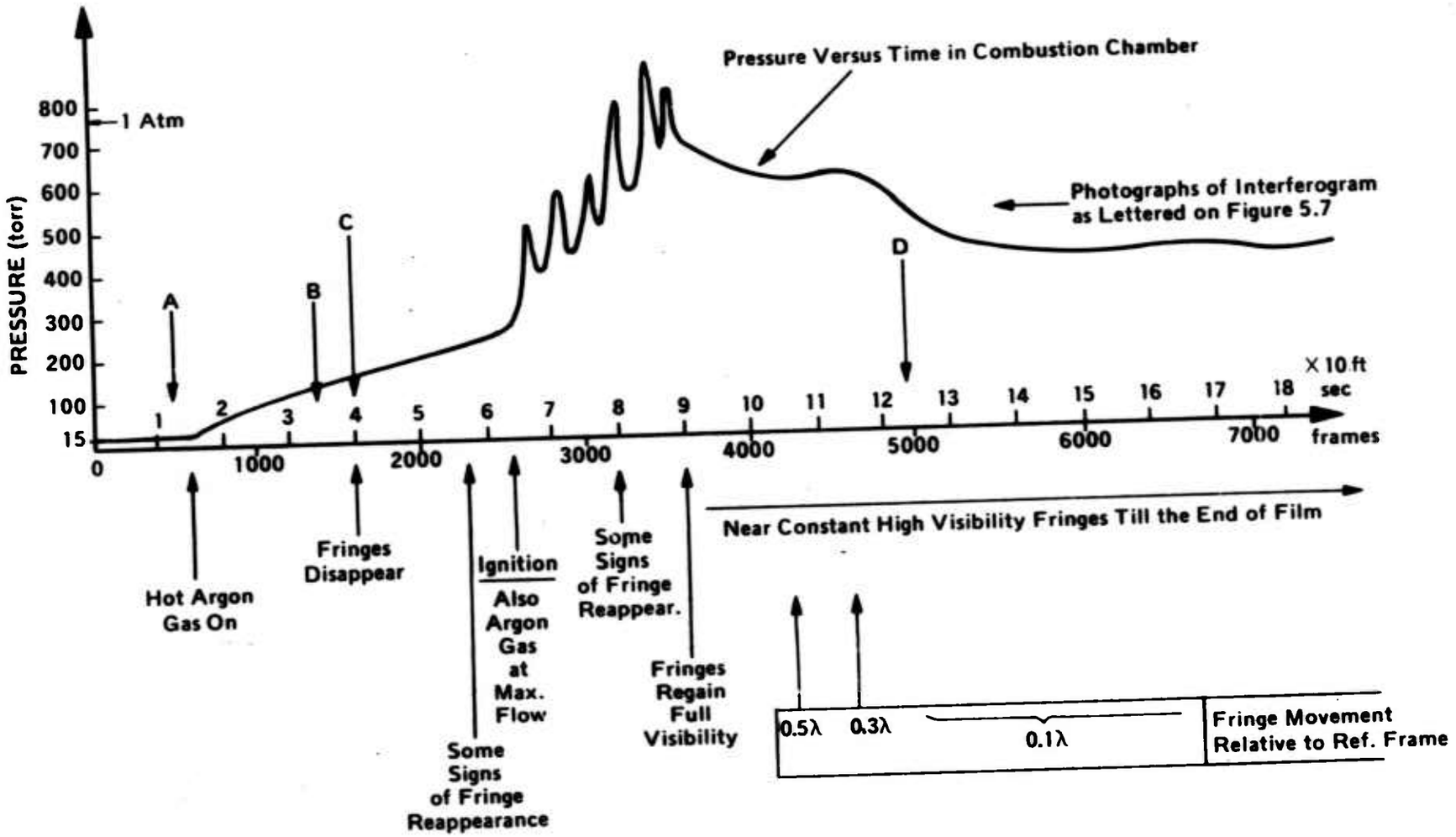

Figure V-6. Interferogram Scenario of a Typical Copper Vapor Generator Firing. A Milliken 16 mm Movie Camera is Used, Recording in the 400 frames/sec Mode.

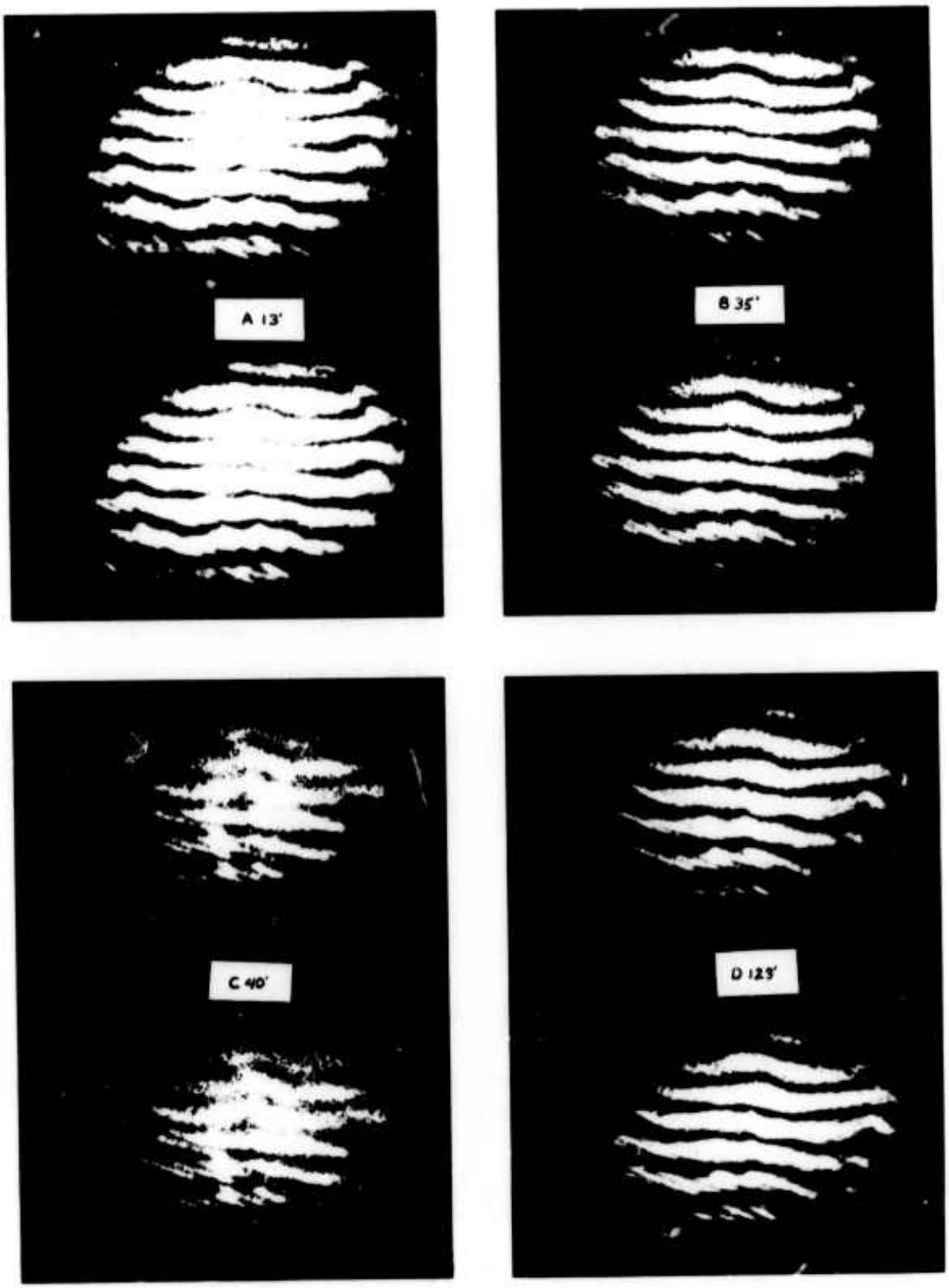

Figure V-7. Interferograms A, B, C and D Exposure Time 5 0 μsec Through IF Filter Centered at λ = 5145 Å, BW = ± 35 Å.

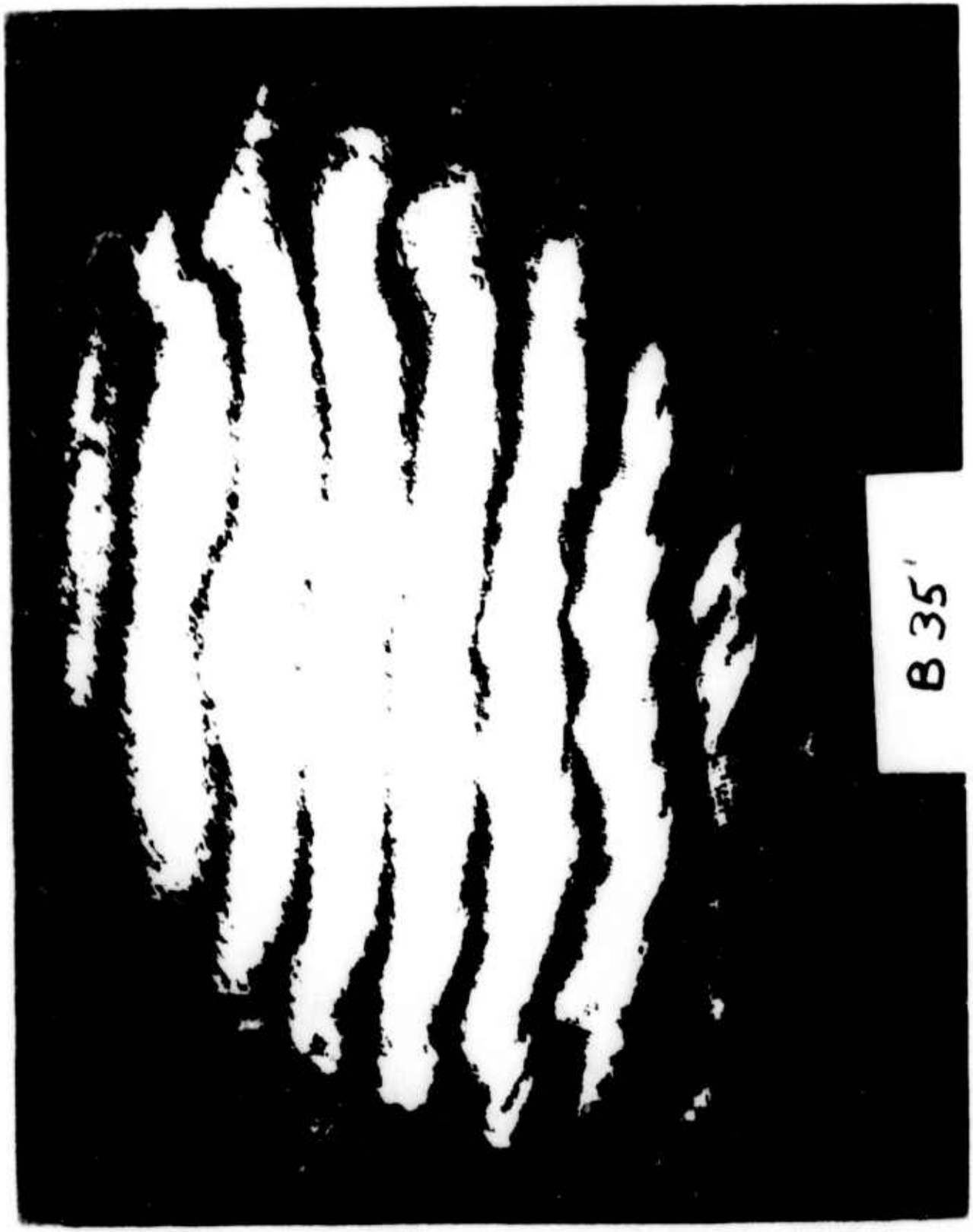
B 35'

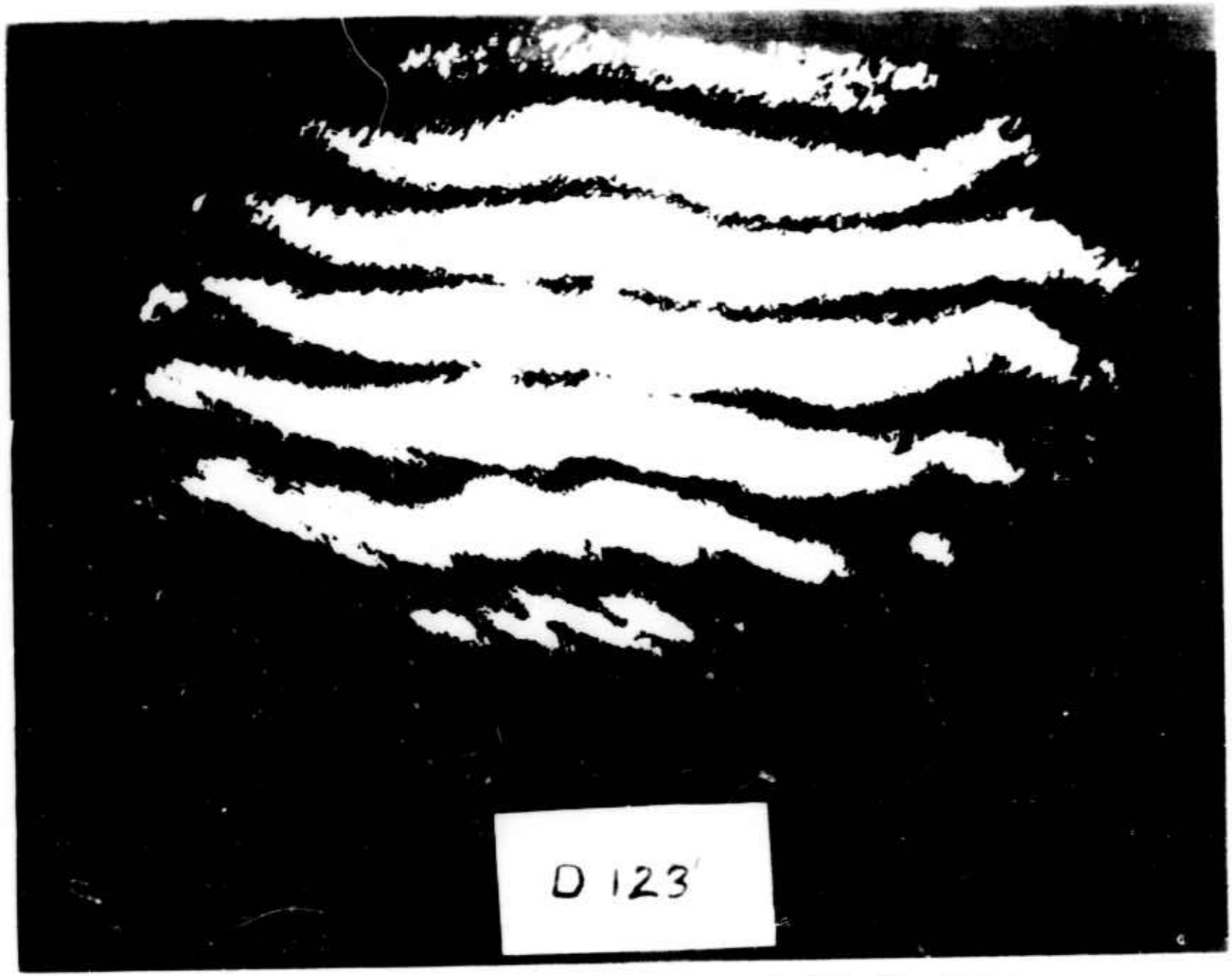

Figure V-8. Overlay of Two Frame Fields of Interferograms, One Taken Before the Burn (Inset B on Figure 5.7) and One Taken During Burn (Inset D on Figure 5.7).

Two adjacent frames on the 16-mm film are shown in each of the four insets, to illustrate the frame to frame repeatability of the interferograms even in the case of inset C which was recorded at a time of rapidly varying densities of mass (or refractive index).

Some movement from frame to frame of the image of the interference pattern was observed with respect to the frame, which is attributed to faulty frame-to-frame registration in the camera.

Fringe movement relative to this moving reference frame is shown as a function of time in Figure V-6. The last, approximately 6 seconds of recording shows a fringe movement of about 1/10 of a fringe. This is about the noise level of this instrumentation which means that optical path difference variations in the cross-sectional plane per double pass is $\lambda/10$ or less. In other words, using the same geometry, i.e., optically active medium length of 1-1/4 inches in a laser cavity, output beam distortions due to medium inhomogeneities would be less significant than beam distortions due to imperfections that are usually present in components of an optical cavity.

Larger intracavity volumes of copper vapor/buffer gases, as are anticipated in scaled-up versions of the copper generator require more stringent requirements on allowed levels of $\frac{d\rho}{\rho}$. On the other hand, the accuracy and resolution of the above used method to determine homogeneity of the flow, also increases proportionately with the length of the optical path through the volume to be tested. In other words, when larger volumes and cross-sections of copper vapor flows will be built, their homogeneities can be tested to the increased requirement on homogeneity.

In Figure V-8, two enlarged interferograms, one taken before the burn (inset B on Figure V-7) and one taken during burn (inset D on Figure V-7) are compared, by superposition. Phase distortions are seen within $\pm 1/10$ of a fringe over the major part of the interferogram.

Homogeneity of the flowing gases was not studied under electrical discharge conditions, because this was outside of the scope of the present work.

SECTION VI

SIMULATED FLOW TESTS

The static CVL apparatus at PIB, which is shown in Figure II-9, had to be modified in two ways to accommodate flowing copper vapor generated by a solid-fuel propellant along with combustion product gases.

a. A ballast volume and an increased pumping capacity were added to the apparatus so that the large volume of gases generated by the burning propellant could be accommodated without a significant pressure increase in the laser cavity.

b. To keep combustion products from depositing on the windows, the axis of the optical cavity was rotated 90 degrees making it perpendicular to the gas flow as indicated in Figure VII-1.

Accomplishment of the second requirement was complicated by the presence of the furnace heating element. The furnace was not required for the final propellant tests; however, inclusion of a furnace enabled an additional series of simulated propellant experiments to be carried out. Tank gases were used to generate the expected mixture of combustion product gases which flowed over molten copper upstream of the laser cavity simulating the expected propellant conditions except for the flow velocity.

The initial BTTN propellant design figures indicated a gas generation of 570 liters/sec at 30 torr and 2000°K for 20 seconds producing a total gas volume of 1710 liters at 300°K. Installation of a 3-foot-diameter by 6-foot-long dump tank (1175 liter volume) and a 150 CFM Kinney pump (20-second pumping volume at 30 torr of 1320 liters) provided sufficient capacity to hold the final pressure in the laser cavity below 30 torr. The final NIBTN propellant designed for burning at 310 torr (Tables IV-4 and IV-5) were expected to generate 3.8373 moles of gas at the equilibrium temperature of 2628.5°K or 3.5378 moles at a reduced temperature of 2200°K. Since the copper condenses on the walls, this corresponds to a final gas pressure of 27 torr at 300°K. The pressures measured during the final propellant tests (Table VII-1) were consistent with this expected pressure.

The more difficult modification was the establishment of an optic axis perpendicular to the gas flow direction. When holes were cut into the alumina tube to permit a light path through gaps in the graphite heating element, as indicated in Figure VII-1, an opportunity was provided for the discharge to short the graphite heating element instead of continuing to the opposite electrode. This situation was overcome by:

a. Placing transverse alumina tubes against the longitudinal alumina tube; the ends of the transverse tubes were cut to fit the 2-inch O.D. of the longitudinal alumina tube.

b. Using boron nitride washers around the ends of the transverse alumina tubes to reduce further the channel through to the heating element; these washers were also cut to fit the 2-inch O.D. of the longitudinal alumina tube.

c. Shifting the circuit ground so that the anode was a few hundred volts below ground instead of at ground; in this way it was possible to establish transverse discharges.

Longitudinal discharges were also operated; however, Step (c) could not be carried out in this case because of the direct electrical connection for one longitudinal electrode to the dump tank. The I.D. of the transverse alumina tubes was 0.47 inch while that of the longitudinal was 1.75 inches.

For the simulated flow experiments, a short heating element was used which displaced the center of the hot zone 1.825 inches upstream of the center of the laser cavity. At this location 40 mg of copper was placed, leaving a spacing of approximately 1 inch between the end of the copper pile and the closest part of the optical cavity. For these tests a smaller 140 liter/min Welch pump was substituted for the 150 CFM Kinney pump. A portion of the gas flow was directed into each transverse tube to prevent copper from depositing on the windows. The flat-flat optical cavity consisted of an opaque aluminum mirror ($\sim$85 percent reflectivity) and a 61 percent transmitting beam splitter for output coupling.

Laser action was observed with transverse electrical excitation but not with longitudinal. With either argon or the expected combustion gas mixture, the laser output reached a maximum when the gas flow rate was $\sim$ 7 liters/min. At flow rates below this value, the copper density decreased because of a reduction in the transport of higher density copper vapor pressure available upstream. Above flow velocities of about 7 liters/min, the flowing tank gases provided sufficient cooling of the copper to again decrease the copper density. Figure VI-1 shows a laser pulse obtained with about 7 liters/min of argon flowing over the molten copper. The peak power was about 1 kW with a half width of 10 nsec. When the argon flow was stopped, the amplitude of the laser pulse fell to 1/3 of this value. The detection system consisted of a TRG 105B vacuum photodiode coupled into a Tektronix 519 oscilloscope.

To investigate the effect of background pressure in the laser cavity on the laser output, the pump was throttled down. The results are shown in Figure VII-2. They are generally in agreement with the additive gas tests conducted in the static CVL and shown in Figure III-3. The argon curve is not as flat as it is in Figure III-3 because of a reduction in the transport of copper vapor as the background pressure increased. One general conclusion of these experiments is that the background pressure of combustion product gases should be limited to 3 torr for optimum propellant-generated CVL performance in this apparatus.

Due to the nature of this apparatus, the mass flow was far less than the predicted propellant mass flow, and the partial pressure of copper could not be accurately determined and controlled. However, these simulated flow experiments show that CVL action can be produced in the environment of the combustion product gases from a solid-fuel propellant containing copper. An output power of 7.7 mW was measured at 2 torr from a 5 cm^3 active volume. The specific pulse generation density was 2 $\mu J/cm^3$ (2 mJ/liter). As indicated in Table II-1, this compares favorably with the results of all other flowing CVL to date, (AVCO 8 mJ/liter, JPL 2.5 mJ/liter, GE 1.7 mJ/liter, UA 1.5 mJ/liter) particularly since, in our case, the flowing gases were not saturated with copper vapor. Use of a pebble bed heater to saturate the flowing gases would have increased the 2 mJ/liter measured value.

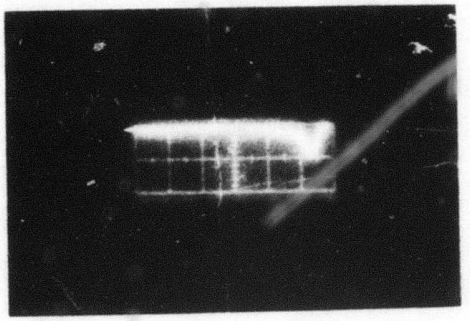

Figure VI-1. Laser Pulse from Transverse Excitation with Flowing Argon. Horizontal scale is 20 nsec/large division. Peak power is approximately 1 kW.

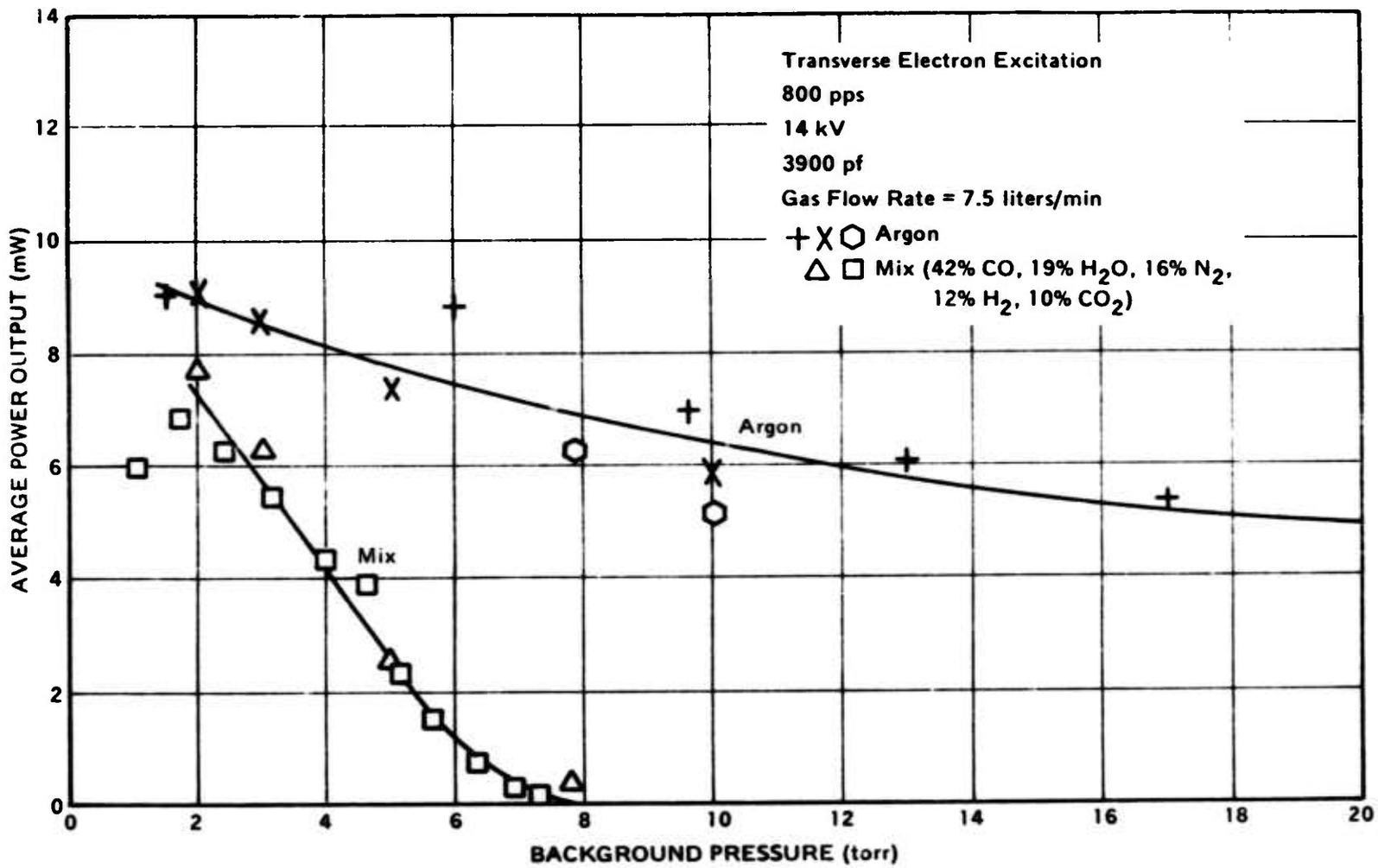

Figure VI-2. Simulated Propellant Copper Vapor Laser.

SECTION VII

PROPELLANT-GENERATED FLOW TESTS

Final testing of the gas generator coupled to the CVL apparatus modified to accommodate flowing gases took place at PIB (see Figure VII-1). Four tests were made, each with the result that neither fluorescence nor laser action was observed at 5106 Å. The fact that green fluorescence was not observed means that the copper vapor density was very low. This fact was verified in the fourth test where an absorption measurement revealed that the density of copper atoms was on the order of 10^{12} atoms/cm^3 in the discharge region.

The experimental arrangement for testing the solid-fuel copper vapor generator is shown in Figure VII-1. The gas generator assembly was attached to the CVL apparatus in which the electrical excitation axis coincided with the optic axis, both being transverse to the direction of flow. The CVL apparatus was located inside a graphite heating element which could be turned on to prevent condensation of copper on the alumina walls.

Ignition of the NIBTN solid-fuel propellant formulation was difficult at pressures less than 20 torr. This situation was remedied by flowing preheated argon through the generator to produce an initial pressure of approximately 200 torr. The argon flow was cut off after initiation of the burn. Current flow through the Kanthal wire raised the temperature of the grain surface sufficiently to initiate the burn. The Kanthal wire melted and open circuited approximately halfway into the burn for all tests.

Pressure and temperature of the generator was monitored by a strain-gauge pressure transducer and a platinum-20 percent rhodium/platinum-40 percent rhodium thermocouple, respectively. Because of conduction losses, the thermocouple did not indicate the true gas temperature. Instead the temperature versus time data was used to evaluate test-to-test reproducibility rather than to measure the value of the gas temperature. Downstream pressure was monitored by a Veeco DV4M thermocouple pressure gauge and a Wallace/Tiernan absolute manometer. The time development of the gas generator pressure during a test is shown in Figure VII-2.

The electrical circuit used to create a discharge in the flowing gas consisted of a 3900 pF capacitor charged to 15 kV and applied to transverse molybdenum wire electrodes by a fast hydrogen thyratron. The pulse repetition rate was 1000 pps.

The optical cavity configuration consisted of an opaque aluminum-coated front-surface mirror (reflectivity – 85 percent) and a 61 percent transmitting output coupling beam splitter, both of which were flats. An interference filter and a 1P28 photodiode were used to monitor the fluorescent output at 5106 Å on the visicorder. Beam splitters coupled part of the light output to a TRG 105B vacuum photodiode, the output of which was applied to a Tektronix Model 519 oscilloscope fitted with a Polaroid camera. The camera was operated in bulb position during each test. The oscilloscope would have been triggered only by presence of a light pulse to record the laser pulse shape. The fluorescent output was also monitored visually.

The following parameters were recorded as a function of time on a visicorder:

a. Generator pressure

b. Downstream pressure

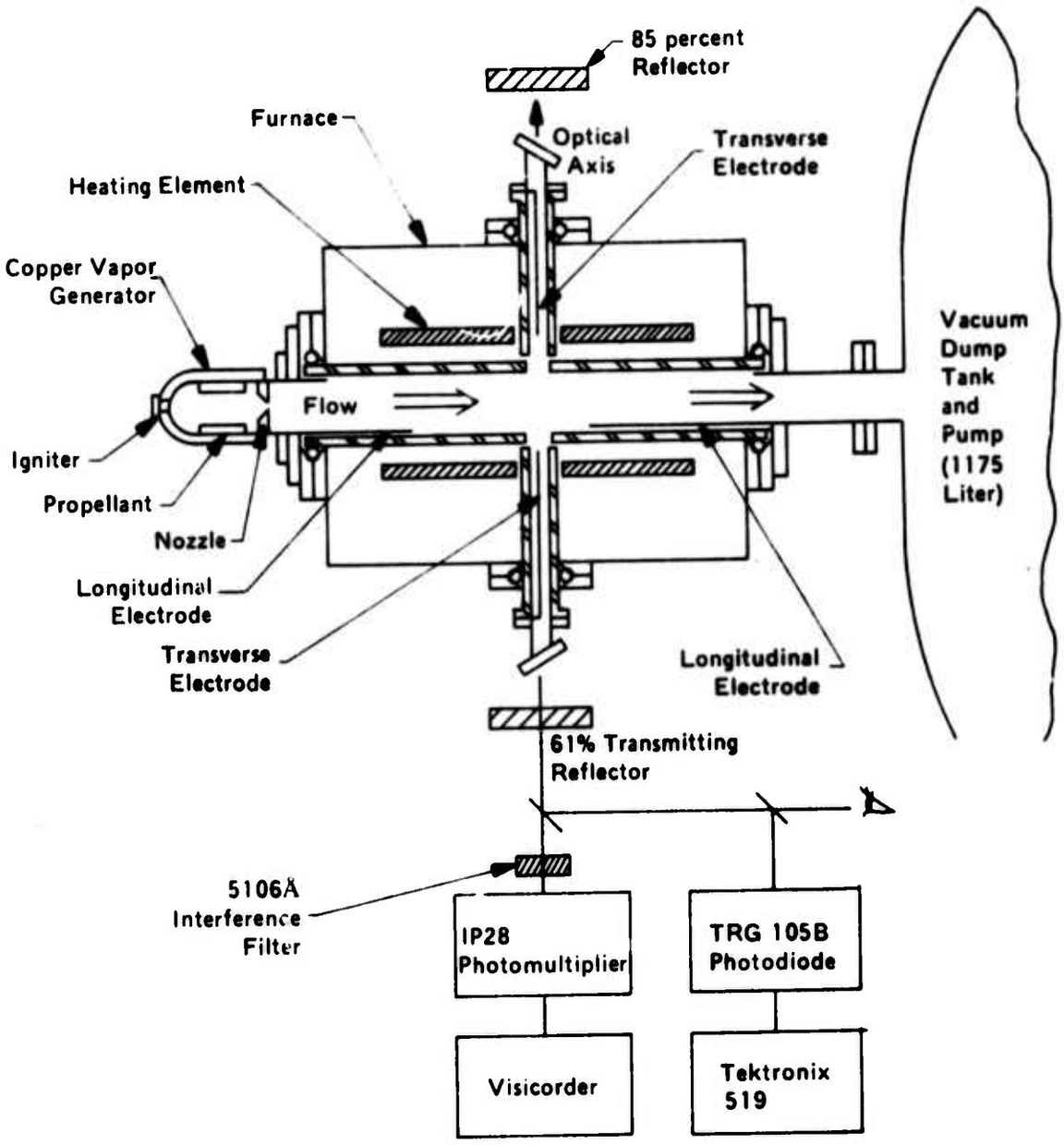

Figure VII-1. Test Apparatus for Investigation of Laser Action Using Solid Fuel Propellant Gas Generator.

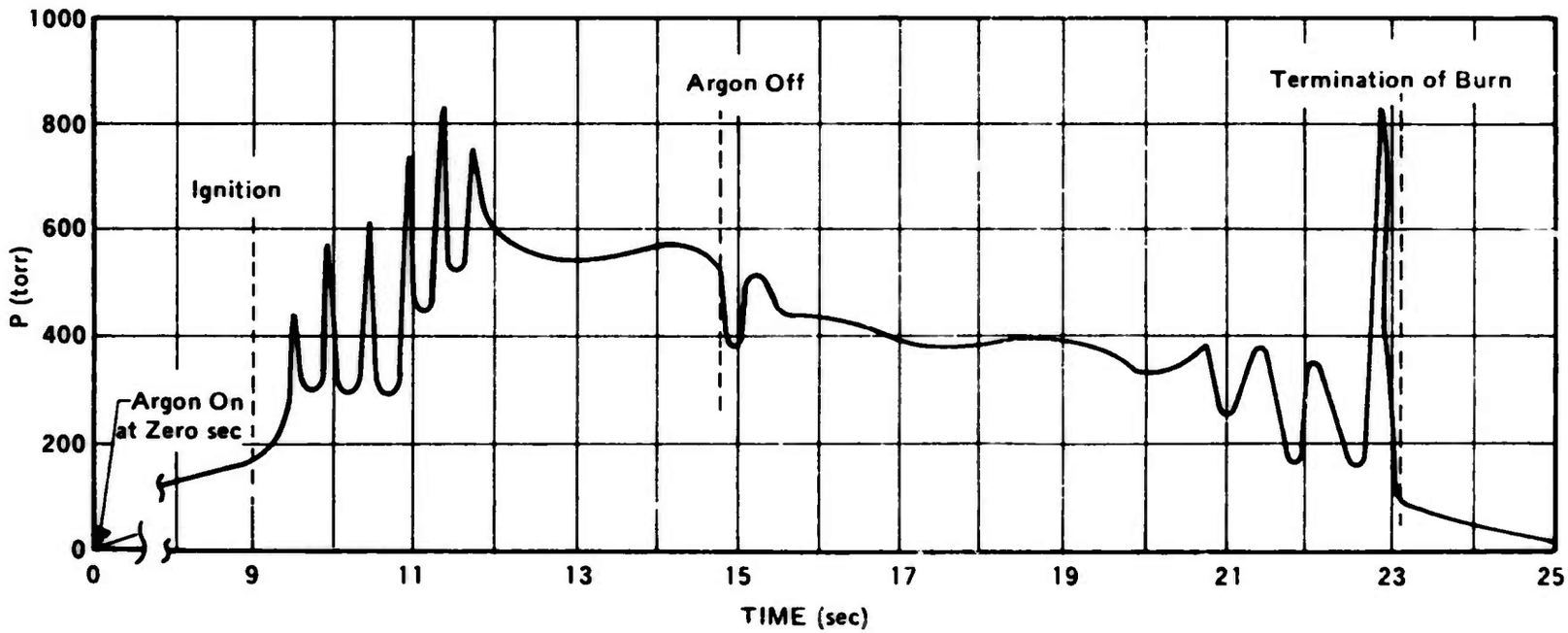

Figure VII-2. Gas Generator Pressure Versus Time (Test No. 3).

c. Generator temperature

d. Fluorescent output at 5106 Å

A summary of the conditions and results for the four tests is given in Table VII-1. Test No. 1 was carried out with the furnace turned off. During this test the Kanthal wire initiator pulled free from its electrical pin connectors and moved into the throat where 3.5 grams of copper deposited onto it. The copper deposited did not have the smooth surface that is characteristic of copper which had been melted. Instead, most of the copper on the Kanthal wire had a very irregular granular appearance as if it had been sintered onto the wire at a temperature somewhat below the melting point of copper, 1083°C. Although the Kanthal wire did not pull free during the subsequent tests, copper was found on the Kanthal wire after each test in smaller quantities as indicated in Table VII-1. The vaporization of the copper seed particles is discussed in Section VII-2.

No green fluorscence was observed during the first run. There was no evidence of any substantial deposit of copper on the alumina tube connecting the gas generator with the laser cavity. However, to minimize the possibility of copper condensing there, the furnace was turned on and operated at ~1200°C during Tests No. 2 and No. 3. Again no fluorescence at 5106 Å was observed, neither with the photomultiplier, nor with the photodiode nor visually. Therefore an absorption measurement was carried out during Test No. 4 to determine the density of copper produced in the laser cavity. This is described in the next section, VII-1.

1. COPPER DENSITY MEASUREMENT

An absorption measurement of the 3274 Å resonance line of copper was carried out during Test No. 4 to determine the density of copper in the laser cavity. A Westinghouse WL22603 copper hollow-cathode lamp was substituted for the 85 percent reflector in Figure VII-1. A 1/2-meter Jarrell-Ash spectrometer with a 1P28 photodetector was substituted for the 61 percent transmitting reflector. Lenses were used on each side of the flowing gas apparatus to produce a collimated light beam through the optical cavity and then to focus it on the entrance slit of the spectrometer. The 3274 Å copper resonance line was used. In retrospect, however, the 3247 Å line would have been preferable because the presence of a weak copper line at 3280 Å from the hollow cathode lamp produced ~2 percent of the signal at 3274 Å.

During the propellant burn of Test No. 4, the maximum absorption measured was 95.8 percent. If a single component with a Doppler line shape is assumed, the transmitted intensity is given by

$$I_{\text{transmitted},\,\nu} = I_{\text{incident}} \cdot e^{-\alpha(\nu)x}$$

where x is the thickness of the absorbing layer ~ 5 cm and at line center

$$\alpha(\nu = \nu_0) = \frac{\lambda_0^3}{8\pi} \frac{g_2 A N}{g_1} \sqrt{\frac{M}{2\pi kT}}$$

Table VII-1. Propellant Test Results.

Test Run No.	Gas Generator Pressure*	Gas Generator Temp	Laser Cavity Pressure	Laser Cavity Temp	Burn Duration	Fraction of 100 gm Propellant Not Burned	Remarks
1	520 torr	820°C		25°C	30 sec		Kanthal wire initiator pulled free, moved into throat, 3.5 gms copper sintered on it Argon on throughout run
2	300 torr	878°C	25 torr	1200°C	19 sec	.545	Unstable burn - chuffing Argon turned on a second time Pressure fluctuations Balls of Cu on Kanthal wire
3	300 torr	820°C	15 torr	1275°C	13 sec	.61	1 gm of Cu sintered on Kanthal wire
4	300 torr	1066°C	25 torr		20 sec	.40	Copper absorption measurement Absorption of 3274Å = 95.8%

*Average pressure after argon was turned off.

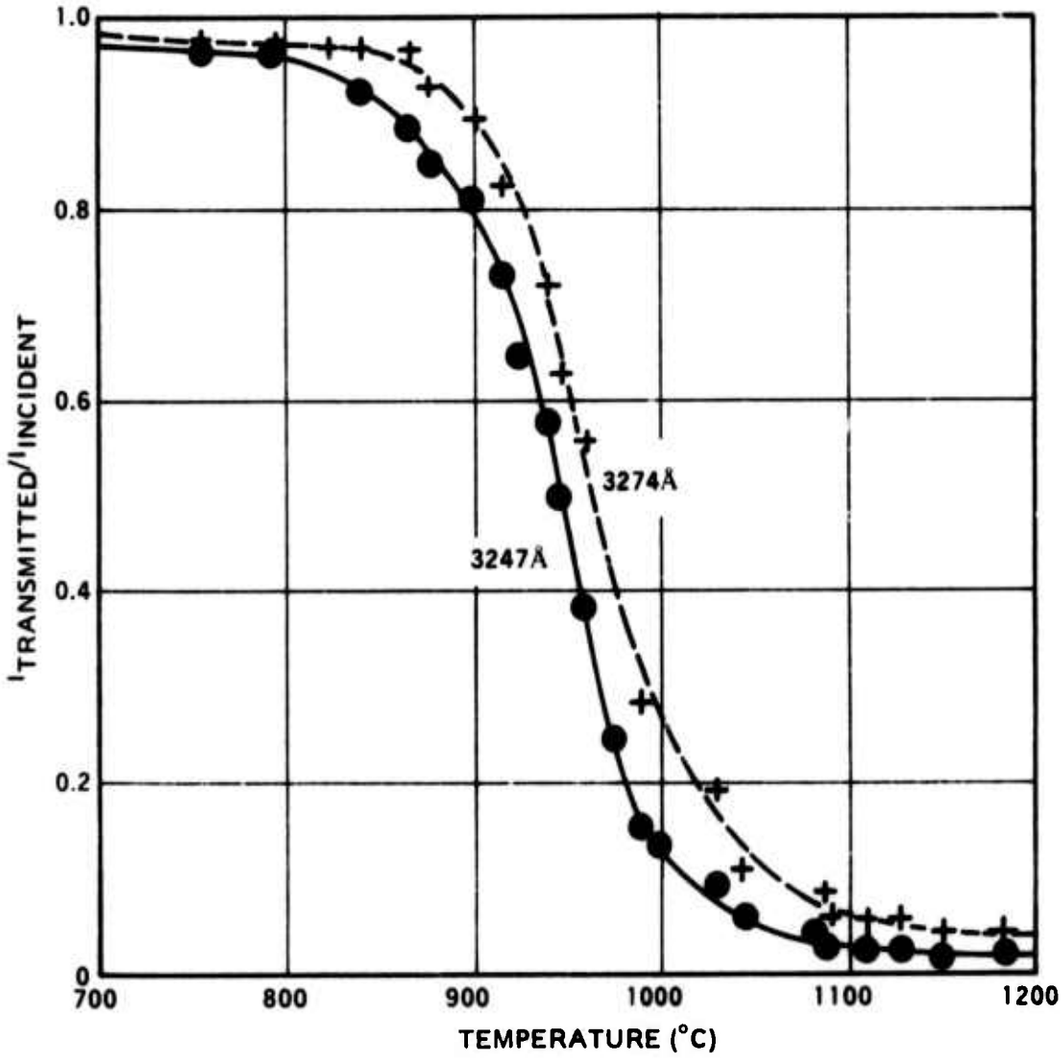

Figure VII-3. Copper Absorption Calibration.

where quantities have already been defined in Section IV. For a transmission of 4.2 percent at a temperature of 1400°K, this corresponds to a copper density

$$N \sim 1.4 \times 10^{12} \text{ atoms/cm}^3$$

which is in agreement with the estimate above.

These results indicate that the copper density produced by the copper-seeded solid-fuel propellant was $\sim 10^{12}$ copper atoms/cm^3 in the laser cavity — only 1/1000 of the expected density. In addition, copper was found sintered on the Kanthal wire initiator as described in Table VII-1 and the accompanying discussion at the beginning of Section VII. This suggests incomplete vaporization of the copper seed particles. This could be caused by a low flame or combustion gas temperature or insufficient residence time within the gas generator. The latter of these possibilities is examined in the next Section, VII-2.

2. COPPER GRAIN SIZE AND TIME REQUIRED FOR VAPORIZATION

Microphotographs of the copper particles used to seed the solid-fuel propellant are shown in Figure VII-4, and a particle size distribution by weight is given in Figure VII-5. The majority of particles were irregularly shaped and had a rough texture. The particle size distribution was fairly wide, the diameter ranging from <9 to >90 microns. The median particle size was 31.7 μ while the weighted average particle size was slightly larger, ~ 35 microns. Approximately 2.2 percent of the sample was 10 microns or less in diameter.

In order to estimate the time required to heat and vaporize a copper particle, a theoretical model was developed which is presented in Appendix II.

The conclusion is that there was insufficient vaporization of the copper seed particles. Probably less than 1 percent of the copper was vaporized. This can partially account for the negative results. From the data in Table IV-2, the propellant was expected to produce 3.56 moles of other gases in addition to the 0.276 mole of Cu vapor. If only 1 percent of this copper were vaporized, then a copper density of 5×10^{13} cm^{-3} would be produced at 15 torr and 2220°K in the laser cavity. Such a density is less than the 10^{14} required for the threshold of laser action. This density is approximately 50 times larger than the 10^{12} cm^{-3} coppe. density measured (Section VII-1). It indicates that the fraction of copper vaporized was probably closer to 0.1 percent. This reduction could be caused by the problems discussed in Section IV.

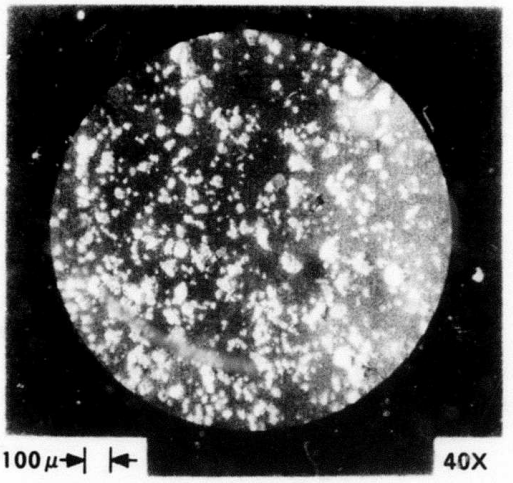

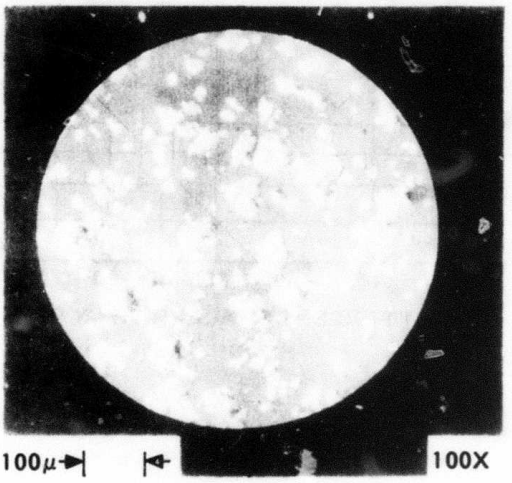

Figure VII-4. Microphotographs of the Copper Seed Particles.

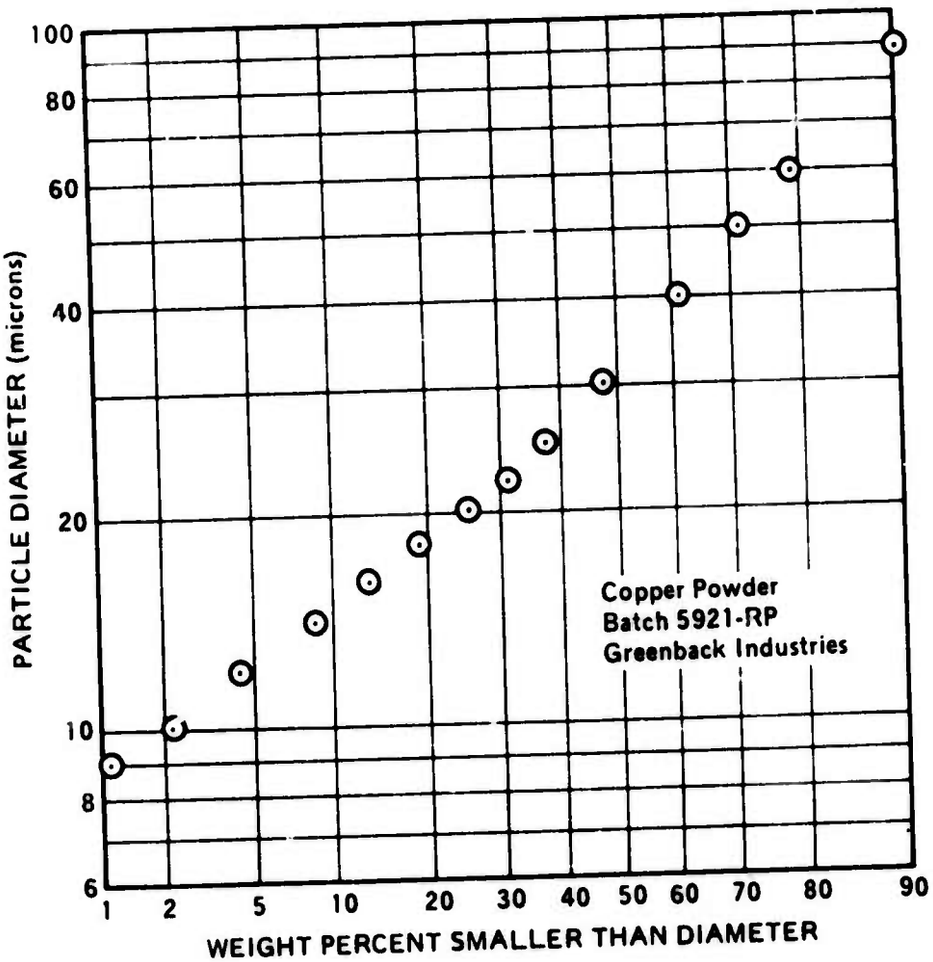

Figure VII-5. Seed Particle Weight Distribution;

SECTION VIII

CONCLUSIONS AND RECOMMENDATIONS

The objective of the present contract work was to develop and demonstrate the concept of using chemical energy for efficiently generating appropriate quantities and densities of copper vapor which is suitable for use in a flowing copper vapor laser. At the conclusion of this work the following observations and recommendations are made:

1. If overall electrical efficiency is of importance, chemical generation of copper vapor is the most promising approach, which should receive continued emphasis in the development of flowing copper vapor systems. In a system, where electrical energy is used to vaporize copper, a substantial portion of the total input electrical energy must go towards vaporizing the copper (approximately 3.86 eV input energy is required to vaporize each copper atom at 1800°K). Further, in a flowing system this invested energy is lost after a single encounter of the copper atoms with the discharge region and optical cavity. In fact, less than one out of five copper atoms complete the lasing cycle because of a large collisional-mixing cross section between the upper and lower laser levels. In a flowing CVL system, therefore, the only approach capable of realizing the potential high inherent efficiency of the CVL has to take advantage of chemical generation of copper vapor.

2. It was experimentally demonstrated, that a steady flow of copper vapor can be generated by burning copper powder loaded solid fuels. Measured values of copper vapor densities produced this way inside the laser cavity were typically 10^{12} copper atoms/cm^3, about 4 orders of magnitude below the analytically predicted densities. A study of the dynamics of copper vaporization under these conditions revealed that one of the causes of the unexpectedly low densities in the discharge/optical cavity region is due to the relatively large sizes of the individual copper particles dispersed in the solid fuel. The 30 micron diameter copper particles used in the tests carried out thus far were too large to completely vaporize during the available residence time within the gas generator.

3. It was shown that the optical homogeneity of the flowing hot diluent gas/copper vapor mixture at the optical cavity was acceptable for laser operation considering the length of the optical path (L = 1.25 inches). Under varying conditions, it was shown that the integrated mass density variation, $\frac{d\rho}{\rho}$, across the cross-sectional area of observation was less than 3 percent (cold, high-pressure condition) and less than 20 percent (hot, low-pressure extreme), and in all cases, the measured values were limited by resolution and accuracy of the instrumentation (Michelson interferometer). Higher resolution would be available with longer optical path lengths.

4. Experimental results show that even though lasing is possible in the presence of diluent gases that are typically generated by the most common (least expensive) solid fuels, at least some of the gases are sufficiently detrimental to the laser performance (efficiency, power output) to warrant an effort to demonstrate the chemical copper vaporizing concept with more exotic fuels that have only very small amounts of H_2 and H_2O (the two most offending gases) in the exhaust products. A hydrogen-free propellant system could be produced as indicated in Section IV by utilizing alkali metal salts, particularly the perchlorates for oxidizer or through the use of nongaseous

systems as discussed below and in Appendix I. The hydrogen-free systems produce alkali halide vapors such as KCl or LiCl as part of the combustion products. Before producing these propellant preparations and subject them to ballistic and other tests, it is necessary to determine the effects of alkali halide vapors on lasing.

5. Chemically generated copper-only and copper-rare gas systems should be investigated. The addition of each molecular gas examined (N_2, CO_2, CO, H_2, and H_2O) degraded the output power of a static CVL as indicated in Figures III-2, III-3, and III-4. The addition of argon, however, did not. Consideration should be given to systems in which the combustion products do not enter the laser cavity. Thermites are one approach, and the thermochemistry of several thermite systems is described in Appendix I.

6. As described in Section III, it was found that higher temperature operating condition (higher copper vapor density) is more tolerant of the detrimental effects of diluent gases. This finding is of particular significance for chemically generated systems, where higher cavity total pressures will make the difficulty of stably and predictably burning solid fuels less severe.

7. Even though not a part of the objectives of the present contract, a better understanding of the fundamental problem of matching into a rapidly varying load impedance is needed in order to gain control of excitation parameters.

The results of this effort clearly show the need for future CVL work to be conducted in a test equipment, which is capable of

a. Generating high copper densities (possibly through high laser operating temperatures)

b. Transmitting the electrical excitation energy through a smooth, high temperature and low impedance transmission line to the electrodes and to the discharge region

c. Accepting a wide variety of electrode and optical configurations

d. Providing good coupling (matching) of the electrical energy into the discharge

e. Handling flowing as well as nonflowing copper vapors.

APPENDIX I

GENERATION OF Cu(g) BY MEANS OF THERMITES

It is of interest to generate Cu(g) undiluted by other gaseous species. This means that hydrocarbon propellant systems, which generate water-gas and N_2 as combustion products in addition to the heat liberated to vaporize and disseminate Cu cannot be considered here. Pyrotechnic compositions that do not generate gas are called thermites, and it is proposed that these types of compositions be modified by the addition of Cu or Cu compounds (especially Cu oxides) to result in the generation of Cu(g) as the only gaseous combustion product. In this concept, Cu(g) is generated and disseminated from the motor chamber, while the condensed combustion products are retained as slag. Described below are two types of compositions of greatest interest, the first concerning generation of Cu(g) as the only gaseous combustion product, and the second concerning generation of Cu(g) as the major gaseous combustion product. For simplicity of discussion, compositions are designed for a flame temperature of 2000°K, which corresponds to a vapor pressure of Cu(g) equal to 2.94 torr.

TYPE I THERMITES

One of the best types of gasless thermites are stoichiometric mixtures of tungstic oxide, $WO_3(c)$, as the oxidizer, and either Zr, Al or Mg as fuels. The equilibrium combustion products of these mixtures are W(c), and either $ZrO_2(c,\ell)$, $Al_2O_3(c,\ell)$, or $MgO(c,\ell)$. At 2000°K, the vapor pressures of these species are, respectively,

$$P_{W(c)} = 4.0 \times 10^{-12} \text{ torr}$$

$$P_{ZrO_2(c)} = 2.5 \times 10^{-8}$$

$$P_{Al_2O_3(c)} = 9.4 \times 10^{-16}$$

and

$$P_{MgO(c)} = 3.8 \times 10^{-4}$$

all of which are considerably less than that of Cu at this temperature. The heat release values of these compositions, defined as the difference between the enthalpy of the combustion products at 2000°K and the reactants at room temperature are listed below for the indicated stoichiometries:

$$WO_3(c) + 1.5\ Zr(c) \rightarrow 1.5\ ZrO_2(c) + W(c) \qquad (1)$$

$$\Delta H_1 = -0.3627 \text{ kcal/gm of reactants}$$

$$WO_3(c) + 2\ Al(c) \rightarrow Al_2O_3(c) + W(c) \qquad (2)$$

$$\Delta H_2 = -0.4804 \text{ kcal/gm of reactants}$$

$$WO_3(c) + 3\ Mg(c) \rightarrow 3\ MgO(c) + W(c) \quad (3)$$

$$\Delta H_3 = -0.5137 \text{ kcal/gm of reactants}$$

These heats represent the energy available to generate Cu(g) at 2000°K. Reaction (1) has been used successfully by workers here as a high-density heater for generating Al(g) and U(g).

The heat required to generate Cu(g) at 2000°K from Cu metal at room temperature is 1.410 kcal/gm Cu. Therefore, Reactions (1), (2) and (3) will generate 0.2572, 0.3407 and 0.3643 grams Cu(g)/gm of reactants respectively, at an equilibrium flame temperature of 2000°K, if the reactants are admixed in the same proportions with Cu metal at room temperature (i.e., 0.2572 gram Cu(c)/gm of reactants of (1)). A superior yield of Cu(g)/unit weight of reaction mass is achieved from mixtures of either (1), (2) or (3) with stoichiometric mixtures of cupric oxide, CuO, and either Zr, Al or Mg, where the CuO is considered to be an oxidizer and the latter as fuels. Heats required to generate Cu(g) and either $ZrO_2(c)$, $Al_2O_3(c)$ or MgO(c) at 2000°K from stoichiometric mixtures of CuO and either Zr, Al or Mg are

$$2\ CuO(c) + Zr(c) \rightarrow ZrO_2(c) + 2\ Cu(g) \quad (4)$$

$$\Delta H_4 = 0.08954 \text{ kcal/gm of reactant}$$

$$[Cu(g)]_4 = 0.5077 \text{ gm Cu(g)/gm of reactant}$$

$$3\ CuO(c) + 2\ Al(c) \rightarrow Al_2O_3(c) + Cu(g) \quad (5)$$

$$\Delta H_5 = 0.1027 \text{ kcal/gm of reactant}$$

$$[Cu(g)]_5 = 0.6515 \text{ gm Cu(g)/gm of reactant}$$

$$CuO(c) + Mg(c) \rightarrow MgO(c) + Cu(g) \quad (6)$$

$$\Delta H_6 = 0.03458 \text{ kcal/gm of reactant}$$

$$[Cu(g)]_6 = 0.6118 \text{ gm Cu(g)/gm of reactant.}$$

The heat requirements of (4), (5) and (6) for Cu(g) generation at 2000°K can be satisfied by admixture with (1), (2) and/or (3). By heat and mass balances, the 3-component mixtures of WO_3/CuO and either Zr, Al or Mg result in the following mixture ratios and yields of Cu(g) at 2000°K:

A. $WO_3/CuO/Zr$

Basis: 1 gm of comp (1)

$$\frac{\Delta H_1}{\Delta H_4} = \frac{0.3627}{0.08954} = \frac{4.051 \text{ gm comp (4)}}{\text{gm comp (1)}}$$

$$\frac{[Cu(g)]_4 \, \Delta H_1/\Delta H_4}{1 + \Delta H_1/\Delta H_4} = \frac{0.5077 \times 4.051}{1 + 4.051} = \frac{0.4072 \text{ gm Cu(g)}}{\text{gm [comp (1) + comp (4)]}}$$

B. $WO_3/CuO/Al$

Basis: 1 gm comp (2)

$$\Delta H_2/\Delta H_5 = 0.4804/0.1027 = 4.678 \frac{\text{gm comp (5)}}{\text{gm comp (2)}}$$

$$\frac{[Cu(g)]_5 \, \Delta H_2/\Delta H_5}{1 + \Delta H_2/\Delta H_5} = \frac{0.6515 \times 4.678}{1 + 4.678} = \frac{0.5366 \text{ gm Cu(g)}}{\text{gm [comp (2) + comp (5)]}}$$

C. $WO_3/CuO/Mg$

Basis: 1 gm comp (3)

$$\Delta H_3/\Delta H_6 = 0.5137/0.03458 = \frac{14.86 \text{ gm comp (6)}}{\text{gm comp (3)}}$$

$$\frac{[Cu(g)]_6 \, \Delta H_3/\Delta H_6}{1 + \Delta H_3/\Delta H_6} = \frac{0.6118 \times 14.86}{1 + 14.86} = \frac{0.5732 \text{ gm Cu(g)}}{\text{gm (comp (3) + comp (6)]}}$$

It is seen that 4-component mixtures, e.g. $WO_3/CuO/Zr/Al$, etc. can also be made up. In the event that the combustion of 3-component mixtures does not form a desirable "melt" for slag formation, and the slag is entrained by Cu(g) rather than retained in the motor chamber, the 4-component mixtures may be of interest. Also, slag-formers, such as iron oxide, may be employed as an additional component, either as the oxide in the mix, or as iron metal in the mix, with the oxide formation taking place as a combustion product. The use of this oxide in selected thermite compositions is described further below.

TYPE II THERMITES

The thermites described previously are based on the use of WO_3 as an oxidizer in order to yield gasless combustion products. More conventional thermite oxidizers, such as the oxides of iron, chromium, and manganese yield Fe, Cr, and Mn, as combustion products, all of which have vapor pressures at 2000°K appreciably greater than that of W, as itemized below:

$$P_{Fe} = 0.244 \text{ torr}$$

$$P_{Cr} = 0.875 \text{ torr}$$

$$P_{Mn} = 121 \text{ torr}$$

These are to be compared with 4.00×10^{-12} and 2.94 torr for the vapor pressures of W and Cu, respectively, at 2000°K. The high vapor pressure of Mn seriously detracts from the energy of compositions based on MnO_2, and certainly would cause the vapor release to be comprised of considerably more Mn(g) than Cu(g). For these reasons, thermite compositions based on MnO_2 as the oxidizer are not considered further here. Both Fe and Cr have vapor pressures considerably less than Cu and for this reason may be permissible in selected applications. Defining heat release values at 2000°K as above, values of this parameter are listed below for thermites based on the use of iron (II) oxide:

$$Fe_2O_3(c) + 1.5\ Zr(c) \rightarrow 1.5\ ZrO_2(c) + Fe(g \text{ or } \ell) \quad (7)$$

$$\Delta H_7 = 0.2327 \text{ kcal/gm to Fe(g)}$$

$$= -0.3714 \text{ kcal/gm to Fe}(\ell)$$

$$Fe_2O_3(c) + 2\ Al(c) \rightarrow Al_2O_3(c) + 2\ Fe(g \text{ or } \ell) \quad (8)$$

$$\Delta H_8 = 0.3063 \text{ kcal/gm to Fe(g)}$$

$$= -0.5323 \text{ kcal/gm to Fe}(\ell)$$

$$Fe_2O_3(c) + 3\ Mg(c) \rightarrow 3\ MgO(c) + Fe(g \text{ or } \ell) \quad (9)$$

$$\Delta H_9 = 0.01984 \text{ kcal/gm to Fe(g)}$$

$$= -0.5717 \text{ kcal/gm to Fe}(\ell)$$

Three-component mixtures of CuO, Fe_2O_3, and either Zr, Al, or Mg are formed by the mixtures 4 + 7, 5 + 8, and 6 + 9, respectively. The mixture ratios, based on a combustion products saturated with both Cu and Fe, and the resultant Cu yields, are itemized below:

D. $Fe_2O_3/CuO/Zr$

Mix ratio = 2.245 gm Comp 4/gm Comp 7

Cu Yield = 0.3512 gm Cu(g)/gm total

E. $Fe_2O_3/CuO/Al$

Mix ratio = 3.521 gm Comp 5/gm Comp 8

Cu Yield = 0.5074 gm Cu(g)/gm total

F. $Fe_2O_3/CuO/Mg$

Mix ratio = 3.837 gm Comp 6/gm Comp 9

Cu Yield = 0.4853 gm Cu(g)/gm total

In each of these cases, the molar ratio of Cu(g)/Fe(g) in the combustion products is the saturation value at 2000°K, 2.94/0.244 = 12.0. Similar results are achieved using Fe_3O_4 as the oxidizer. The best of the Cr oxides to use as an oxidizer is the "anhydride," CrO_3. With Zr, Al, and Mg, the heat release values at 2000°K are

$$CrO_3(c) + 1.5\ Zr(c) \rightarrow 1.5\ ZrO_2(c) + Cr(g) \qquad (10)$$

$$\Delta H_{10} = -0.4881 \text{ kcal/gm}$$

$$CrO_3(c) + 2\ Al(c) \rightarrow Al_2O_3(c) + Cr(g) \qquad (11)$$

$$\Delta H_{11} = -0.7701 \text{ kcal/gm}$$

and

$$CrO_3(c) + 3\ Mg(c) \rightarrow 3\ MgO(c) + Cr(g) \qquad (12)$$

$$\Delta H_{12} = -0.8004 \text{ kcal/gm}$$

and the mixture ratios and Cu(g) yield for the 3-component mixtures of CrO_3, CuO, and either Zr, Al, or Mg are:

G. $CrO_3/CuO/Zr$

Mix ratio = 5.451 gm Comp 4/gm Comp 10

Cu Yield = 0.4290 gm Cu(g)/gm total

Cu(g)/Cr(g) = 10.9 molar

II. CrO_3/CuO/Al

Mix ratio = 7.498 gm Comp 5/gm Comp 11

Cu Yield = 0.5748 gm Cu(g)/gm total

Cu(g)/Cr(g) = 22.8, molar

I. Cr_3/CuO/Mg

Mix ratio = 23.15 gm Comp 6/gm Comp 12

Cu Yield = 0.5864 gm Cu(g)/gm total

Cu(g)/Cr(g) = 23.2, molar

In all cases, the combustion products are saturated with respect to Cu(g) and unsaturated with respect to Cr(g). The sesquioxide of Cr, Cr_2O_3, is a considerably inferior oxidizer. For example, the 3-component mixture formed by admixture of Comp 5 and the stoichiometric mixture Cr_2O_3 + 2 Al yields only 0.2492 gm Cu(g)/gm total, and the molar ratio Cu(g)/Cr(g) in the combustion products is the saturation value, 2.94/0.875 = 3.36.

In summary, the yields of Cu(g) from 3-component mixtures of CuO and either WO_3, Fe_2O_3, Fe_3O_4, or CrO_3 and either Zr, Al, or Mg are comparable. The use of WO_3 as an oxidizer permits the generation of Cu(g) as the only gaseous combustion product. The use of Fe_2O_3 or Fe_3O_4 as oxidizers yields Fe(g) as a minor combustion product. Similarly, CrO_3 yields Cr(g) as a minor combustion product. Cr_2O_3 yields Cr(g) as a major combustion product and results in poor yields of Cu(g).

APPENDIX II

TIME REQUIRED FOR VAPORIZATION OF A COPPER SEED PARTICLE

For the copper vapor generator it is of interest to determine to what extent a seed particle is vaporized at the time of its introduction into the laser cavity. In order to estimate the time required to heat and vaporize a copper particle the following model is used. We assume a copper sphere of diameter D leaves the burning grain surface at a temperature T_s and is immersed in the combustion gases at a temperature T_o. The heat transfer rate per unit area is given by

$$h(T_o - T)$$

where h is the heat transfer coefficient and T is the temperature of the sphere. The rate of evaporation is given approximately by:

$$\frac{1}{3}\bar{v}\frac{\lambda}{\ell}(N_{eq} - N)$$

if diffusion limited or by

$$\frac{1}{4}\bar{v}(N_{eq} - N)$$

if not, where

$\bar{v}$ = mean velocity of Cu atom

λ = mean free path of Cu atom

ℓ = stagnant film thickness

N_{eq} = Cu vapor density at equilibrium

N = Cu vapor density

The second expression for the rate of vaporization is expected to apply only when $\lambda \lesssim \ell$. In addition to convective heat transfer and vaporization, it may be necessary to include radiative heat loss. For this we assume the particle emissivity is unity, the combustion gas is optically thin and the enclosure wall temperature is much lower than the particle temperature. Then the radiative heat loss per unit area is given by

$$\sigma T^4$$

where σ is the Stefan-Boltzmann constant.

For spherical particles we obtain the following rate equations when the above mentioned processes are considered

$$\frac{dT}{dt} = \frac{6}{\rho CD}\left(h(T_o - T) - W\epsilon_v - \sigma T^4\right)$$

$$\frac{dD}{dt} = -\frac{2W}{\rho}$$

where

C = heat capacity

D = particle diameter

W = rate of evaporation per unit area

ϵ_v = heat of vaporization

The rate of evaporation is

$$W = \sqrt{\frac{M}{2\pi RT}}\,(P_{eq}(T) - P)\theta$$

where

M = molecular mass

R = gas constant

P_{eq} = equilibrium vapor pressure

P = actual vapor pressure

and

$\theta = \frac{\lambda}{\ell}$ when $\lambda < \ell$

$= 1$ when $\lambda \gtrsim \ell$

The equilibrium vapor pressure as a function of temperature may be expressed as

$$P_{eq}(T) = e^{(a-b/T)}$$

and the stagnant film thickness ℓ may be approximated by assuming that

$$h = \frac{k}{\ell}$$

where k = thermal conductivity of combustion gases and using

$$h = \frac{kN_u}{D}$$

where N_u is Nuesselt's number. A good approximation is $N_u = 2$, so that $\ell = D/2$. Furthermore we take P = O which in effect means we neglect the recondensation of the vapor on the existing particles.

Tables VII-2 through VII-5 give the time development of the diameter D(microns) and temperature T (°K) of a copper sphere in a heat bath of the combustion product gases at a temperature T_0 (°K) where X is the elapsed time in microseconds. A Runge-Kutta integration procedure was used. The accuracy was checked by decreasing the step size. No significant changes were observed.

The results given in Tables AII-1 through AII-4 account for the low copper densities observed and suggest a way to overcome this problem. Table AII-1 indicates that 30-micron particles would not be vaporized. Table AII-2 indicates that 10-micron particles would be partially vaporized while Table AII-3 indicates that 3-micron particles would be completely vaporized.

Two temperatures are considered in these tables. It was indicated in Table IV-5 that if the propellant burned completely to thermal equilibrium, the final temperature would be 2628.5°K. Therefore, $T_0 = 2500$°K was used as a more conservative estimate of the temperature of the combustion product gases. Without the copper seeding, the NIBTN propellant would generate a flame temperature of 2775.4°K, so $T_0 = 2775.4$ was used for an optimistic estimate of the gas heat bath temperature.

Two times should be considered in examining these tables; the residence time within the gas generator and a transit time of 1.1 msec to travel the 33 cm from the throat to the laser cavity. Initially based on the propellant burn rate and combustion gas velocity, the gas generator residence time was estimated to be 0.5 to 1.0 msec.

Table AII-1 shows that even if the optimistic 2775.4°K temperature is assumed for a full 2.1 msec, a 30-micron particle does not vaporize. Its diameter will still be 29.9 microns. If the temperature of the 30-micron particle is examined at the throat of the gas generator and compared with the experimental finding of sintered copper on the Kanthal wire in Test No. 1 with a granular structure similar to the original seeding distribution, this suggests that T (residence time) $\lesssim$1356°K = melting point of copper or that the "effective" residence time was ~0.5 msec.

Table AII-2 examines the 2.2 percent of the copper particles whose size was 10 microns or less. These particles will just be vaporized if the optimistic 2775.4°K flame temperature is assumed for a full 2.1 msec. If the gas temperature is 2500°K for the entire trip, then 52 percent of a 10-micron particle's mass would have vaporized when

it arrives at the laser cavity with a diameter of 7.8 microns. In view of the foregoing, 1 percent appears to be an optimistic upper limit for the amount of copper which was vaporized during a test run.

Table AII-3, on the other hand, indicates that 3 micron-copper particles would be fully vaporized in 0.41 msec which is less than the 0.5 msec "effective" residence time of the gas generator. Propellant seeding with smaller copper particle size distributions is possible. Distributions with average copper particle sizes as small as 1 micron are commercially available. Slow precipitation and classification are two methods which can produce copper particle distributions with a mean diameter by weight that is less than 1 micron. Oxidation, however, becomes a problem for distributions this fine. Handling, mixing, and casting the propellant should be carried out under an inert atmosphere. The more practical possibility is to use a commercially available distribution with a mean particle size of 2.7 microns by weight, 99 9 percent of which would pass through a 10-micron screen. This distribution can be handled in air which will facilitate the propellant formulation.

The passage of a copper seed particle through the burning propellant surface and its release into the hot combustion product gases is a complex process. The results of Tables AII-1 through AII-3 apply to copper particles at 700°K which are suddenly released into a 2500°K environment. A more realistic set of conditions might include (1) a relatively long dwell time ($\gtrsim$40 msec) on the burning surface whose temperature ~1400°C and (2) a dwell time in the hot combustion gas zone which accounts for the time required to accelerate a copper particle up to the gas velocity. The following scenario might represent a "more realistic" set of conditions for a 30-micron copper seed particle. The results are given in Table AII-4. A 30-micron copper particle starting at an initial propellant temperature T_s = 700°K is exposed to a burning surface temperature of 1400°C for 47 msec, then released into the combustion gas heat bath at 2775.4°K for 1 to 6 msec and finally undergoes an expansion through the throat during which the temperature of the gas heat bath drops to 0.8 times its initial value or to 2220.3°K for the 1.1 msec transit time to the laser cavity. After 49.1 msec a 30-micron particle still is 29.85 microns in diameter which corresponds to 1.5 percent vaporization of the sphere's mass. Even if 6 msec are spent at a flame temperature of 2775.4°K, the 30-micron copper particle has a 26.77-micron diameter when it arrives at the laser cavity after 54.1 msec. Actually these "more realistic" conditions predict the 30-micron copper particle's temperature to be 2216°K or 2460°K at the throat which does not correspond to the $<$1356°K temperature indicated by the copper sintered on the Kanthal wire. It might also be noted that under this "more realistic" set of conditions, a 3-micron copper particle would be fully vaporized in 47.15 msec. At this point it would probably be more productive to experimentally test a solid fuel propellant seeded with 3-micron copper particles than to attempt to develop better computer models.

Table AII-1. Vaporization of 30-Micron Copper Spheres.*

DIFFUSION LIMITED WITH RAD LOSS

TO = 2775.4

SKIP NO = 1

X	T	D
0.00	700.00	30.000
100.00	860.70	30.000
200.00	1008.80	30.000
300.00	1145.20	29.999
400.00	1270.72	29.999
500.00	1386.14	29.999
600.00	1492.16	29.999
700.00	1589.44	29.999
800.00	1678.61	29.999
900.00	1760.24	29.999
1000.00	1834.86	29.999
1100.00	1902.97	29.998
1200.00	1965.01	29.997
1300.00	2021.42	29.995
1400.00	2072.56	29.992
1500.00	2118.78	29.987
1600.00	2160.42	29.980
1700.00	2197.78	29.970
1800.00	2231.17	29.958
1900.00	2260.88	29.942
2000.00	2287.18	29.923
2100.00	2310.38	29.900

DIFFUSION LIMITED WITH RAD LOSS

TO = 2500.0

SKIP NO = 1

X	T	D
0.00	700.00	30.000
100.00	839.36	30.000
200.00	967.81	30.000
300.00	1086.13	29.999
400.00	1195.06	29.999
500.00	1295.27	29.999
600.00	1387.39	29.999
700.00	1472.02	29.999
800.00	1549.69	29.999
900.00	1620.91	29.999
1000.00	1686.16	29.999
1100.00	1745.89	29.999
1200.00	1800.51	29.999
1300.00	1850.40	29.999
1400.00	1895.92	29.998
1500.00	1937.39	29.997
1600.00	1975.14	29.996
1700.00	2009.44	29.994
1800.00	2040.55	29.991
1900.00	2068.73	29.988
2000.00	2094.21	29.983
2100.00	2117.21	29.978

*Vaporization of copper spheres of diameter D (microns) and temperature T(°K) in a heat bath of combustion product gases at a temperature TO(°K) where X is the time in microseconds.

Table AII-2. Vaporization of 10-Micron Copper Spheres.*

DIFFUSION LIMITED WITH RAD LOSS

TO = 2775.4

SKIP NO = 50

X	T	D
0.00	700.00	10.000
10.00	845.30	10.000
250.00	2384.62	9.939
500.00	2509.03	9.365
1000.00	2515.35	7.816
1500.00	2521.28	5.799
1600.00	2522.77	5.293
1700.00	2524.43	4.728
1800.00	2526.35	4.078
1900.00	2528.68	3.292
1925.00	2529.36	3.062
1950.00	2530.09	2.812
1975.00	2530.91	2.537
2000.00	2531.83	2.226
2025.00	2532.91	1.862
2050.00	2534.27	1.403
2060.00	2534.97	1.168
2070.00	2547.20	0.876
2075.00	2568.90	0.704
2080.00	2600.09	0.506
2082.00	2617.64	0.415
2084.00	2640.81	0.314
2086.00	2674.92	0.198
2086.50	2686.67	0.165
2087.00	2700.67	0.129
2087.50	2717.98	0.091
2088.00	2740.75	0.049

DIVISION LIMITED WITH RAD LOSS

TO = 2500.0

SKIP NO = 20

X	T	D
0.00	700.00	10.000
10.00	826.01	10.000
100.00	1626.36	9.999
200.00	2064.47	9.996
400.00	2330.76	9.896
600.00	2363.24	9.693
800.00	2366.78	9.468
1000.00	2367.74	9.235
1200.00	2368.52	8.995
1400.00	2369.32	8.747
1600.00	2370.14	8.490
1800.00	2371.00	8.223
2000.00	2371.89	7.946
2100.00	2372.35	7.804

*Vaporization of copper spheres of diameter D (microns) and temperature T(°K) in a heat bath of combustion product gases at a temperature TO(°K) where X is the time in microseconds.

Table AII-3. Vaporization of 3-Micron Copper Spheres.*

DIFFUSION LIMITED WITH RAD LOSS

TO = 2500.0

SKIP NO = 50

X	T	D
0.00	700.00	3.000
1.00	839.49	3.000
25.00	2243.09	2.992
50.00	2382.78	2.911
100.00	2389.03	2.689
150.00	2389.84	2.444
200.00	2390.75	2.170
250.00	2391.79	1.854
300.00	2393.07	1.468
350.00	2398.51	0.931
360.00	2408.24	0.793
370.00	2419.84	0.647
380.00	2434.18	0.487
385.00	2442.87	0.402
390.00	2453.03	0.311
392.00	2457.62	0.274
394.00	2462.60	0.235
396.00	2468.02	0.194
398.00	2473.99	0.153
400.00	2480.61	0.109
401.00	2484.22	0.087
401.50	2486.23	0.075
402.00	2488.19	0.064
402.50	2490.21	0.052
402.70	2491.04	0.047
402.80	2491.46	0.045
402.90	2491.88	0.043
403.00	2492.30	0.040

Table AII-3. (Continued).

X	T	D
403.10	2492.73	0.038
403.20	2493.16	0.036
403.30	2493.60	0.033
403.40	2494.03	0.031
403.50	2494.48	0.028
403.60	2494.92	0.026
403.70	2495.37	0.024
403.80	2495.82	0.021

*Vaporization of copper spheres of diameter D (microns) and temperature T(°K) in a heat bath of combustion product gases at a temperature TO(°K) where X is the time in microseconds.

Table AII-4. Vaporization of 30-Micron Copper Spheres Under "More Realistic" Conditions.*

DIFFUSION LIMITED WITH RAD LOSS
SKIP NO = 10

X	T	D	TO
0.00	700.00	30.000	1673.0
100.00	775.29	30.000	
500.00	1021.90	29.999	
1000.00	1235.18	29.999	
2000.00	1467.47	29.999	
3000.00	1566.23	29.999	
4000.00	1607.72	29.999	
5000.00	1625.05	29.999	
10000.00	1637.25	29.997	
20000.00	1637.41	29.994	
30000.00	1637.42	29.990	
40000.00	1637.42	29.987	
47000.00	1637.42	29.984	2775.4
47100.00	1722.63	29.984	
47200.00	1800.57	29.984	
47300.00	1871.76	29.983	
47400.00	1936.67	29.982	
47500.00	1995.73	29.981	
47600.00	2049.34	29.978	
47700.00	2097.86	29.974	
47800.00	2141.64	29.968	
47900.00	2181.00	29.960	
48000.00	2216.23	29.949	2220.3
48100.00	2205.21	29.936	
48200.00	2195.38	29.925	
48300.00	2186.60	29.915	
48400.00	2178.75	29.905	
48500.00	2171.73	29.896	
48600.00	2165.45	29.887	
48700.00	2159.81	29.878	
48800.00	2154.76	29.870	
48900.00	2150.24	29.862	
49000.00	2146.18	29.855	
49100.00	2142.53	29.848	

DIFFUSION LIMITED WITH RAD LOSS
SKIP NO = 10

X	T	D	TO
0.00	700.00	30.000	1673.0
100.00	775.29	30.000	
500.00	1021.90	29.999	
1000.00	1235.18	29.999	
2000.00	1467.47	29.999	
3000.00	1566.23	29.999	
4000.00	1607.72	29.999	
5000.00	1625.05	29.999	
10000.00	1637.25	29.997	
20000.00	1637.41	29.994	
30000.00	1637.42	29.990	
40000.00	1637.42	29.987	
47000.00	1637.42	29.984	2775.4
47100.00	1722.63	29.984	
47200.00	1800.57	29.984	
47300.00	1871.76	29.983	
47400.00	1936.67	29.982	
47600.00	2049.34	29.978	
47800.00	2141.64	29.968	
48000.00	2216.23	29.949	
48500.00	2340.71	29.841	
49000.00	2403.80	29.646	
49500.00	2433.14	29.387	
50000.00	2446.23	29.091	
50500.00	2452.15	28.775	
51000.00	2455.06	28.447	
51500.00	2456.78	28.110	
52000.00	2458.03	27.767	
52500.00	2459.11	27.417	
53000.00	2460.15	27.060	2220.3
53100.00	2410.53	26.998	
53200.00	2369.54	26.951	
53300.00	2335.20	26.914	
53400.00	2306.13	26.885	
53500.00	2281.35	26.860	
53600.00	2260.10	26.839	

Table AII-4. (Continued).

X	T	D	TO
53700.00	2241.80	26.821	
53800.00	2225.99	26.805	
53900.00	2212.29	26.790	
54000.00	2200.40	26.777	
54100.00	2190.06	26.765	

*Vaporization of copper spheres of diameter D (microns) and temperature T(°K) in heat baths at the burning surface TO = 1673°K for 47 msec, then in combustion product gases at TO = 2775.4°K for 1 - 6 msec and finally at TO = 2220.3°K during a transit time of 1.1 msec. X is the time in microseconds.

REFERENCES

1. W.T. Walter, "40-kW Pulsed Copper Laser," Bull. Am. Phys. Soc. 12, 90(1967) and W.T. Walter "High Power Copper Laser," Final Report NADC Contract N62269-3584 (1966).

2. W.T. Walter, "Metal Vapor Lasers," IEEE J. Quantum Electron. QE-4, 355 (1968).

3. R. Chimenti and W.T. Walter, "Coherence Properties of the Pulsed Copper Vapor Laser," Bull. Am. Phys. Soc. 16, 41 (1971).

4. W.T. Walter, N. Solimene, M. Piltch, and G. Gould, "Efficient Pulsed Gas Discharge Lasers," IEEE J. Quantum Electron. QE-2, 474 (1966).

5. C.H. Corliss and W.R. Bozman, "Experimental Transition Probabilities for Spectral Lines of Seventy Elements," National Bureau of Standards Monograph 53 (U.S. GPO, Washington, D.C., 1962), p. 80.

6. D.A. Leonard, "A Theoretical Description of the 5106-Å Pulsed Copper Vapor Laser," IEEE J. Quantum Electron. QE-3, 380 (1967).

7. L.A. Weaver, C.S. Liu, and E.W. Sucov, "Superradiant Laser Emission at 5106-Å in Pulsed Copper Iodide Discharges," IEEE J. Quantum Electron. QE-9, 645 (1973).

8. C.S. Liu, E.W. Sucov, and L.A. Weaver, "Copper Superradiant Emission from Pulsed Discharges in Copper Iodide Vapor," Appl. Phys. Lett., 23, 92 (1973).

9. W.T. Walter, M. Piltch, N. Solimene, and G. Gould, "Pulsed–Laser Action in Atomic Copper Vapor," Bull. Am. Phys. Soc. 11, 113 (1966).

10. W.T. Walter, "Improved Copper Vapor Laser," Progress Report No. 36 to JSTAC, Polytech. Inst. of Brooklyn, Report No. R-452.36-71, p. 112 (1971).

11. A.A. Isaev, M.A. Kazaryan, and G.G. Petrash, "Effective Pulsed Copper-Vapor Laser with High Average Generation Power," JETP Lett. 16, 27 (1972).

12. G.G. Petrash, A.A. Isaev, and M.A. Kazaryan, "Pulsed Metal Vapor Lasers," IEEE J. Quantum Electron. QE-9, 644 (1973).

13. J.F. Asmus and N.K. Moncur, "Pulse Broadening in a MHD Copper Vapor Laser," Appl. Phys. Lett. 13, 384 (1968).

14. D. Leonard, "Airborne Laser Development," Final Report ABMDA Contract DAHC60-70-C-0030 (1970).

15. G.R. Russell, N.M. Nerheim, and T.J. Pivirotto, "Supersonic Electric-Discharge Copper Vapor Laser," Appl. Phys. Lett. 21, 565 (1972).

16. T.W. Karras, R.S. Anderson, B.G. Bricks, T.E. Buczacki, and L.S. Springer, "Copper Vapor Generator," Final Report AFWL Contract F29601-72-C-0079 (1973).

17. W.R. Bennett, Jr., "Gaseous Optical Masers," Appl. Optics Suppl. 1, 29 (1962).

18. C.M. Ferrar, "Copper-Vapor Laser with Closed-Cycle Transverse Vapor Flow," IEEE J. Quantum Electron. QE-9, 856 (1973).

19. W.T. Walter and R. Chimenti, "Metal Vapor Lasers," Progress Report No. 35 to JSTAC, Polytech. Inst. of Brooklyn, Report No. R-452.35-70, p. 130 (1970).

20. R. Chimenti, "The Copper Vapor Laser," Ph. D. Dissertation, Polytechnic Institute of Brooklyn (1972).

21. R. Bleekrode and W. vonBenthem, "Resonance Fluorescence of Cu Atoms in the Gas Phase," J. Chem. Phys. 51, 2757 (1969).

22. G.M. Grover, T.P. Cotter, and G.F. Erickson, "Structures of Very High Thermal Conductance," J. Appl. Phys. 35, 1990 (1964).

23. C.R. Vidal and J. Cooper, "Heat-Pipe Oven: A New, Well-Defined Metal Vapor Device for Spectroscopic Measurements," J. Appl. Phys. 40, 3370 (1969).

24. P.P. Sorokin and J.R. Lankard, "Infrared Lasers Resulting from Giant Pulse Laser Excitation of Alkali Metal Molecules," J. Chem. Phys. 54, 2184 (1971).

25. R.T. Hodgson, "Vapor Discharge Cell," U.S. Patent No. 3,654,567, April 4, 1972.

26. P.P. Sorokin and J.R. Lankard, "Emission Spectra of Alkali-Metal Molecules Observed with a Heat-Pipe Discharge Tube," J. Chem. Phys. 55, 3810 (1971).